DEVELOPMENT OF BIOASSAYS FOR THE DETECTION OF BENZYLISOQUINOLINE ALKALOIDS,HIGENAMINE AND BERBERINE

ポームラフィ, ヌンタウォン

DEVELOPMENT OF BIOASSAYS FOR THE DETECTION OF BENZYLISOQUINOLINE ALKALOIDS, HIGENAMINE AND BERBERINE

POOMRAPHIE NUNTAWONG

A DISSERTATION SUBMITTED IN PARTIAL FULFILLMENT OF THE REQUIREMENT FOR THE DEGREE OF DOCTOR OF PHILOSOPHY

DEPARTMENT OF PHARMACOGNOSY
GRADUATED SCHOOL OF PHARMACEUTICAL SCIENCES
KYUSHU UNIVERSITY
2023

TABLE OF CONTENTS

LIST OF ABBREVIATIONS

(*S*)-HM	*S*-configuration higenamine
4-HPAA	4-hydroxyphenylacetaldehyde
AAF	Adverse analytical finding
ABTS	2,2'-azino-bis(3-ethylbenzothiazoline-6-sulfonic acid)
Apt	Aptamer
BBR	Berberine
BSA	Bovine serum albumin
CDI	*N,N'*-Carbonyldiimidazole
CR	Cross-reaction
CV	Coefficient of variation
Da	Dalton
DMF	Dimethyl formamide
DNA	Deoxyribonucleic acid
dNTP	Deoxyribonucleotide triphosphate
dsDNA	Double strand deoxyribonucleic acid
e-RDF	Enriched RPMI1640-Dulbecco's-Ham's F12
EDTA	Ethylenediaminetetraacetic acid
ELISA	Enzyme-linked immunosorbent assay
FBS	Fetal bovine serum
FCA	Freund's complete adjuvants
FIA	Freund's incomplete adjuvants
Fig.	Figure
GOLD-SELEX	Colloidal gold nanoparticles-based aptamer selection
HAT	Hypoxanthine-aminopterin-thymidine
HM	Higenamine
HPLC	High-performance liquid chromatography
HRP	Horseradish peroxidase
IC_{10}	10% Inhibitory concentration
IC_{50}	50% Inhibitory concentration

icELISA	Indirect competitive ELISA
iELISA	Indirect ELISA
IgG	Immunoglobulin G
LB	Luria-Bertani
LFA	Lateral flow immunoassay
LOD	Limit of detection
MAb	Monoclonal antibody
MAb E8	Monoclonal antibody from colony E8
MALDI-TOF-MS	Matrix-assisted laser desorption/ionization time-of-flight mass spectrometry
MeOH	Methanol
MW	Molecular weight
ND	Not detected
OD	Optical Density
OVA	Albumin from chicken egg white
PAb	Polyclonal antibody
PBS	Phosphate-buffered saline
PBS-T	PBS with 0.05% (v/v) tween 20
PCR	Polymerase chain reaction
PEG	Polyethylene glycol
RNA	Ribonucleic acid
ROI	Region of interest
SD	Standard deviation
SDS-PAGE	Sodium dodecyl-sulfate polyacrylamide gel electrophoresis
SDW	Sterile distilled water
SELEX	Systematic evolution of ligands by exponential enrichment
ssDNA	Single strand deoxyribonucleic acid
Tween 20	Polyoxyethylene sorbitan monolaurate
UV	Ultraviolet
WADA	World Anti-Doping Agency

LIST OF PUBLICATIONS

[1] Nuntawong P, Tanaka H, Sakamoto S, Morimoto S. ELISA for the detection of the prohibited doping agent higenamine. *Planta Med*. 2020 Jul;86(11):760-766. doi: 10.1055/a-1181-2084. Epub 2020 Jun 8. PMID: 32512615.

[2] Nuntawong P, Ochi A, Chaingam J, Tanaka H, Sakamoto S, Morimoto S. The colloidal gold nanoparticle-based lateral flow immunoassay for fast and simple detection of plant-derived doping agent, higenamine. *Drug Test Anal*. 2021 Apr;13(4):762-769. doi: 10.1002/dta.2981. Epub 2020 Nov 25. PMID: 33217196.

[3] Nuntawong P, Tayama Y, Tanaka H, Morimoto S, Sakamoto S. Aptamer-based berberine detection for quality control of Kampo medicines. In preparation.

LIST OF TABLES

LIST OF FIGURES

Chapter I
General Introduction

1. Benzylisoquinoline alkaloids

Secondary metabolites, such as terpenoids, phenolic compounds, and alkaloid, are compounds produced by the plants but do not play a role in the growth and development of the plants. Alkaloids are valuable secondary metabolites and potential medicinal candidates because of their potent biological activities. Alkaloids are generally produced in plants through the decarboxylation of amino acids such as histidine, ornithine, lysine, tyrosine, and tryptophan. Thus, the common structure of alkaloids is low-molecular-weight, nitrogen-containing compounds found in more than 20% of plant species.

One of the primary classes of alkaloids with pharmacological activity is benzylisoquinoline alkaloids. As their name implies, the main structural elements of these compounds (Fig. 1) are a benzene ring linked to an isoquinoline and a benzene ring fused to a pyridine ring. More than 2,500 identified structures have been isolated from plants [1]. The actions of benzylisoquinoline alkaloids in the form of plant crude extract are well known to humans. For example, opium poppy (*Papaver somniferum* Linn.) was recognized as the traditional source of analgesia [1], while greater celandine (*Chelidonium majus* Linn.) was widely recognized in Asia and Europe as a medicinal herb [1]. Using contemporary scientific data, it was possible to corroborate their traditional usage. The quaternary ammonium salts of protoberberine and benzophenanthridine alkaloids have demonstrated antibacterial properties. Additionally, sanguinarine and berberine exhibit anticancer properties by stabilizing human telomeric G-quadruplex DNA [2]. The primary alkaloid present in opium poppy, papaverine, is a nonspecific vasodilator [1] and has been linked to erectile dysfunction [3]. It was discovered that dauricine, a dimer of the 1-benzylisoquinoline alkaloid found in moonseed (*Menispermum dauricum* DC.), is a calcium channel blocker [4]. (+)-Tubocurarine, a bisbenzylisoquinoline alkaloid extracted from curare (*Chondrodendron tomentosum* Ruiz & Pav.), was known as a neuromuscular blocking agent [5]. Morphinan and promorphinan alkaloids, morphine and codeine, are also excellent drugs for narcotic analgesics [6]. These compounds were helpful for direct usage and as important precursors in the synthesis of naloxone and naltrexone, two drugs used to treat opiate addiction [1]. The benzylisoquinoline

alkaloids are vital not only to the pharmaceutical sciences but also to other sectors, including agriculture. Berberine is an effective insect antifeedant against a broad range of insect species [7–9] and also has antiherbivore action [10].

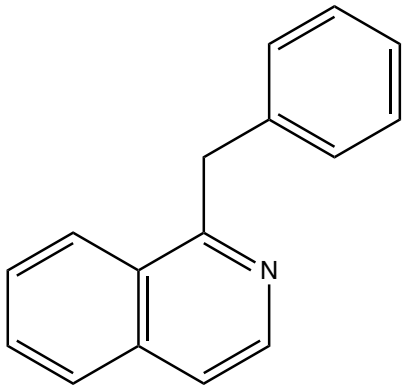

Figure 1 Core structure of benzylisoquinoline alkaloids

The benzylisoquinoline alkaloid is a category of chemicals that are very significant to humans under certain conditions. To ensure effectiveness and reduce side effects, it is vital to ensure the quality of the natural source, which may be indicated by the concentration of essential substances in these plants.

1.1 Higenamine

Higenamine (HM; 1-[(4-hydroxyphenyl)methyl]-1,2,3,4-tetrahydroisoquinoline-6,7-diol; Fig. 2A), also known as norcoclaurine in the biosynthesis literature, is a benzyltetrahydroisoquinoline alkaloid with β-adrenoreceptor agonist activity. The activation of the receptor might be because of the structural similarity of the well-known catecholamines, epinephrine (Fig. 2B) and norepinephrine (Fig. 2C), which are the β-adrenoreceptor activators. The attachments of the piperidine ring-linked *p*-hydroxybenzyl group to the catechol ring make the structure of HM stand out from the classical catecholamines.

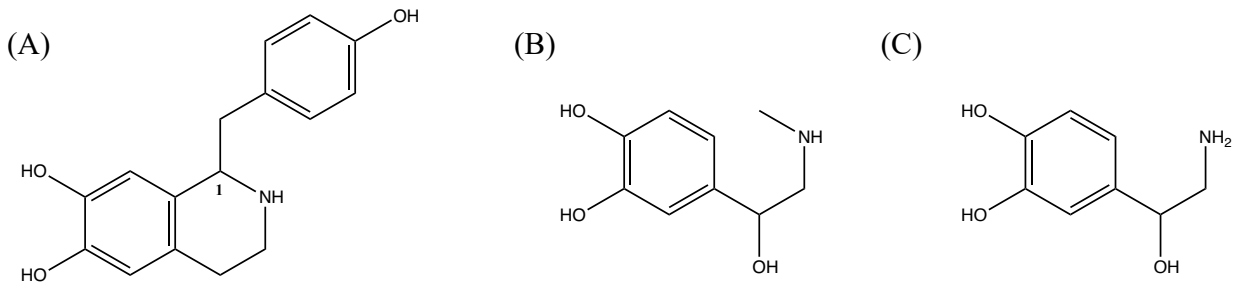

Figure 2 Chemical structure of (A) higenamine, (B) epinephrine, and (C) norepinephrine

Chiral carbon is present in the HM structure (C-1; Fig. 2A). Thus, the HM was present in nature in two optical isomer: (*S*)-HM and (*R*)-HM. As the precursor, the S-configuration is essential for the production of benzylisoquinoline alkaloids in plants [11]. The HM is produced in the plant as a result of the Pictet–Spengler condensation (Fig. 3) of L-dopamine and 4-hydroxyphenylacetaldehyde (4-HPAA) catalyzed using norcoclaurine synthase (NCS) [12, 13]. The enzyme's stereoselectivity leads to *S*-configuration condensation of the HM [12, 13]. However, HM was also isolated in racemic [14] and *R*-form [15] in many plants.

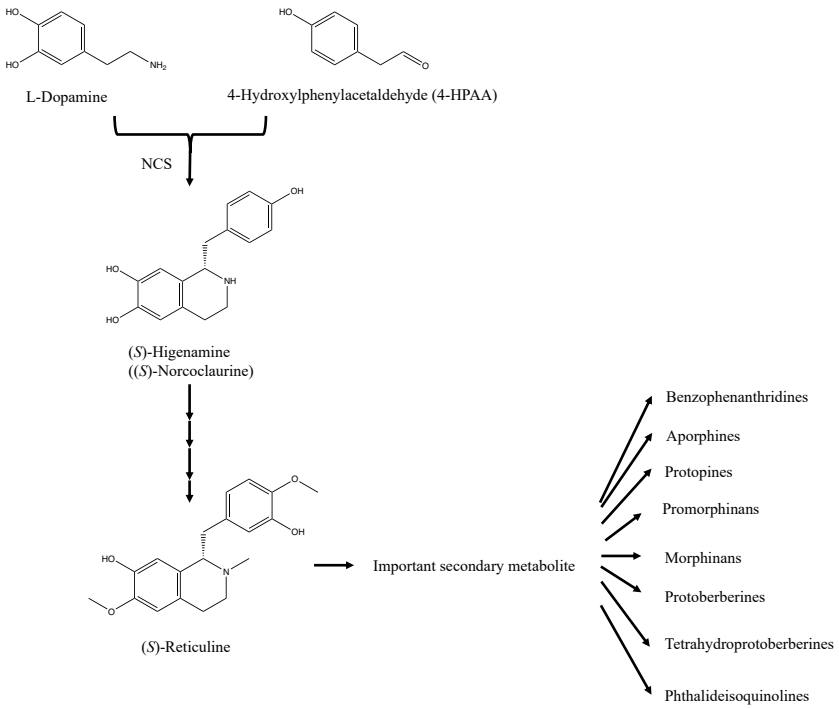

Figure 3 Involvement of (*S*)-HM for plant secondary metabolites production

(*S*)-HM has been shown to be a more potent antiplatelet agent than its counterparts in terms of pharmacological activity [16]. Additionally, it has been reported that (*S*)-HM might be more advantageous than *R* and the racemic form in diseases associated with iNOS overexpression, such as septic shock [17]. Since HM was first isolated and identified in 1976 as a cardiac stimulant, Aconite (*Aconitum carmichaelii* Debeaux) is a well-known source of HM [14]. Then, it was discovered that HM has been extracted from several medicinal plants, including *Nelumbo nucifera* Gaertn. [15], *Nandina domestica* Thunb. [18], *Tinospora crispa* Hook. f. & Thomson [19], *Asarum siebodii* Miq. [18], *Evodia reutaecarpa* (Juss.) Benth. [20], *Sinomenium acutum* (Thunb.) Rehder & E.H. Wilson [21], and *Gnetum parvifolium* (Warb.) W.C. Cheng [22]. Traditional medical preparations, such as Japanese Kampo medicine, Traditional Chinese medicine, and Thai traditional medicine, may also include HM because HM is present in certain medicinal plants. HM is a molecule with wide-ranging pharmacological actions, including analgesic [23], antioxidative [22, 24], and anti-inflammatory properties (interleukin-1 suppression) [25]. However, adrenergic receptor-related actions were usually emphasized as the most important pharmacological impact. Several investigations have demonstrated that the agonistic activities of β_1 and β_2 adrenergic receptors on HM result in positive inotropic and chronotropic effects [26]. Additionally, it has a hypotensive effect, which may be a result of α1-adrenergic receptors' antagonistic effect [27]. HM was widely used as a dietary supplement since it was believed to have anabolic and lipolytic properties in addition to being a β-adrenoreceptor agonist [11].

Although HM is abundant in medicinal plants and has several favorable pharmacological benefits, it is inappropriate for athletes. Since 2017, the World Anti-Doping Agency (WADA) has listed HM in the category of S3, β_2-agonists on its list of banned substances [28]. Athletes should avoid the unintended use of medicinal plants containing measurable levels of HM. Adverse analytical findings (AAF) will be produced from the athlete sample when the urinary HM concentration exceeds 10 ng/mL [11]. HM-positive plants must be screened using trustworthy analytical procedures to prevent athletes from unintended usage of HM from these medicinal herbs.

1.2 Berberine

Berberine (BBR; 16,17-dimethoxy-5,7-dioxa-13-azoniapentacyclo [11.8.0.02,10.04,8. 015,20] henicosa-1(13),2,4(8),9,14,16,18,20-octaene; Fig. 4) is a benzylisoquinoline alkaloid

containing quaternary ammonium. The BBR is distinguished by its yellow color, which may be attributed to the structure's conjugated *pi*-bonds. BBR was reportedly isolated from a number of medicinal plants, including *Berberis aristata* DC. [29], *Coptis chinensis* Franch. [30], *Coptis japonica* (Thunb.) Makino [31], *Hydrastis canadensis* L. [32], *Xanthorhiza simplicissima* Marshall [33], and *Phellodendron amurense* Rupr. [34]. Several traditional therapeutic formulations contain these medicinal plants. BBR is present in two important crude drugs used in Japanese Kampo medicine: Coptis rhizome [35] (*Coptis japonica*, *Coptis chinensis*, *Coptis deltoidea*, C. Y. Cheng et Hsiao, or *Coptis teeta* Wallich) and Phellodendron bark [36] (*Phellodendron amurense* or *Phellodendron chinense* Schneider). These herbs served as the foundation for over 10 Kampo medicinal formulations. It has been shown that the BBR has various pharmacological effects, particularly in relation to metabolic syndromes [37], which are the most prevalent health issues in an aging population. Additionally, BBR was found to have antioxidative [38], antitumor [39], and antibacterial properties [40]. According to a recent study, BBR may be administered in conjunction with probiotics to enhance the hypolipidemic effect on postprandial lipidemia [41]. Although BBR has a variety of intriguing pharmacological activities, it is important not to neglect its negative effects. Long-term exposure to BBR may induce gastrointestinal distress [42] and raise the incidence of jaundice [42]. Reliable and time-saving methods for BBR detection are required for a balanced BBR intake.

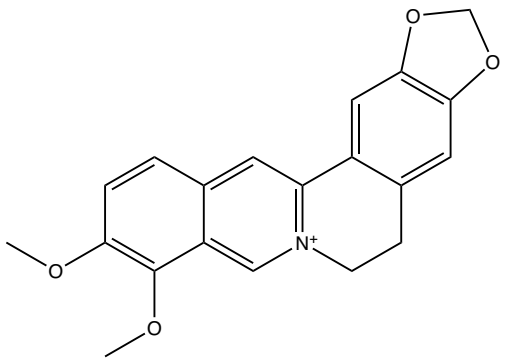

Figure 4 Structure of BBR

2. Biochemical assays development

Various analytical methods have been established for the detection or determination of the analytes of interest. Among them, biological assays are one of the major groups of assays generally used for quantifying the metabolic reaction, cellular process, and binding activity of the

biomolecules. The biochemical assay could be developed to aid the target characterization to clarify the function of the biomolecular unit, such as immunoglobulin, enzymes, RNA, and DNA. Some researchers used the biomolecular unit to develop the analytical method for tracking molecules that might interact with biomolecular units.

2.1 Immunoassays

Immunoassays are biochemical assays designed to detect and/or quantify an analyte based on the immunological interaction between an antigen (as the analyte) and an antibody (as a detection element). The immunoassays were created based on the Berson and Yalow's (1960) discovery that the half-life of their synthesized radioiodinated insulin was longer in adults with insulin-dependent diabetes than in healthy patients [43]. The anti-insulin antibody was attached to the produced insulin as a consequence of this occurrence, resulting in a prolonged duration of their clearance. The number of the insulin molecules bound to an antibody was followed by the equilibrium constants of the binding reaction, which were derived from the law of mass action. Ultimately, the immunoassay could be developed by labeling either the antigen or the antibody. The quantity of the antigen or antibody could be read from the known labeled signal. Therefore, there are various types of labels, such as radioactive compounds, fluorophores, nanoparticles, and enzymes. Each label has its own pros and cons depending on the situation and proposed immunoassay. Until now, the immunoassays have been extremely important in various bioanalytical settings, including clinical diagnostics, biopharmaceutical analysis, environmental monitoring, security, forensic science, and food testing.

Several businesses, such as medicines, cosmetics, and food, rely heavily on secondary metabolites from plants. The majority of beneficial secondary metabolites are produced as small-molecule organic compounds (MW < 900 Da) with a structural deviation. Immunoassays often examine relatively macromolecules that may stimulate the animal immune system. Therefore, proteins are the preferred analytes for this technique. However, small molecules' protein attachment enabled their immunosensitization and generation of antibodies against them. Small molecules, including plant secondary metabolites, were initially examined using immunoassay. Immunoassay frequently uses a protein-bondable microplate, membrane, paper, or another platform. However, owing to multiple washing steps, it is challenging to immobilize small molecules on the platform. Therefore, the immunoassay for small molecules is mostly a

competitive method. The small molecule was conjugated with a protein carrier to provide it the platform binding property. Through competitive binding, the antibody was attached to both the free antigen in the sample and the antigen on the carrier. The greater the concentration of free antigen introduced into the system, the lesser the number of antibodies on the immobilized platform. Various secondary metabolites, including alkaloids, flavonoids, chromenes, and secoiiridoid glycosides, are currently being investigated for either measuring them as the active molecules or as the toxins in the sample [44, 45].

2.1.1 Enzyme-linked immunoassay

Enzyme-linked immunoassay (ELISA) was a test that used enzyme-conjugated antibodies/antigens to develop an analytical technique. A protein-bondable plastic microplate is typically used for the experiment. For macromolecules, the analyte or sample may be directly coated on the plate; however, for small molecule detection assays, proteins coupled with small molecules were used. The system was then reintroduced with the antibody to detect the analytes. The signal obtained from the enzyme substrate, where the enzyme was often coupled to the antibody molecule, served as a representation of the reaction between the antibody and antigen. There were many types of ELISA, including direct ELISA, indirect ELISA (iELISA), direct competitive ELISA, and indirect competitive ELISA (icELISA). However, the majority of the assays discussed in this thesis were iELISA and icELISA. These tests shared several protocol steps, including coating, blocking, addition of primary antibody, addition of secondary antibody, and enzyme-based signal development. Every stage was followed by a washing procedure to ensure that any surplus molecules were eliminated. Typically, the concentration of an analyte is calculated by determining the relationship between the signal produced from a known concentration of a standard analyte and concentration of the analyte of interest, also known as the standard curve.

2.1.2 Lateral flow immunoassay

Lateral flow immunoassay (LFA), also known as the immunochromatographic strip test, was an antibody-based assay, in which the reaction was conducted on a membrane rather than a microplate. The whole device was streamlined to be portable, have a quick analysis time, and be user-friendly. As a result, the assay gained popularity as a point-of-care device. The LFA has been

used for qualitative, semiquantitative, and quantitative investigations of several substances, including small molecules. Small compounds were used in the immunoassay's competitive basis. The antibody and antigen reactions took place competitively in the test zone, where the small molecule-protein conjugate was accumulated. The color of a nanoparticle–antibody conjugate was typically used to determine the signal. Thus, the color was easily observed without the need of additional equipment.

2.2 Antibody and monoclonal antibody

Antibody, or immunoglobulin, is a protein that reacts to foreign substances (antigens). The antibody was composed of two pairs of polypeptide chains that formed a y-shaped structure. The stem of this y-shaped protein, which extends to the inner arm, consists of two identical heavy chains, but the outermost portion of each arm comprises light chains. The stem and base of the arms' portions are identical in many antibodies. Therefore, they are known as constant regions. These y-shaped arms' tips are the parts that bind antigens. The unique arrangement of amino acids per antigen was noticed in this location. Consequently, it was known as the variable region. The role of the antibody was to capture the antigen via its recognition property and facilitate the antigen elimination from the body. The molecule that differs from the host was recognized as an antigen when it was introduced into the host body. B lymphocytes bound to antigen could mature and secrete antigen-specific antibodies into the bloodstream. Each antibody might be able to recognize the antigen in different parts. Thus, it is possible to obtain different antibodies for an antigen that generally originates from different clones of B cells. The total antibodies per antigen could be called polyclonal antibodies (PAb). The advantages of antigen recognition were used for diagnostic purposes where the antibody served as the detection element and the antigen served as the analyte.

Typically, PAb is derived from animal serum. Therefore, it was impossible to regulate the consistency of these antibodies from batch to batch. Moreover, the increased cross-reactivity of PAbs is due to their multiple recognition sites. The monoclonal antibody (MAb) was developed to address the aforementioned issues. Typically, MAb is derived from an immortalized cell line that generates an antibody with identical characteristics. Splenocytes from an immunized animal are often fused with myelomas to produce the cell line. Screening was performed to acquire homogenous cells in the culture. The obtained cells called hybridoma can be preserved for long-

term MAb synthesis. Due to their single characteristic and single epitope recognition, cross-reactivity was believed to be minute compared to that of PAb [44].

2.3 Aptamer

DNA is well known as the macromolecule primarily responsible for storing genetic information in an organism. Different nucleotide sequences make up the DNA strand. The double helix structure of DNA is created when it is kept with its complementary strand. The DNA strand may take on a three-dimensional form depending on its sequence. These three-dimensional structures can form noncovalent bonds with other molecules. This binding characteristic of DNA is used as a biosensing molecule called an aptamer. When a single-stranded, synthetic oligonucleotide (DNA or RNA) can accurately connect to the target molecule, it is referred to as an aptamer. The most popular *in vitro* selection method for producing aptamers is systematic evolution of ligands by exponential enrichment (SELEX). Several forms of SELEX are available now. SELEX, conversely, shared the same three primary processes: selection, partitioning, and amplification. Generally, the aptamer is chosen from a pool of random DNA, which is created with a random region flanked by two known primer binding sequences. The size of random library is determined by the purpose, cost, and diversity. The advantage of adopting an aptamer as the detection molecule is the shorter selection and production time (a few months) of the aptamer compared to an antibody. Additionally, the target size of aptamer is as tiny as 60 Da. Moreover, its production cost and stability are considerably superior to those of an antibody. The aptamer stock can be stored digitally; however, the antibody requires equipment to retain the valuable hybridomas for sustained antibody production. Therefore, the aptamer could be a good replacement for the antibody as a detection molecule.

The aptamer has been used for macromolecule detection, especially protein analytes. This might be because the differences between the size of the protein and aptamer enable the ease of selection. Moreover, the protein is easier to partition because its molecule can bind to various support materials. The aptamer-based assay was recently used to identify small compounds [46]. There were two main methods: First, the small molecule was bound to the small molecule binder support. The aptamer, which could bind to the small molecule, would be further eluted. Second, the library was attached to the support materials, which were later eluted with the target molecule.

The aptamer used for the detection of the plant secondary metabolite was still lacking, although aptamers for small molecules had received greater attention.

Aptamer-based assays, in contrast to immunoassays, cannot be easily classified. The aptamer could be studied in different manners. The changes in fluorescence of the target molecule could be one of them. The differences in fluorescence in terms of excitation and emission wavelength shift or the intensities of the emission signal could be used as observing parameters. Additionally, there is a technique called the gold nanoparticle protective assay that is based on the competition between the weak bonds between the aptamer's supporting material and target compound. Circular dichroism spectroscopy, nuclear magnetic resonance (NMR) spectroscopy, and isothermal titration calorimetry could all be used to observe the binding of an aptamer and a target molecule. This increases the potential use of using aptamers for various analytes and matrices.

This study aimed to investigate the following topics:

- Anti (*S*)-HM monoclonal antibody production and development of icELISA for (*S*)-HM detection in plant samples
- Development of LFA for rapid (*S*)-HM detection in plant samples
- Selection, characterization, and application of the aptamer for berberine detection method

CHAPTER II

Anti (*S*)-HM Monoclonal Antibody Production and Development of icELISA for (*S*)-HM Detection in Plant Samples

1. Introduction

HM, also known as norcoclaurine and *dl*-demethylcoclaurine, is an intermediate in the biosynthesis of benzylisoquinoline alkaloids. HM is found in several important medicinal plants that are used in traditional medicine, including aconite roots (*Aconitum carmichaelii* Debeaux) [14], *Nandina domestica* Thunb. [18], *Tinospora crispa* Hook. f. & Thomson [19], *Sinomenium acutum* (Thunb.) Rehder & E.H. Wilson [21], and *Gnetum parvifolium* (Warb.) W.C. Cheng [22]. Additionally, several plants, which make up the majority of diets, contain HM. Given the existence of a chiral center in the structure, there are two forms of HM [(*S*)-HM and (*R*)-HM]. The (*S*)-HM is expected to be present in plants owing to the stereoselective nature of norcoclaurine synthase [12, 13]. The production of various benzylisoquinoline alkaloids depends on the (*S*)-HM conformation. However, racemic [14] and *R*-form [15] HM were also detected in plant-isolated samples. The beta-adrenergic receptor is the primary receptor to which HM binds in humans because of its structural similarity to catecholamines. Additionally, several pharmacological properties of HM have been identified, including analgesic [23], antioxidative [24, 47], and anti-inflammatory activities [25]. Because of these pharmacological effects, the first phase of a clinical trial study was conducted to examine the potential use of HM as a medicinal molecule [22]. Despite its potential as a medicinal agent, WADA has classified HM as a class S3, β_2-agonists prohibited drug [28]. As doping substances, HM enhances athletic performance by boosting heart rate and air inhalation volume. WADA's standard for an adverse analytical finding is 10 ng/mL in urine. With this low AAF, athletes must be very cautious about the medications and foods they consume to avoid unintentionally consuming products containing HM.

Several methods for HM detection in plants and other matrices have been developed as a result of the aforementioned issue, including HPLC with various kinds of detectors [48], UHPLC–MS/MS [18], and gas chromatography–mass spectrometry (GC–MS) coupled with derivatization [49]. However, due to the specialized equipment required, these analytical approaches are inapplicable for particular laboratory settings. Moreover, these procedures require a lot of steps for sample handling and large consumption of organic solvent. Low-throughput analytical

techniques that were time-consuming and labor-intensive were another drawback of the approaches.

This chapter describes the production, characterization, and use of MAb against HM for the development of icELISA. To create the specific antibody, HM was conjugated with bovine serum albumin (BSA) as an immunogen (Fig. 5). Then, a sustainable source of antibody production was created using hybridoma technology. The chosen MAb was characterized, including its cross-reactivity and reactivity against immobilized HM and free HM. Validation of the icELISA verified the reliability of the test. With this method, a sensitive assay for the detection of (*S*)-HM was developed. These methods could be used as supporting analytical methods for HM-including plants or further product screening.

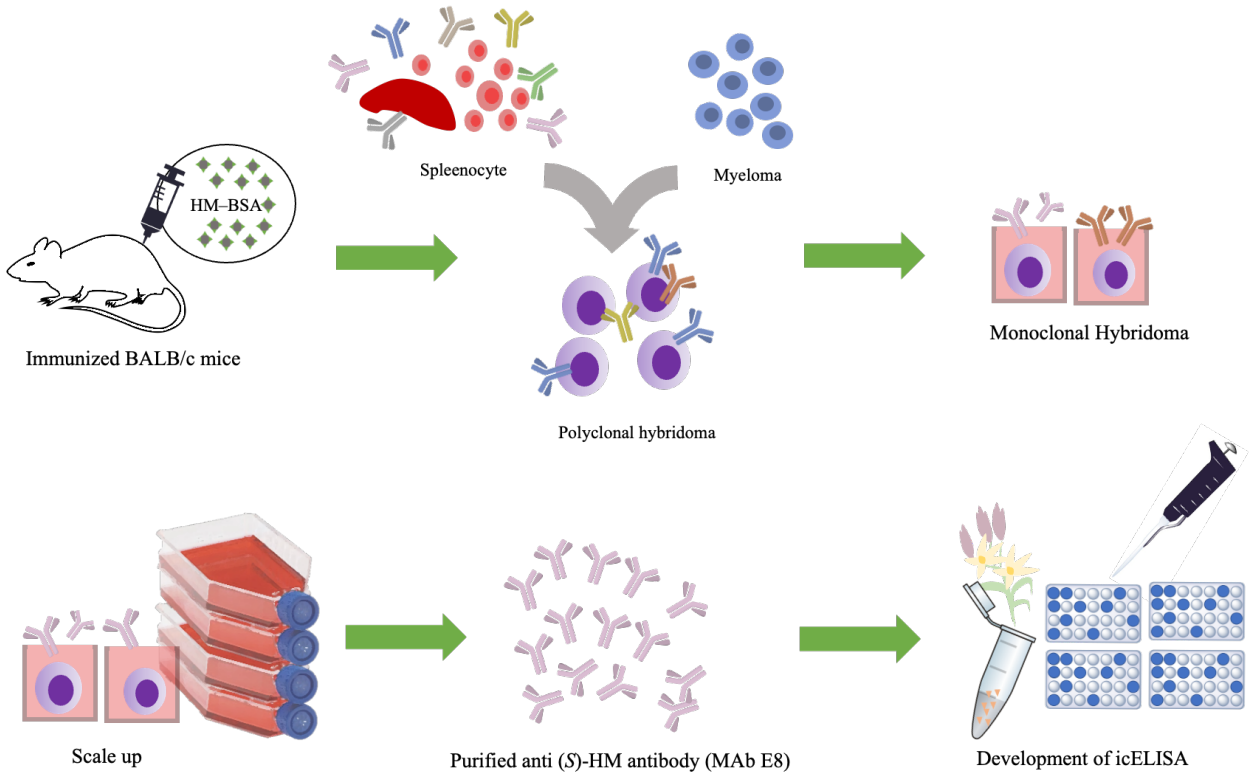

Figure 5 Production of MAb against HM and its application

2. Material and methods

2.1. Experimental materials and reagents

Benzylisoquinoline alkaloids (≥90% purity) and other cross-reacted compound candidates (≥ 90% purity) were purchased from different compound manufacturers. Higenamine HBr (98%) and (*S*)-higenamine HBr (98%) were provided by Toronto Research Chemicals (Toronto, Canada). BSA (97%), albumin from chicken egg white (OVA; 98%), and *N,N′*-Carbonyldiimidazole (CDI) were provided from Sigma-Aldrich (MO, USA) in this experiment. For immunization emulsion forming, Freund's complete and incomplete adjuvants (FCA and FIA, respectively) were obtained from Difco Laboratories (MI, USA). Polyethylene glycol (PEG; Hybri-max) for cell fusion was obtained from Sigma-Aldrich (MO, USA). Fetal bovine serum (FBS; Gibco Invitrogen, MA, USA), enriched RPMI1640-Dulbecco's Ham's F12 (e-RDF; Kyokuto Pharmaceutical Industrial Co., Tokyo, Japan), and RD-1 additives (Kyokuto Pharmaceutical Industrial Co., Tokyo, Japan) were used as the main components of the hybridoma media. To establish the ELISA, the hybridomas screening secondary antibody, goat anti-mouse IgG H&L (HRP) (ab6789), and icELISA secondary antibody, goat anti-mouse IgG1 (HRP) (ab97240), were purchased from Abcam (Cambridge, UK). Other nonmentioned reagents were either analytical HPLC or reagent grade and were obtained from appropriate commercially available sources.

2.2 Plant samples and products containing *Nandina domestica* Thunb. preparation

To better understand the performance of icELISA, well-known HM-containing plants were used as samples for HM analysis using icELISA and HPLC–UV. Uchida Wakanyaku Co., Ltd. (Tokyo, Japan) supplied seven samples of medicinal plants. Additionally, brown sugar-flavored and honey-plum flavored Tokiwa Nanten Nodo Ame (Kobe, Japan; 22 tablets per pouch) were used as a source of *Nandina domestica* Thunb. Three distinct kinds of Aconite root samples (Bushi, Shuchi-Bushi, and Houbushi) were used for the experiment. The plant fragments were ground into powder and passed through a 300 μm mesh sieve to increase particle size homogeneity. The sieved powder (50 g) was macerated in methanol (MeOH; 300 mL) overnight at 25°C . The MeOH extract was concentrated using an evaporator. The resultant MeOH extract (10 mL) was reconstituted with MeOH (10 mL). The resulting extract was centrifuged and filtered through a 0.22 μm filter before being used. The dry weight of the remaining plant samples, which included *Nandina domestica* Thunb. (fruit and leaf), *Asarum siebodii* Miq. (root), and *Evodia reutaecarpa* (Juss.) Benth. (fruit),

was 30 g. The procedure for preparing samples was the same as that used for preparing aconite root samples.

Nandina domestica Thunb. (candy)-containing products were dissolved in 5% MeOH (2 mL) and then filtered through a 0.22 μm filter. Using HPLC–UV and icELISA, the (*S*)-HM concentration in the samples was measured.

The studies were conducted with greater caution due to the well-known presence of strong toxins in aconite roots. The chosen samples were detoxicated and processed aconite roots. Additionally, gloves, safety goggles, and masks were used when aconite root samples were utilized in tests.

2.3 Synthesis of immunogen (HM–BSA conjugates) and coating antigen for ELISA (HM–OVA conjugates)

Like other small molecules, the mouse immune system did not detect free HM as an immunogen. Additionally, it can be difficult to immobilize the free HM on the immunoplate. Therefore, carrier proteins (i.e., BSA and OVA) were used to facilitate immunization and ELISA preparation. Typically, small molecules can bind to other molecules by a chemical modification of the reactive functional group. Three hydroxy functional groups can be found on the HM molecule. As shown in Figure 6, the CDI-mediated conjugation method was adopted for the synthesis of conjugates. Between the small molecule and the carrier protein, CDI often contributes no more carbon. Therefore, the carbamate bond between the active hydroxyl of the small molecule and the carrier protein's amino group served as the connecting moiety. To activate the functional group of HM, HM (3.28 mg) and CDI (3.19 mg) were dissolved in dimethyl formamide anhydrous (DMF; 0.6 mL) and agitated at 30°C for 3 h. The BSA solution (6.02 mg of BSA in 2.4 mL of distilled water) was continuously agitated as the activated HM solution was added drop by drop. The coupling process was conducted at 30°C and in the dark for one night. The reaction mixture was then dialyzed against distilled water at 4°C for four days with a 6-h interval to eliminate extraneous molecules (i.e., nonreacted CDI, free activated HM, and any small molecular weight byproducts). Through lyophilization, the dialysate was powdered to produce HM–BSA conjugates (5.04 mg). HM–OVA conjugates were synthesized for the ELISA coating antigen using the same procedure as HM–BSA conjugates. However, the weights of HM (2.51 mg), CDI (2.60 mg), and OVA (5.14 mg) were different from those of their equivalents. The yield of the HM–OVA

conjugates was thus 4.86 mg. The conjugates were inherently resistant to water solubility. All conjugates were diluted in 50 mM Tris-HCl (pH 8.0) containing 8 M urea and then were used immediately for immunization or stored at −20°C until ELISA usage.

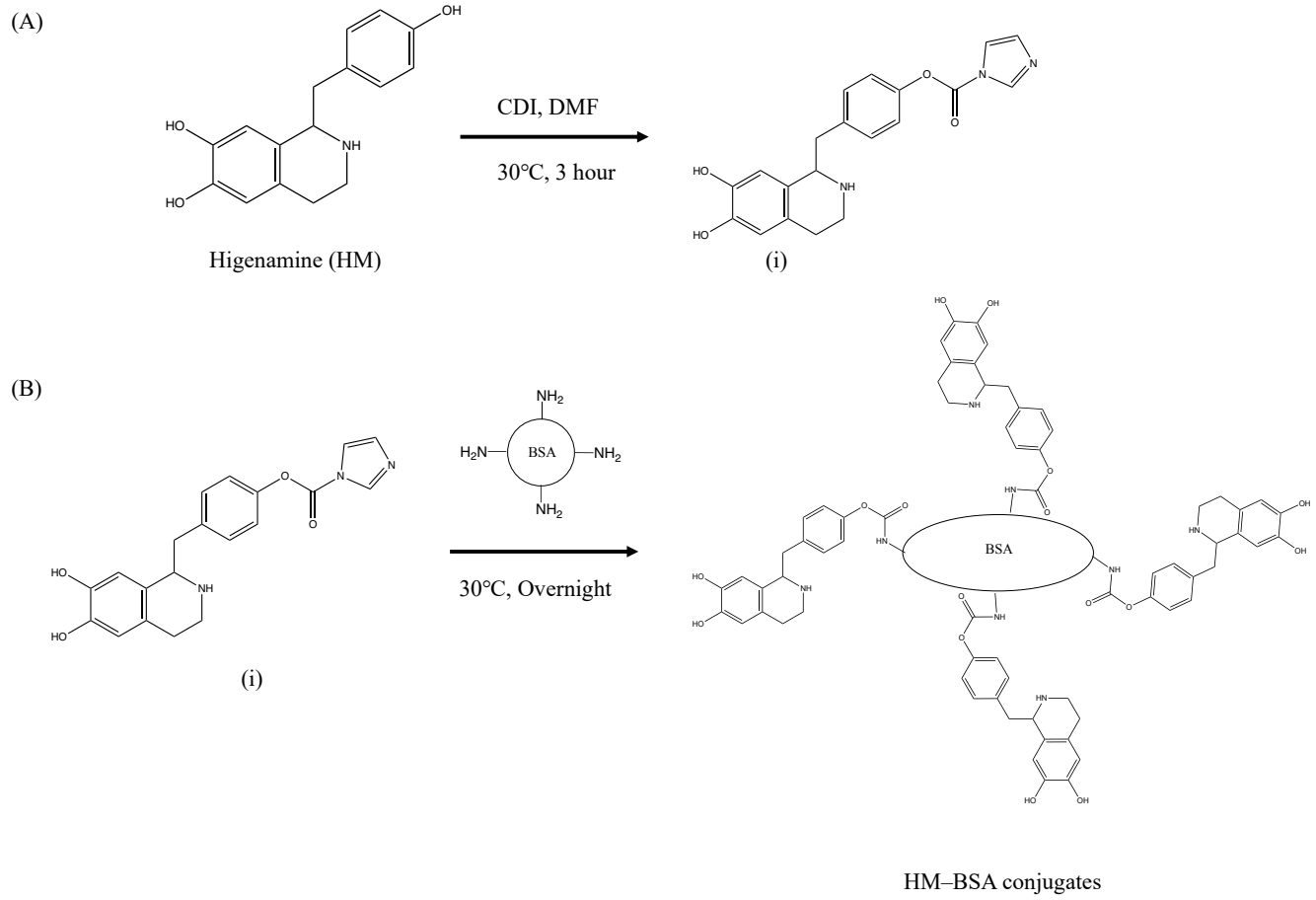

Figure 6 Proposed synthetic reaction of HM–BSA conjugates. (A) The reaction between HM and CDI is expected to form the reactive intermediate (i). (B) The reactive intermediate (i) can be reacted with amine groups of BSA yielding HM–BSA conjugates

The hapten number, also known as the number of bound HM molecules per carrier protein, was measured using matrix-assisted laser desorption/ionization time-of-flight mass spectrometry (MALDI–TOF–MS; Bruker Autoflex III, Bruker Daltonics) with an optimized technique. Comparative dilutions of HM–BSA conjugates and BSA (2.5–20 mg/mL) were generated when BSA was used as a protein carrier. The matrix solution was saturated with sinapinic acid in 0.15% (v/v) trifluoroacetic acid in HPLC-grade water and acetonitrile in a 2:1 ratio. Finally, the matrix solution was used as a diluent for the obtained protein sample to produce a 10-fold dilution of each protein concentration. The sample was applied and allowed to dry on the MTP 384 ground steel target plate (Bruker Daltonics). The nitrogen laser used for analysis had a maximum firing rate of 337 nm at 200 Hz. The data were processed using software (Bruker Daltonics). The OVA carrier protein underwent a similar procedure. In contrast, HM–OVA conjugates and OVA were used in place of protein samples.

2.4 Animal immunization

After obtaining approval from the animal experiment ethics committee at Kyushu University (approval no. A30-003-3), the animal experiment was conducted under the animal experimental guidance from the Graduate School of Pharmaceutical Sciences, Kyushu University. Five-week-old male BALB/c mice (KBT Oriental Co., Ltd., Saga, Japan) were housed with freely accessible food (MF; Oriental Yeast Co.) and water. The immunization started when HM–BSA conjugates, which were emulsified with FCA (50 μg), were intraperitoneally administered to the subject mice. To enhance the immune response, HM–BSA conjugates emulsified with FIA (50 μg) were used in the second immunization. Then, the following doses until the fifth dose were administered using HM–BSA conjugates (100 μg) in phosphate-buffered saline (PBS). The immunizations were done every 2 weeks. The mouse antibody titer and reactivity of the serum-derived polyclonal antibody against free HM were monitored using iELISA and icELISA.

2.5. Somatic hybridization for generation of anti (*S*)-HM antibody-producing hybridomas

The process of hybridoma production is described in Figure 7. Because splenocytes lack the ability to proliferate, the cells were fused with mouse myeloma to obtain it. Splenocytes were harvested from the spleen of the immunized mouse when the antibody titers of the mice reached the desired level. The nonimmunoglobulin-producing mouse myelomas, SP2/0, were chosen as

hybridizing partners. To maximize cell-to-cell contact, the splenocytes and SP2/0 cells were combined, and the supernatant was removed. Then, polyethylene glycol (PEG) was added to the cell mixture to fuse adjacent splenocytes, resulting in a heterokaryon in which the hybridomas formed naturally. There are three types of cells: nonfusing myeloma cells, nonfusing splenocytes, and hybridomas. Hypoxanthine–aminopterin–thymidine (HAT) medium was used to promote the growth of hybridomas while inhibiting the growth of nontarget cells. The selection medium contains e-RDF, RD-1, and 10% FBS in addition to the HAT reagent. The hybridomas were grown in an incubator with the standard culture atmosphere of 5% carbon dioxide (CO_2) at 37°C. iELISA screening test results were used to select the antibody-producing cells. In this test, only hybridomas producing anti carrier protein antibodies and anti (*S*)-HM antibodies could be distinguished from others. The supernatant of colonies that tested positive with iELISA was evaluated with icELISA to determine the antibody reactivity against (*S*)-HM to further select hybridomas producing only anti (*S*)-HM antibodies. Subsequently, the positive colonies were cloned using a hypoxanthine–thymidine (HT) medium instead of a HAT medium. To ensure the monoclonal nature of the cell lines, they were cloned via limiting dilution. The hybridomas producing highly reactive anti (*S*)-HM antibody (colony E8) were serially expanded into an 800 mL culture. The cells were then grown in a 1,000 mL culture. In this step, however, the serum was removed from the culture medium, resulting in a serum-free medium.

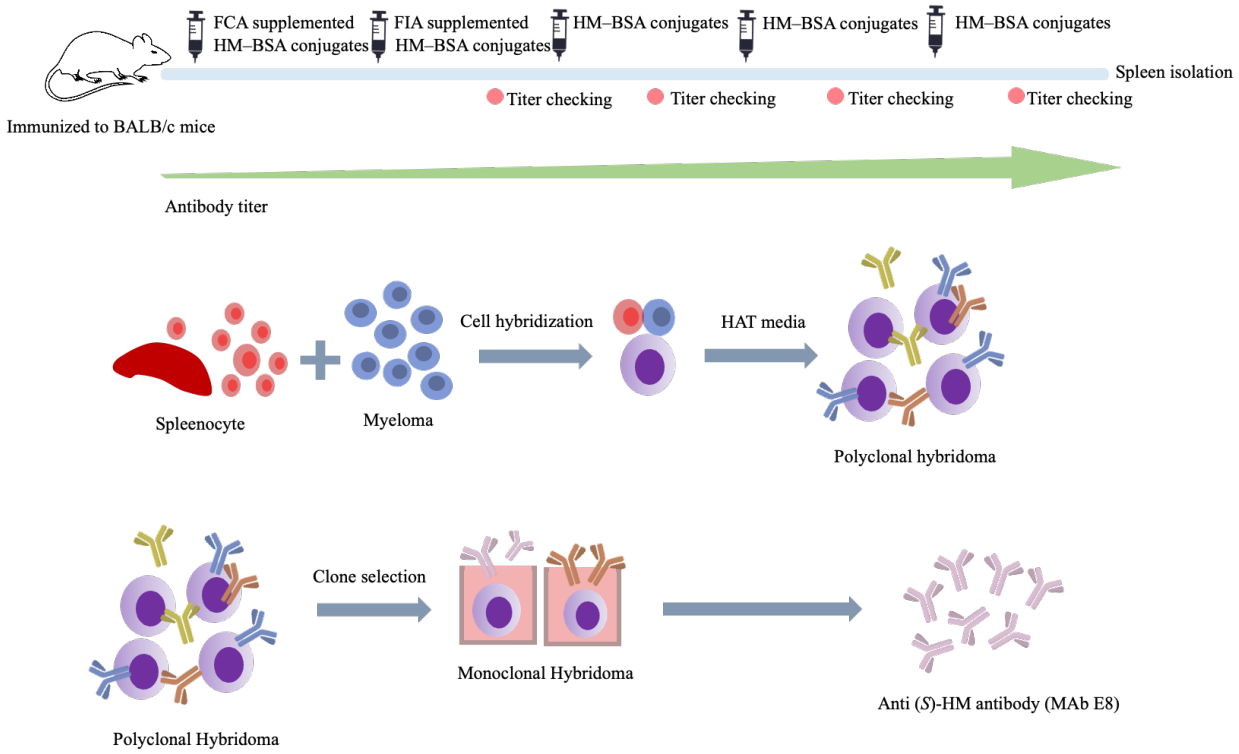

Figure 7 Brief antibody production scheme. The polyclonal antibody against (*S*)-HM was induced to be increased as the dosage was increased. The spleen was taken from the immunized mice yielding the splenocytes, which were later hybridized with SP2/0 cells. The reactive clone was selected among the polyclone to obtain colony E8, which can produce the anti (*S*)-HM antibody, MAb E8.

2.6 Purification of anti (*S*)-HM MAb (MAb E8)

To select the appropriate affinity ligand for the selection of purification resin, it is necessary to identify the isotype of the MAb. The MAb isotype was determined using the supernatant of the positive colonies and using the IsoStrip mouse MAb isotyping kit's standard protocol (Roche Diagnostics GmbH, Mannheim, Germany). It was revealed that MAb E8 was an IgG1 kappa light chain antibody. Thus, a protein G sepharose fast-flow column was chosen as the purification column (GE Healthcare Bioscience AB, Uppsala, Sweden). The purification procedure began with the separation of the supernatant by centrifugation at 6,300 × *g* for 10 min at 4°C. The pH of the medium was adjusted to 7.0 using a 1 M Tris-HCl solution (pH 9.0). The solution was stirred for

10 min in a cold room to ensure that no precipitant formed after pH adjustment. Under reduced pressure, the supernatant was filtered with 0.22 μm filters to remove any unwanted particles or leftover cell debris. The purification column was equilibrated with an excess of 50 mM phosphate buffer (>5 column volumes) (pH 7.0). The filtered culture medium was then passed twice through the purification column. The unbound residues of protein G were washed with an equilibrating buffer (5 column volumes). The elution per fraction was performed using 100 mM citrate buffer (pH 2.7; ~8 mL) through the continuously shaking fraction receiving tube containing 1 M Tris-HCl (pH 9.0; ~3 mL) for immediate neutralization of the MAb to prevent the prolonged exposure of an antibody to extreme pH conditions. The fractions were continuously analyzed using UV spectrometry. The positive fractions (absorbance at 280 nm [OD280] > 0.25) were collected. The positive fractions were pooled and dialyzed against deionized water at 4°C and 6-h intervals for a week to desalt from the MAb E8. The desalted MAb was powdered using lyophilization to obtain the purified MAb E8 (59.3 mg).

2.7. Evaluation of the antibody reactivity against immobilized antigen using iELISA

iELISA is very useful for evaluating the antibody titer in mouse serum, screening for hybridoma-positive colonies, and determining the appropriate concentration of primary antibody for icELISA. The assay derives its name from the signal produced by the secondary antibody rather than the primary antibody, which directly reacts with the target. In this study, the reaction products of the enzyme (horseradish peroxidase [HRP]) that was attached to the secondary antibody molecule demonstrated the bonding between immobilized HM and MAb. The steps involved in the iELISA procedure are depicted in Figure 8. iELISA was conducted on a 96 well immunoplate (Nunc, Maxisorb) coated with HM–OVA conjugates (2 μg/mL) in 50 mM carbonate buffer (pH 9.6, 100 μL/well) and incubated for 1 h at 37°C. To prevent nonspecific antibody binding to the uncoated area, the wells were blocked with a known protein-containing solution, 5% skim milk in PBS (300 μL/well). To allow the antibody–antigen interaction, the primary antibody produced from immunized mouse serum (diluted in PBS with 0.05% (v/v) tween 20; PBS-T), hybridoma supernatant, or MAb (diluted in PBS-T) was applied in equal amounts (50 μL/well) as a 5% solution of MeOH in distilled water (50 μL/well). A plate mixer was used to ensure that these solutions were homogenous. The plate was then incubated for 1 h at 37°C. The antibody capable of reacting with HM–OVA conjugates was reacted with peroxidase-labeled goat anti-mouse IgG

H&L (HRP) (ab6789; 100 µL/well) for titer checking of immunized mouse serum or hybridoma supernatant with peroxidase-labeled goat anti-mouse IgG1 (HRP) (ab97240; 100 µL/well) for MAb E8. Before detection, the plate was incubated at 37°C for 1 h. The detection signal was peroxidase-catalyzed oxidation of 2,2′-azino-bis(3-ethylbenzothiazoline-6-sulfonic acid) (ABTS). The reaction was initiated by the addition of 0.3 mg/mL ABTS diluted in a 100 mM citric acid buffer (pH 4.0) containing 0.003% (v/v) H_2O_2 (ABTS substrate solution; 100 µL/well) to the microplate. The reaction was conducted at 37°C for 20 min. The observable signal in the experiment was the absorbance of the solution in each well at 405 nm. The plate was washed three times with PBS-T to eliminate unreacted unbound residues following the incubation of each step other than the detection step (coating, blocking, addition of primary antibody, and addition of secondary antibody).

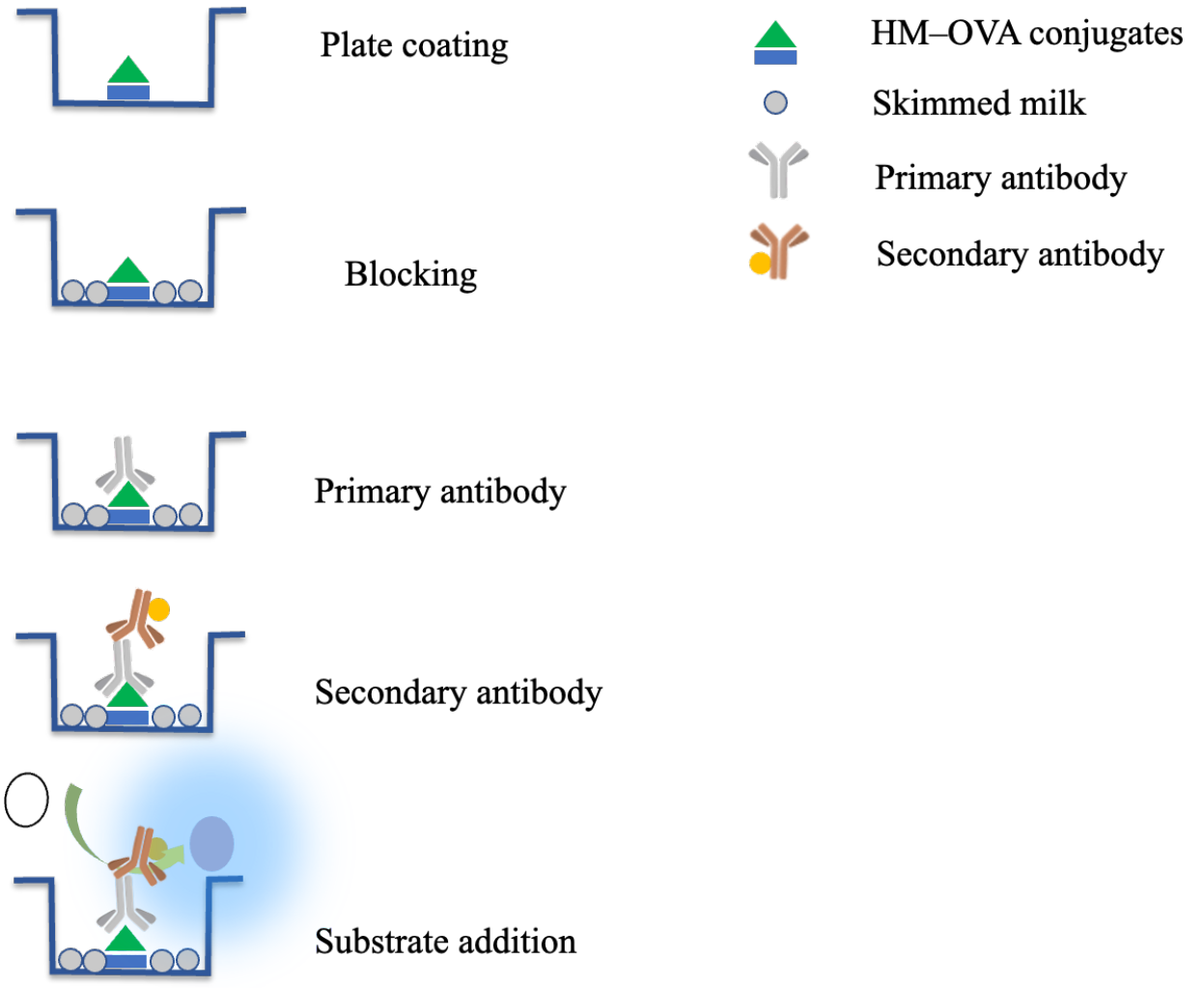

Figure 8 Brief diagram of the iELISA procedure

2.8 Development of icELISA and systemic validation of the assay

The icELISA is the system in which the amount of free (*S*)-HM molecules can be determined. The name was derived from the competition between free (*S*)-HM molecules and bound HM molecules on the microplate to react with the primary antibody. The procedure is depicted in Figure 9. As depicted in Figure 9, the technique was nearly identical to the iELISA with minor modifications. Coating the plate with HM–OVA conjugates (2 µg/mL; 100 µL/well) and incubating it at 37°C for 1 h commenced the assay. The plate was then blocked with 5% skim milk in PBS (300 µL/well) and incubated under conditions identical to plate coating. An antibody produced from immunized mouse serum (diluted in PBS-T) or hybridoma supernatant (50 µL/well) was used as the primary antibody when the reactivity of antibody against free (*S*)-HM was required. In the development of icELISA for the detection of (*S*)-HM in plant samples, the optimal concentration of MAb E8 (in PBS-T) obtained from iELISA (50 µL/well) was utilized. The primary antibody was mixed with the testing samples, that is, (*S*)-HM, cross-reactivity test candidates, plant samples, or plant-containing products, which was prepared in 5% MeOH (50 µL/well). The sample could be diluted to get the desired concentration. The plate was then shaken using a plate mixer. Peroxidase-labeled goat anti-mouse IgG H&L (HRP) (ab6789; 100 µL/well) was used as a secondary antibody for immunized mouse serum or hybridoma supernatant after 1 h of incubation at 37°C. Instead, peroxidase-labeled goat anti-mouse IgG1 (HRP) (ab97240; 100 µL/well) was used as the secondary antibody for MAb E8. The plate was then incubated for 1 h at 37°C. The signal was measured as absorbance at 405 nm following the addition of the ABTS substrate solution (100 µL/well) at 37°C for 20 min. After 1 h of incubation at 37°C for each step, the plates were washed three times using PBS-T.

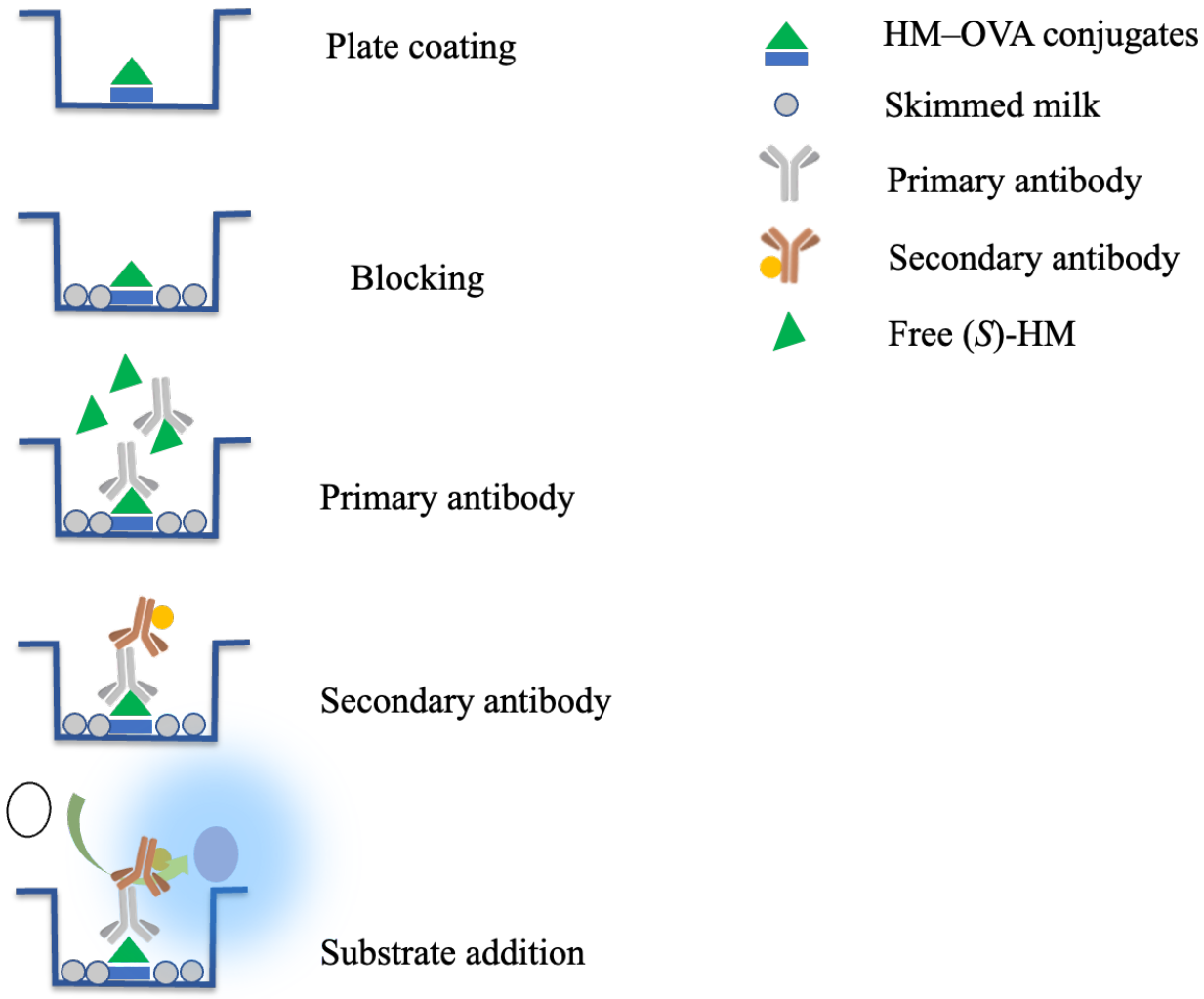

Figure 9 Brief diagram of the icELISA procedure

The ultimate purpose of the assay is to be used as the (*S*)-HM determination tool in complex matrices such as plants and plant-containing products. Thus, various validation methods were applied to ensure the reliability of the assays. The assay was validated only when the MAb E8 was used as the primary antibody.

Various concentrations of (*S*)-HM were used in the primary antibody addition step to evaluate icELISA's sensitivity. The obtained result was shown as a correlation between applied (*S*)-HM concentration and the proportion of the signal (A/A_0) obtained from (*S*)-HM at the concentration of interest (A) and that obtained from control (5% MeOH; A_0). The limit of detection (LOD) was defined as the concentration of (*S*)-HM which could decrease A/A_0 by 10% when compared to the control (5% MeOH). The determination range of the assay was defined by the

concentration range which could provide the linear correlation between applied (*S*)-HM concentration and A/A_0 when the applied (*S*)-HM concentration was plotted on the semilog scale.

Specificity is an important factor when the assay was developed using an antibody as the detection element. It is more challenging to use the antibody as a detecting element when it exhibits strong cross-reactivity with substances other than the target. The plant extracts were the major target sample for the developed assay. There is a possibility that the plant samples contain (*S*)-HM structurally related compounds. Thus, 27 compound candidates (50 μL/well in 5% MeOH) were coincubated with the primary antibody, MAb E8. The comparative binding activity was reported as a percentage of cross-reactivity as described in the following equation:

$$\text{Cross-reaction (CR, \%)} = \frac{\text{IC}_{50} \text{ of } (S)\text{-HM}}{\text{IC}_{50} \text{ of candidate compounds}} \times 100$$

where IC_{50} denotes the concentration of those compounds that caused 50% of A/A_0 reduction from A/A_0 of control (5% MeOH).

Precision of the assay was demonstrated using the coefficient of variation (CV, %). The concentrations in the determination range were used for the precision test. In an individual plate, the variation between wells (n = 3) was evaluated. The results were mentioned as an intraplate assay. Additionally, the variation among various plates (n = 3) was assessed, with three wells from each plate being included in the calculation. The results were mentioned as an interplate assay.

The accuracy of the assay was assessed using a spike-recovery test. The test would measure the ability to determine the known concentration of the (*S*)-HM that was added on top of the plant extract that contained some amount of (*S*)-HM. The gradient of known amount of (*S*)-HM (0.5, 1, 2, and 4 μg) was spiked into the diluted extract of *Aconitum carmichaelii* Debeaux (1.0 mL). icELISA was used to determine the amount of (*S*)-HM of either spike or nonspike samples. The percentage of recovery was reported using the following calculation:

$$\text{Recovery rate (\%)} = \frac{\text{Measured amount of } (S)\text{-HM} - (S)\text{-HM amount in nonspike sample}}{\text{spiked amount of } (S)\text{-HM}} \times 100$$

2.9. HM detection using HPLC–UV

The HPLC–UV was selected as the method for assay reliability comparison. The assay was set based on the method described by Chung et al. [48] with some modifications. The flowrate of the LC-10AD VP HPLC pump (Shimadzu) was set to 1.0 mL/min. The detection wavelength was set at 225 nm on the SPD-10A UV/VIS detector (Shimadzu). The separation condition was reverse-phase chromatography (Cosmosil-packed column 5C18-MS-II, 4.6 mm × 250 mm, 5 μm particle size, Nacalai Tesque). The mixture of 10% (v/v) CH_3CN and 50 mM phosphate buffer containing 0.1% (v/v) trifluoroacetic acid was used as the isocratic mobile phase. The filtered sample was loaded (20 μL) and subjected to the aforementioned conditions for 50 min. The peak of (*S*)-HM standard was detected at the retention time of ~11 min. The HPLC–UV had a detection range of 0.16–5.00 μg/mL and a limit of detection (LOD) of 0.08 μg/mL. The analytical results were obtained from the average of triplicate samples injection.

3. Results and discussion

3.1 Profiling of immunogen and coating antigen through MALDI–TOF–MS

There are various tests for verifying the binding of small molecules to the carrier protein. Physical difference analysis and UV-identification analysis might be classified as the two primary methodologies for the study. For the examination of physical differences, the test was based on the measurement of the molecular mass or molecular size of the conjugates and carrier proteins and the determination of their differences. Sodium dodecyl sulfate–polyacrylamide gel electrophoresis (SDS–PAGE) and MALDI–TOF–MS were the primary techniques used for this strategy. Due to the drawbacks of SDS–PAGE, such as unclear findings of low hapten number of conjugates, difficulty in identifying the actual molecular size, and electrophoresis conditions that are prone to inaccuracy, MALDI–TOF–MS was used to determine the quantity of HM molecules conjugated to the carrier molecule. As demonstrated in Fig. 10, the peak of HM–BSA conjugates, which corresponded to its molecular mass, was determined to be 67,787, whereas that of BSA was determined to be 66,453. The mass differences between the molecular mass of HM–BSA and BSA (1,334) were divided by HM's molecular weight (271.31), yielding four hapten numbers for HM–BSA conjugates. The hapten number for the OVA as the carrier could not be calculated with precision because the peak could not be verified. However, iELISA and icELISA verified the conjugation. Thus, the conjugates produced were eligible for further research.

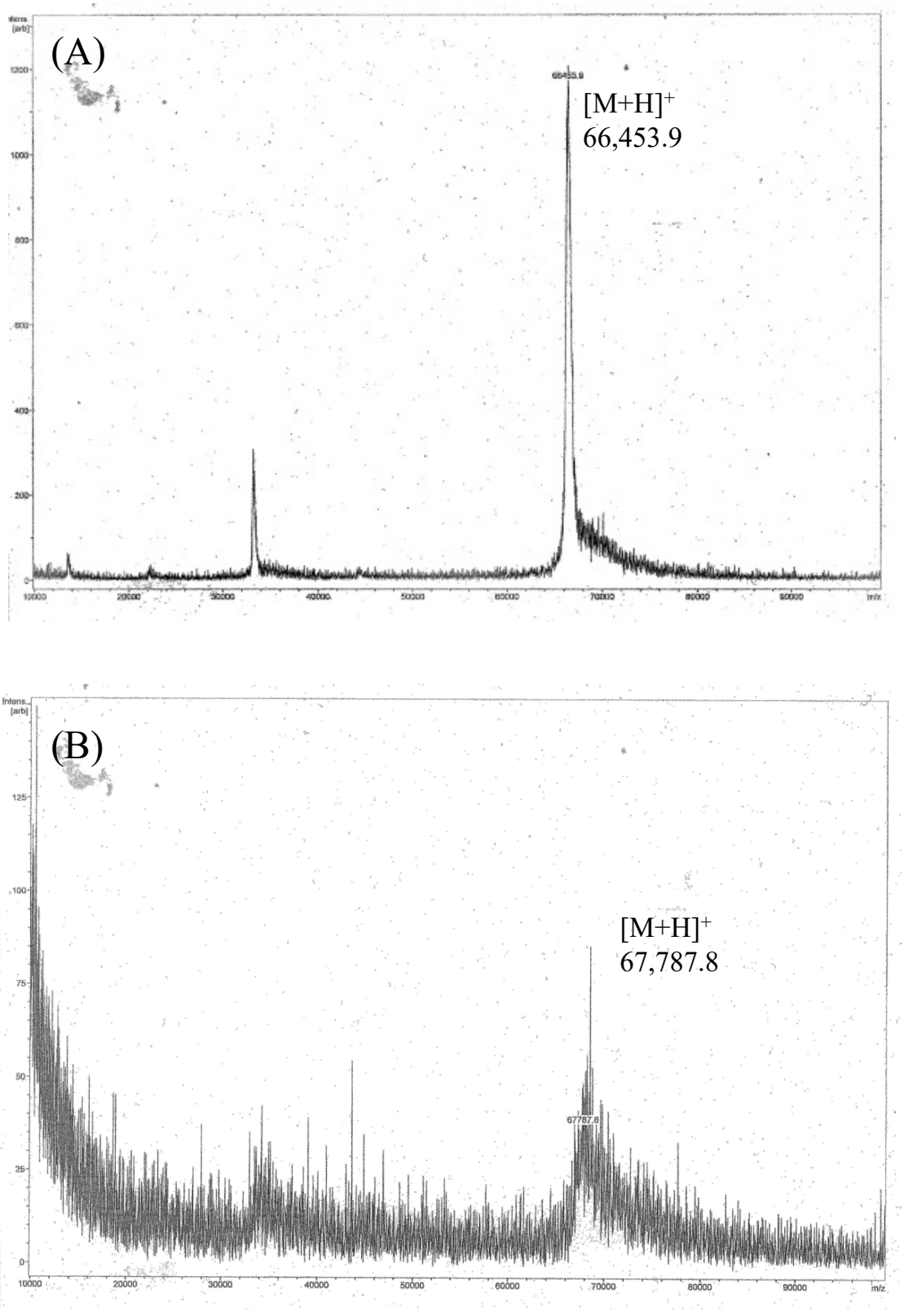

Figure 10 MALDI–TOF–MS spectrum of (A) BSA and (B) HM–BSA conjugates

3.2 Immunization monitoring and antibody production

From the second to the last dosage, the antibody titer and reactivity to (*S*)-HM were measured. The serum taken four days after immunization showed binding activity against both bound HM–OVA conjugates and free (*S*)-HM from the second immunization. Up to the fourth dosage, the antibody titer and reactivity against free (*S*)-HM increased dose by dose. This shows that the immunogen can stimulate the formation of anti (*S*)-HM PAb in mice. The optimal number of haptens for small molecule immunization was found to be between 8 and 25 molecules [50]. Nonetheless, the antibody titer was still seen when the HM–BSA conjugates with an approximate hapten number of 4 were utilized as immunogens. This study might correspond to earlier data revealing antibody production with low hapten number immunization [51–53]. Immunization was administered until the fifth injection to increase the number of splenocytes expressing anti (*S*)-HM antibodies by prolonged exposure to the immunogen. Splenocytes obtained from the immunized spleen were fused with myeloma cells (SP2/0) through PEG-mediated cell fusion. A systematic cloning procedure was used to create colony E8, a hybridoma clone that secretes anti (*S*)-HM antibodies. The expansion of colony E8 was intended to reach 1 L (serum-free medium). IgG1 with a kappa light chain was identified as the isotype of MAb using the Isostrip Mouse Monoclonal Isotyping kit (Roche Diagnostics). Thus, the protein G resin was selected to match the antibody's isotype. Eventually, the colony E8–derived antibody (MAb E8) was generated effectively (59.3 mg).

3.3 Assessment of reactivity of the MAb E8

Using the inherent property of MAb E8 to bind either immobilized or free (*S*)-HM, icELISA was developed. The development of the test began with the selection of the optimal concentration of MAb E8 using iELISA. Various amounts of MAb E8 were reacted with a specific concentration of HM–OVA conjugates (2 μg/mL). Using iELISA, the optimal concentration of MAb E8 was determined. To plot the correlation curve, the correlation between absorbance and antibody concentration on a log scale was plotted (Fig. 11). The absorbance increased with the increase in MAb E8 concentration. As a result, 100 ng/mL was the optimal MAb E8 concentration defined as the concentration that yields an absorbance of roughly 1.0 for further study.

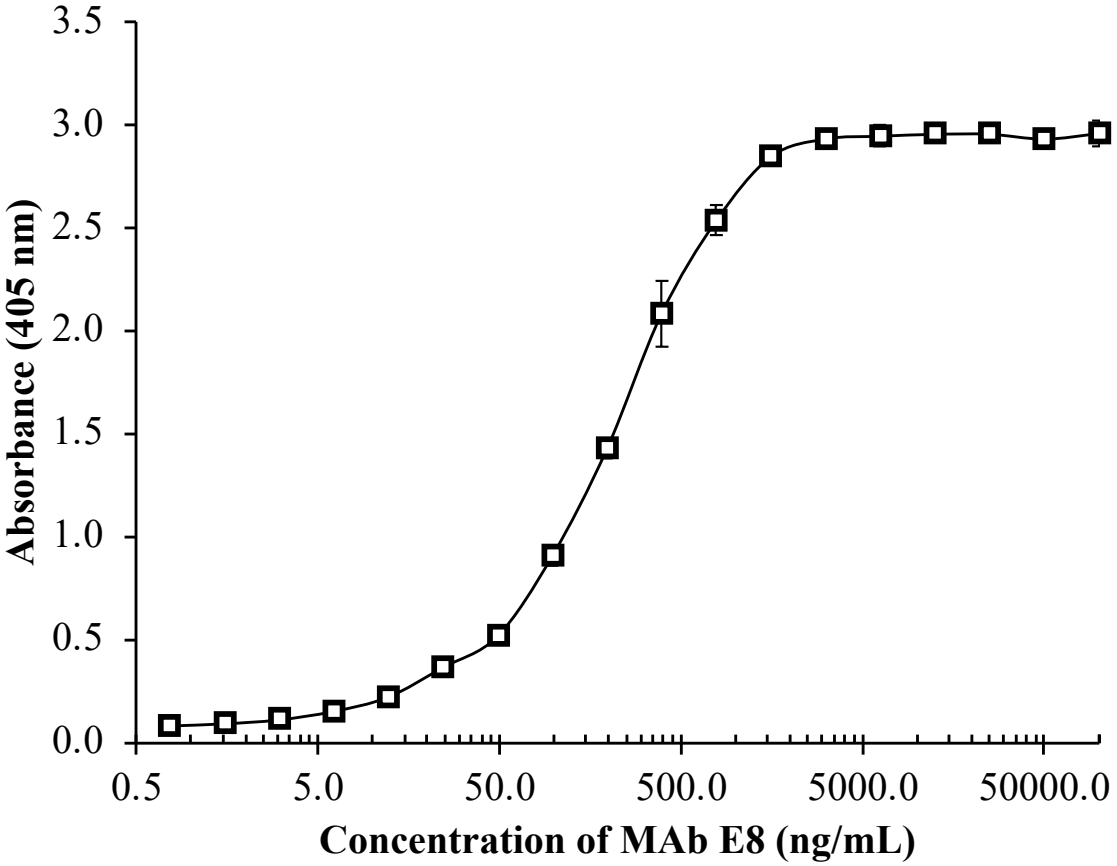

Figure 11 iELISA reaction of MAb E8 against HM–OVA conjugates. As the primary antibody, various concentrations of MAb E8 were serially diluted with PBS-T and applied. The concentration of HM–OVA conjugates was 2 μg/mL

Dopamine and 4-hydroxyphenylacetaldehyde are stereospecifically condensed by the enzyme norcoclaurine synthase (NCS) to produce (*S*)-HM [12, 13]. For the development of icELISA, (*S*)-HM was used as the standard antigen to represent the actual HM concentration in plants. The combination of MAb E8 (100 ng/mL; 50 μL) and (*S*)-HM at varied concentrations were used for making icELISA standard curve. Inverse sigmoid curve revealed the competition between bound HM on HM–OVA conjugates and free (*S*)-HM. The binding of MAb E8 to HM–OVA conjugates induced a decrease in absorbance when the concentration of (*S*)-HM was increased. Based on these results (Fig. 12), a determination curve with a range of 7.81–125 ng/mL, an IC_{50} of 26.1 ng/mL, and a LOD of 4.41 ng/mL was obtained. The developed method demonstrated more sensitivity

than HPLC–UV (0.08 μg/mL; LOD). Therefore, the outcome indicated that the MAb E8 obtained was relatively sensitive. The MAb E8 was an excellent choice for use in a variety of immunoassays to optimize its usefulness. There are numerous detection methods established for HM that are more sensitive than the developed icELISA, such as UHPLC–MS/MS with a LOD of 1 ng/mL [18] and GC–MS combined with derivatization with a LOD of 1.52 ng/mL [49]. However, icELISA has an advantage over these techniques: it is a high-throughput technique that can handle many samples at the same time. Moreover, sophisticated equipment was not required. Although icELISA has a lower sensitivity than these approaches, its sensitivity for (*S*)-HM detection in plant samples was sufficient.

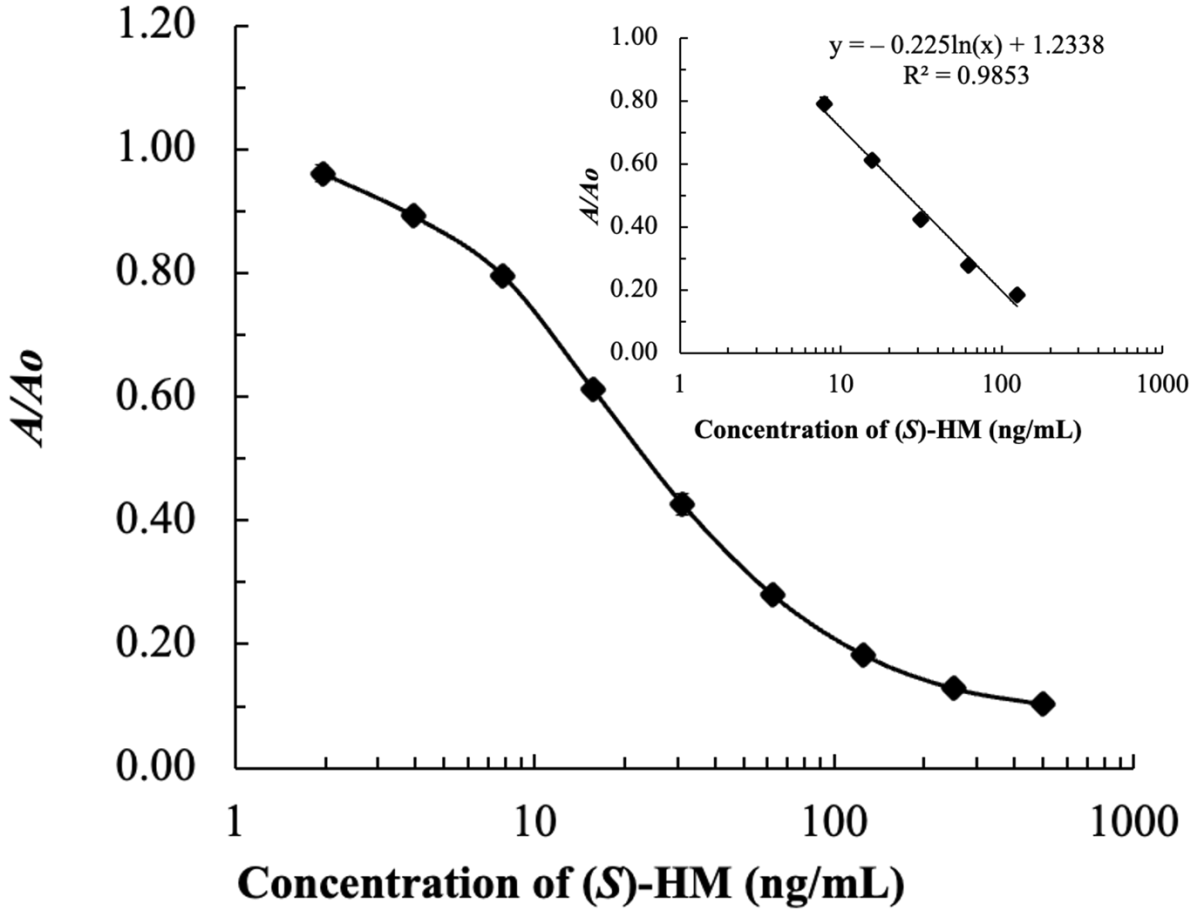

Figure 12 Standard curve for determination of (*S*)-HM using icELISA. The constant concentration of HM–OVA conjugates and MAb E8 were applied at 2 μg/mL and 100 ng/mL, respectively. A_0 and A refer to the absorbance without and with (*S*)-HM, respectively. The insert shows the linear determination range for (*S*)-HM (7.81–125 ng/mL)

3.4 Selectivity of MAb E8

MAb is a molecule composed of various arrangements of limited amino acids. The formation of the binding pocket and/or the side chain functional group of amino acids is controlled by a specific pattern of amino acid sets. Thus, there is no doubt that the CR of structurally similar compounds can occur, especially to the small molecular target. Therefore, the CR test was carried out in general immunoassay validation. In this icELISA development, the CR (%) was investigated with 26 different compounds, as listed in Table 1. The MAb E8 appeared to have selectivity against (*S*)-HM based on the low CR of almost all candidate compounds (<5.00%) except for one unique compound, norlaudanosoline (Fig. 13D), which has a high CR (223%). However, the isolation of norlaudanosoline from plants has never been documented. Thus, the effect of this compound's CR was minimized. It is noteworthy that MAb E8 could differentiate between nonhydroxy group benzyltetrahydroisoquinoline (Fig. 13C) and (*S*)-HM. This ensures that the specificity of MAb E8 is as high as the functional group level. In these conditions, the MAb E8 was an excellent candidate for immunoassay development for (*S*)-HM detection in plant samples.

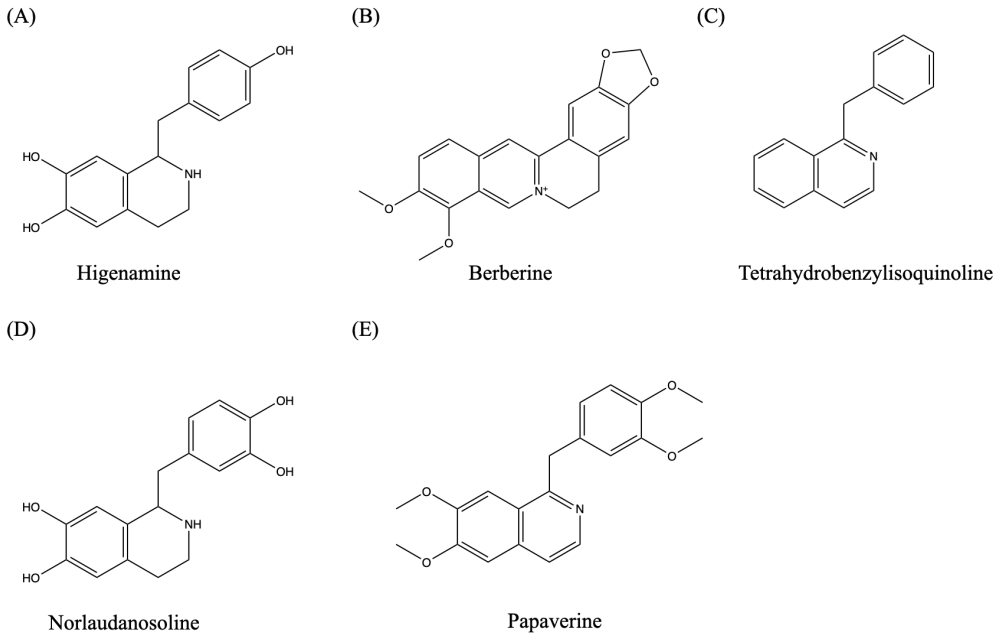

Figure 13 Structures of structurally related compounds of HM. The structures of (A) HM, (B) berberine, (C) tetrahydrobenzylisoquinoline, (D) norlaudanosoline, and (E) papaverine were provided.

Table 1. CR (%) of various compounds when using MAb E8-based icELISA

Class	Compound	CR (%)
Alkaloid	Irinotecan	<0.06
	Ergotamine	<0.06
	Ajmalicine	<0.06
	Hyoscyamine	<0.06
Anthraquinone	Sennoside A	<0.06
Benzyl isoquinoline alkaloid	Berberine	3.48
	Tetrahydrobenzylisoquinoline	4.16
	Norlaudanosoline	223
	Papaverine	<0.06
Flavonoid glycoside	Luteolin-7-*O*-glucoside	<0.06
	Apigenin-7-*O*-glucoside	<0.06
	Baicalin	<0.06
Isoflavone	Genistein	<0.06
Naphthoquinone	Plumbagin	<0.06
Phenylpropanoid	Cinnamaldehyde	<0.06
Steroid glycoside	Ginsenoside Rg1	<0.06
Taxanes	Paclitaxel	<0.06
	10-deacetylbaccatin	<0.06
	Xylosyltaxol	<0.06
	Docetaxel	<0.06
Terpenoid	Andrographolide	<0.06
Terpenoid glycoside	Paeoniflorin	<0.06
	Swertiamarin	<0.06
	Geniposide	<0.06
	Glycyrrhizic acid	<0.06
Cyclosporin	Cyclosporin A	<0.06

3.5 icELISA development and method validation

The CV value indicated the repeatability of the developed icELISA. The variation of each detectable concentration of (*S*)-HM (125, 62.5, 31.3, 15.6, and 7.81 ng/mL) was evaluated using intra ($n = 3$) and interassay ($n = 3$) tests (Table 2). The variation within the plate was ranged from 0.144% to 11.6% but the variation between the plates ranged from 1.19% to 10.2%. This indicates sufficient repeatability for the assay that was created.

Table 2. Variation of the developed icELISA indicated using intra and interassay CV (%)

(*S*)-HM concentration (ng/mL)	CV (%)	
	Intra-assay ($n = 3$)	Interassay ($n = 3$)
125	11.6	1.19
62.5	0.144	6.68
31.3	1.88	5.81
15.6	7.04	1.78
7.81	4.25	10.2

Above values indicated the CV calculated using the below formula:
CV = standard deviation (SD)/mean × 100.

The spike-recovery test was conducted to validate the accuracy of the assay. The spike-recovery assay here not only validates the accuracy of the assay but also tests the performance of the assay in the real plant matrix. *Aconitum carmichaelii* Debeaux was diluted and spiked with various amounts of (*S*)-HM (0.500, 1.00, 2.00, and 4.00 μg). The results (Table 3) showed that the recovery was between 100% and 117%, which indicated that icELISA was accurate enough for plant sample analysis.

Table 3. Percentages of recovery obtained from spiked (*S*)-HM in methanol extract of *Aconitum carmichaelii* Debeaux determined using icELISA

Spiked amount of (*S*)-HM (μg)	Measured amount of (*S*)-HM (μg)[a]	CV (%)[b]	Expected amount of (*S*)-HM (μg)	Recovery (%)[c]
0	$7.17 \pm 3.66 \times 10^{-1}$	4.22		
0.500	$7.67 \pm 3.11 \times 10^{-1}$	2.94	7.67	100
1.00	$8.28 \pm 5.48 \times 10^{-1}$	4.74	8.17	111
2.00	$9.51 \pm 2.35 \times 10^{-1}$	2.29	9.17	117
4.00	$11.6 \pm 4.75 \times 10^{-1}$	4.03	11.2	111

[a]Measured amount of (*S*)-HM was calculated from mean ± standard deviation (SD) from triplicate samples for each level.

[b]CV= SD/mean × 100.

[c]Recovery (%) = (measured amount − 7.17 μg/spiked mount) × 100.

3.6 Actual application of the developed icELISA

The validated icELISA was intended to be used as the (*S*)-HM detection tool for various plant samples. the amount of (*S*)-HM amount detected using icELISA and HPLC–UV were compared. The amount of (*S*)-HM obtained from both methods are given in Table 4. When using icELISA as the detection method, the (*S*)-HM could be noticeably detected higher in some samples. This might be due to the CR of the MAb E8. Because it was noted in some samples, the benzylisoquinolines, especially berberine, could increase the detectable amount of (*S*)-HM [54]. Even so, the amount of (*S*)-HM detected still corresponded to that detected by HPLC–UV (Fig. 14).

Table 4. (*S*)-HM content in the various plants and plant containing samples determined using developed icELISA and HPLC–UV.

Sample	icELISA		HPLC–UV	
	(*S*)-HM amount (%wt/dry wt)	SD	(*S*)-HM amount (%wt/dry wt)	SD
Aconitum carmichaelii (root, Shuchi-Bushi)	2.10×10^{-4}	8.46×10^{-6}	3.04×10^{-4}	5.43×10^{-7}
Aconitum carmichaelii (houbushi, Uchida)	1.61×10^{-4}	5.69×10^{-6}	1.42×10^{-4}	7.99×10^{-6}
Aconitum carmichaelii (Bushi, Uchida)	3.39×10^{-5}	1.19×10^{-6}	2.58×10^{-5}	1.71×10^{-6}
Nandina domestica (fruit)	1.22×10^{-3}	5.39×10^{-5}	1.40×10^{-3}	1.06×10^{-4}
Nandina domestica (leaf)	5.63×10^{-3}	2.22×10^{-4}	3.47×10^{-3}	4.80×10^{-4}
Nandina domestica containing candy				
Nanten nodo ame (Brown sugar flavored)	5.01×10^{-4}	5.01×10^{-5}	3.98×10^{-4}	1.38×10^{-5}
Nanten nodo ame (Honey-Plum flavored)	3.21×10^{-4}	2.37×10^{-5}	4.46×10^{-4}	2.30×10^{-5}
Asarum siebodii (root)	3.11×10^{-3}	2.87×10^{-4}	2.31×10^{-3}	2.28×10^{-4}
Evodia rutaecarpa (fruit)	6.48×10^{-4}	7.74×10^{-5}	9.22×10^{-4}	5.39×10^{-5}

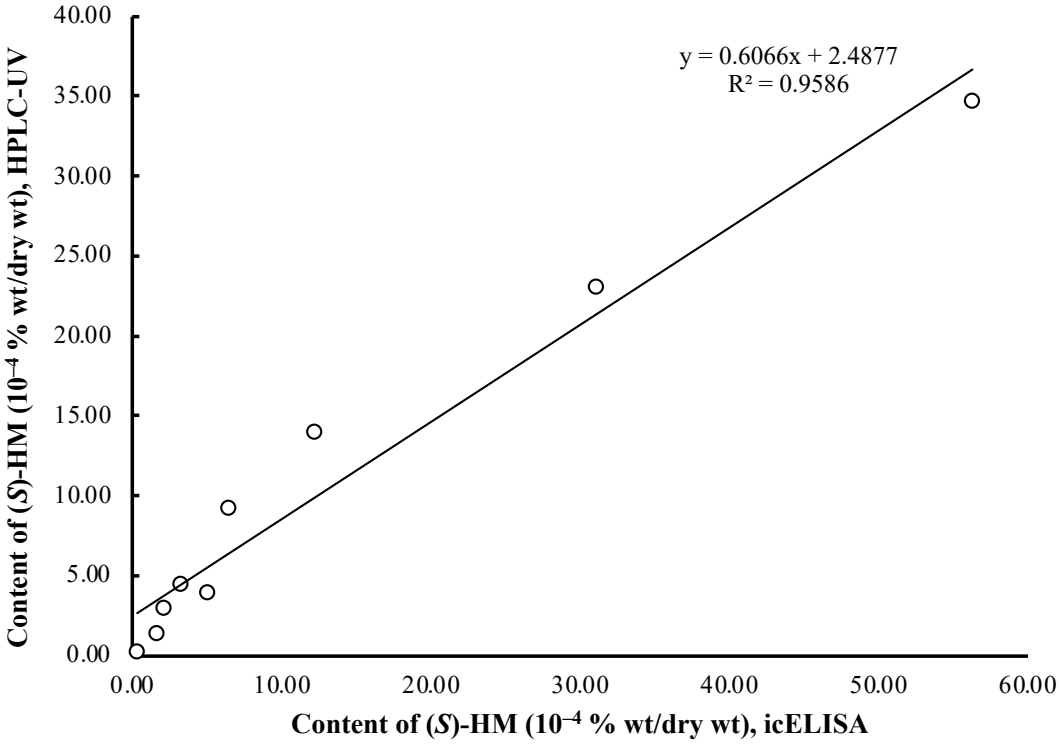

Figure 14 Correlation plot between the (*S*)-HM content obtained from HPLC–UV and icELISA

4. Conclusion

In this study, the anti (*S*)-HM MAb (MAb E8) was successfully produced. The icELISA was developed using the MAb E8 as the detection element. Various validation methods were used to ensure the reliability of this assay. Benefits of this developed assay are its cost-effectiveness, high throughput, and simplicity. Additionally, the analysis could be done with ease without the need for complex sample pretreatment. Because the icELISA using MAb E8 could be used to detect the (*S*)-HM in plant containing samples, it could be applied as the alternative or coanalysis with conventional methods for simple screening of the plant containing (*S*)-HM. Notably, this is the first immunoassay for the detection of (*S*)-HM.

CHAPTER III

Development of Lateral Flow Immunoassay for Rapid (*S*)-HM Detection in Plant Samples

1. Introduction

HM is an alkaloid isolated from several medicinal plants, including *Nandina domestica* Thunb., *Nelumbo nucifera* Gaertn., and *Asarum heterotrophies* F. Schmidt [11]. Thus, athletes who use medicinal plants as medicine or consume certain diets containing these medical plants as components need to be more concerned. Since WADA determined 10 ng/mL as the minimum analytical finding of HM in urine, the need for the development of sensitive HM detection techniques was highlighted. HM was a significant cardiac muscle activator in terms of pharmacology [14]. Therefore, the analytical techniques for HM identification in diverse matrices were established before WADA listed this molecule as a banned drug in 2017 [28]. In 1987, HPLC–UV was utilized to identify HM in rabbit blood samples [27], marking the beginning of the development. After that, more sensitive techniques are used, such as gas chromatography–mass spectrometry (GC–MS) coupled with derivatization [49] and UHPLC–MS/MS [18]. These established procedures yielded impressive and trustworthy outcomes. However, the demand for expensive equipment restricts the assay's use in some laboratory settings. Additionally, these techniques use a substantial volume of organic solvent, require many sample treatments, and are time-consuming.

To decrease the limitations of the chromatographic approach, the microplate-based immunoassay, ELISA, was created and has been utilized for a variety of natural substances. The concept depends on the unique interaction between the antibody and antigen. ELISA may be utilized for either quantitative or qualitative examination. This can be used as an alternative to chromatography or to screen samples before sending them for chromatographic analyses. Consequently, the MAb E8-based icELISA was developed as described in the preceding section. However, the icELISA is not an appropriate detection tool in all circumstances. icELISA requires a certain microplate reader for particular signals. These restrictions prevent detection outside of a laboratory.

Detection methods are not only important for detecting the misused compounds from athletes' secretion samples but also necessary for preventing athletes from consuming questionable meals or medications. Unintentional HM consumption prevention ideally requires a detection method that is sensitive, portable, and does not require difficult result interpretation. The procedure should be simple enough for athletes to independently monitor their consumption on sites.

In this study, lateral flow immunoassay (LFA), a point-of-care test, was developed to enable the on-site detection of (*S*)-HM. The LFA is a well-known rapid assay with a long history of use for a wide variety of compounds, including small molecules. The assay can be formatted to be semiquantitative, qualitative, or even quantitative analysis with the aid of a strip reader. This approach is beneficial for the development of plant secondary metabolite detection due to its ease of preparation, straightforward interpretation, ecofriendliness, and reduced time and cost. To our knowledge, this is the first LFA for the detection of (*S*)-HM. The purpose of this study is to build an LFA for the detection of (*S*)-HM in plant samples using colloidal gold nanoparticles and our previously generated MAb E8. While icELISA requires several hours, the LFA analyzes samples in about 20 min. Moreover, this approach does not require a microplate reader. Visual observation or basic picture analysis tools can be used to quickly comprehend the data. Additionally, the developed strip test is a preincubation format that eliminates the need for production of reservoir conjugate pads.

2. Material and methods

2.1. Experimental materials and reagents

Toronto Research Chemicals (Toronto, Canada) supplied both (*S*)-HM HBr (98%) and HM HBr (98%). CDI (*N,N′*-Carbonyldiimidazole) was acquired from Sigma-Aldrich (St. Louis, MO, USA). Albumin from chicken egg white (OVA; 98%) was obtained from Sigma-Aldrich (St. Louis, Missouri, USA); γ-globulin from human serum (95%) was obtained from Wako Pure Chemical Industries, Ltd. (Osaka, Japan). The colloidal solution of gold nanoparticles (0.0070% wt; 15-nm mean size) was received from Tanaka Holding Co. (Kanagawa, Japan). The antibody used for the control zone was rabbit anti-mouse IgG PAb (ab6709) and that for the icELISA was goat anti-mouse IgG1 (HRP) (ab97240), all of which were bought from Abcam (Cambridge, MA, USA). All other required reagents were acquired at either an analytical or reagent grade.

2.2 Medicinal plant samples preparation

Uchida Wakanyaku Co., Ltd. supplied the plant candidates, including *Nandina domestica* Thunb. (fruit and leaf), *Asarum siebodii* Miq. (root), *Evodia reutaecarpa* (Juss.) Benth. (fruit), and *Aconitum carmichaelii* Debeaux roots (Bushi, Shuchi-Bushi, and Houbushi) (Tokyo, Japan). Tokiwa Nanten Nodo Ame (22 tablets per pouch) was used as *Nandina domestica* Thunb.–containing products. Brown sugar-flavored and honey-plum-flavored candies were acquired at a Japanese pharmacy (Fukuoka, Japan). To improve the extraction efficiency and raise the homogeneity, the plant materials were separately milled into powders, with particle sizes generally restricted by a 300 μm mesh screen. For nonaconite root samples, the powders of the plant (30 g) were steeped in MeOH (300 mL) overnight at room temperature with intermittent shaking to create a methanolic extract. Under decreased pressure, the filtered methanolic extract of the plant was concentrated by a rotary evaporator. After drying the samples, 10 mL of MeOH was used to reconstitute them into the concentrated methanolic extract. For aconite root samples, the same process was followed, but the plant weight was altered (from 30 g to 50 g). For *Nandina domestica* Thunb.–containing candies, 5% MeOH (2.0 mL) was applied to the samples.

After the final concentration of MeOH was adjusted to 5%, these samples were used as candidate samples for LFA and icELISA.

2.3 Preparation of test zone protein for lateral flow immunoassay and coating antigen for icELISA

The test zone of the LFA was coated with HM-γ-globulin from human serum (γ-globulin) conjugates. In icELISA, HM–OVA conjugates were used for plate coating in the comparative approach. The conjugation was performed according to the method described in the preceding section. HM (3.2 mg) and CDI (3.1 mg) were dissolved using anhydrous DMF (0.6 mL) as a solvent in the same container. The reaction was maintained at 30°C for 3 h with constant stirring. Through dropwise addition (2.4 mL), the reactive HM from the reaction solution was combined with γ-globulin (6.1 mg) that has been dissolved in distilled water. The solution was stirred at room temperature overnight. With three changes of dialyzing solution every 8 h, the remaining residue was removed by dialysis against 1 L of distilled water for 2 days at 4°C. After lyophilization of the dialysate, 4.1 mg of HM-γ-globulin conjugates were obtained as a powder. HM–OVA

conjugates (5.4 mg) were obtained using the same procedure. HM (3.3 mg), CDI (4.1 mg), and OVA (6.5 mg) all had slightly different weights.

2.4 MAb E8-colloidal gold nanoparticles conjugation

In this investigation, the MAb E8 was used as the direct detecting element for the LFA. A colorimetric signal was used to report the competitive interaction between MAb E8 and free (*S*)-HM, or immobilized HM in the test zone. Thus, MAb E8 was conjugated with colloidal gold nanoparticles using a modified version of a previously published procedure [55]. Briefly, by adding enough potassium carbonate solution (20 µL) to the colloidal gold nanoparticle suspension (1.0 mL), the pH was brought down to mild alkali (pH 9.0). The MAb E8 (1 mg/mL; 50 µL) was then added to the solution. The mixture was incubated on an orbital shaker at 50 rpm at room temperature for 10 min. To stabilize the conjugated particle, 10% (w/v) BSA and 5% polyethylene glycol (PEG20000) in 100 mM Tris-buffer at pH 8.0 were added to the suspension to achieve final concentrations of 1% BSA and 0.5% PEG20000, respectively. The mixture was returned to the orbital shaker and incubated at 50 rpm at room temperature for 1 h. The unreacted residue in the supernatant was removed by centrifuging the mixture at 7,400 × *g* for 30 min, 4°C. To ensure the total elimination of the undesired reagent, the pellets were redispersed in 1% (w/v) BSA in a 100 mM Tris-buffer solution at pH 8.0 (1.0 mL) and centrifuged at 7,400 × *g* for 30 min at 4°C. Three repetitions of dispersion and centrifugation were performed. The pellets were not resuspended with the washing solution in the last cycle. They were resuspended in 35 µL of 1% (w/v) BSA solution and kept at 4°C until use. The MAb E8 conjugates were used as a detection mixture in the test. The detection process was immediately followed by the preparation of the detection mixture. The detection mixture per strip consisted of MAb E8 conjugates suspension (8 µL), 10% (w/v) sucrose in distilled water (45 µL), 1% (v/v) Tween 20 in distilled water (21 µL), 1% (w/v) BSA in 100 mM Tris-HCl buffer (pH 8.0, 32 µL), and distilled water (24 µL).

2.5 Development of the detection strip for lateral flow immunoassay

As demonstrated in Figure 15, the produced strip comprised three major components: the sample pad, nitrocellulose membrane, and an adsorbent pad. The cellulose pad serves both as the detection mixture bridge to the nitrocellulose membrane (sample pad; bottom of the strip) and as the detection mixture bank to avoid system back pressure (adsorbent pad; top of the strip). A sample pad and an absorbent pad were made from cellulose-based paper by cutting it into 1.5 × 0.6 cm squares. The nitrocellulose membrane, which was laminated with a plastic backing card, Hi Flow Plus 240 (Millipore, Temecula, California, United States), was cut to a strip size of 5.4 × 0.6 cm. The test mainly focused on the test zone and control zone on the nitrocellulose membrane. The antibody–antigen responses occurred in the test zone or the free (*S*)-HM in the sample, whereas the control zone was used to detect system anomalies. The test zone and control zone on the strip were coated with protein using pipet dispensing. The control zone was placed in the center of the strip, 0.5 cm from the top, and away from the adsorbent pad region, whereas the test zone was placed 0.5 cm from the control zone. 0.5 μL of diluted HM-γ-globulin conjugates (2 mg/mL) in 50 mM carbonate buffer containing 0.25% (w/w) sodium dodecyl sulfate (SDS) was applied three times to the test zone (equivalent to 3 μg). 0.5 μL of rabbit anti-mouse IgG PAb diluted in 50 mM carbonate buffer containing 0.25% (w/v) SDS was added to the membrane for the control zone (equivalent to 0.5 μg). When repeated applications of the solution were necessary on the same region, the membrane was allowed to incubate at room temperature before the subsequent application. The membrane was ultimately dried at room temperature for 15 min after the test zone and control zone were fully prepared. The membrane was soaked for 2 h in a blocking solution (1% (w/v) BSA in PBS). The membrane was washed thrice with PBS-T and dried at room temperature. A sample pad and an adsorbent pad were then attached to the dried modified nitrocellulose strip, making it ready for analysis.

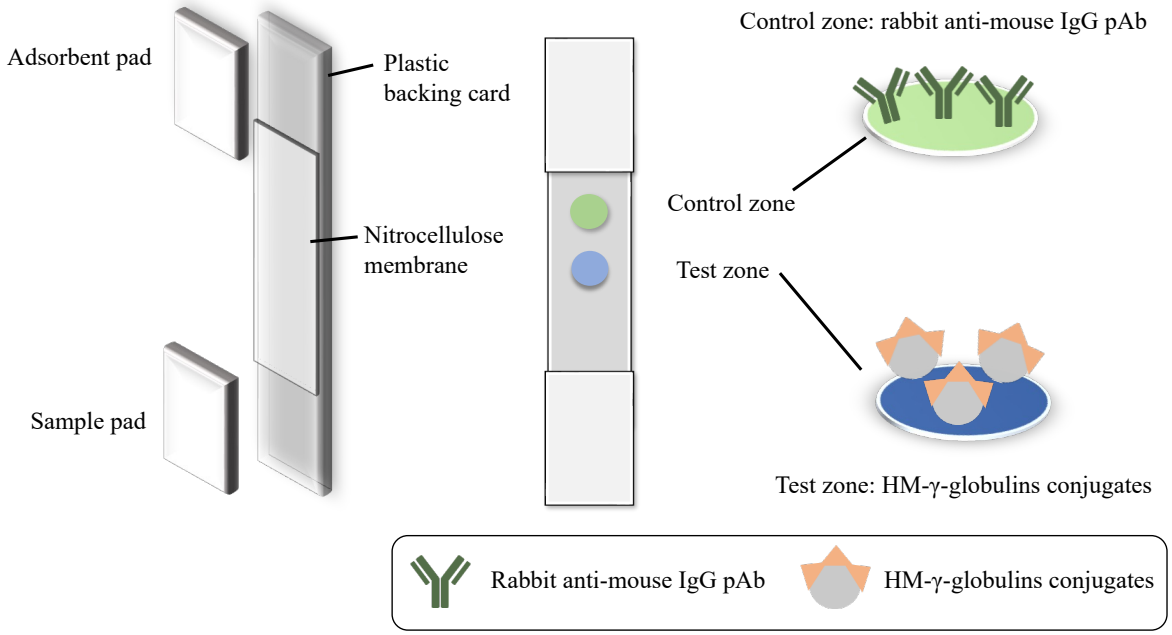

Figure 15 Schematic of strip components

2.6 Performance of the lateral flow immunoassay and result interpretation

The detection may be performed in any container that can store the detection mixture, such as a glass test tube, a 1.5 mL centrifuge tube, or a 96 well plate. Because the solution could be mixed easily and multiple strips could be placed in the plate, a 96 well plate was used as the container in this experiment. The detection mixture (130 µL), and analyte (20 µL), which might be standard (*S*)-HM, plant extracts, or CR compound candidates, were combined on a plate mixer and then incubated for 5 min to allow the antibody to react with free (*S*)-HM. The constructed strip was then immersed in the detection mixture. In a few minutes, the liquid flow should be visible on the strip. The results were interpreted after 15 min of dipping. The signal with the pinkish spot was anticipated to emerge in either the control zone or the test zone. The abnormalities of the detecting system were identified when the control zone included no pinkish spot. If a strip was performed without any color on the control zone, the result was deemed invalid and was not included in the analysis. The data were acquired in the form of digital photographs captured by a phone camera or a scanner. In addition to picture analysis, eye observation was used to assess the actual strips. In this test, the photographs were postprocessed using ImageJ software (National Institutes of Health, Maryland, United States) to accurately estimate the intensity of the test zone. Using the

region of interest management tool, the intensity for each strip test zone was acquired. On a logarithmic scale, these data were plotted against the (*S*)-HM concentration (ng/mL).

2.7 Validation of lateral flow immunoassay

The developed LFA was validated to ensure sensitivity, repeatability, and CR. LOD findings indicated the sensitivity of the LFA. Various concentrations of (*S*)-HM standard (9.77 ng/mL–2.50 µg/mL) were used as the LFA samples. The LOD was defined as the highest concentration of (*S*)-HM at which the pinkish spot of the test zone first appeared. Additionally, CV(%) was used to illustrate the assay's variation. The CV% was calculated by the intensity value obtained from ImageJ software. Because the excess amount of (*S*)-HM produced no spot on the test zone and too low amount of (*S*)-HM produced a spot on the test zone with the same intensity as the control, the (*S*)-HM concentration that showed linear correlation to the intensity (19.0–156 ng/mL) was repeatedly challenged to the developed LFA within the day (intraday; $n = 3$) and different day (interday; $n = 3$) assays.

CR test for LFA evaluates not only the antibody's ability to bind to the candidate antigen but also the interaction between colloidal gold nanoparticles that might adsorb some compound on its surface. Total effects of these interactions were shown as the color of the test zone. Even though CR of MAb E8 against various small molecules was clearly evaluated in a previous study, the CR might be somehow altered during the conjugation with colloidal gold nanoparticles. In these conditions, the developed LFA was used to examine 27 natural compounds. Initially, the compounds were screened at a concentration of 20.0 µg/mL. The compounds that showed no spot on the test zone (positive compound) were picked for further investigation by performing the LFA with various concentrations of that compound. The CR of that compound was evaluated and reported as the percentage of CR. The LODs of both the compound and standard (*S*)-HM were used for calculation with the formula below:

$$\text{CR (\%)} = \frac{\text{LOD of (}S\text{)-HM}}{\text{LOD of the candidate compound}} \times 100$$

2.8 (*S*)-HM detection in plant samples using lateral flow immunoassay

Actual plant samples were used to test the effectiveness of LFA. The produced methanolic extract and candies containing *Nandina domestica* Thunb. were used as samples when their final concentration was diluted to 5%. In the absence of the pinkish spot in the test zone, a very positive (+) result was recorded. A spot that developed on the test zone and was weaker than the control (5% MeOH) was the faint positive (±) result, indicating a low concentration of (*S*)-HM. On the test zone, a negative result (−) was recorded when a pinkish spot with the same intensity as the control (5% MeOH) appeared. Using the procedure outlined in the preceding section, the LFA findings were compared with those from icELISA and HPLC–UV.

3 Results and discussion

3.1 Development of lateral flow immunoassay-based (*S*)-HM detection tools

The HM detection technique was deemed essential because HM is a WADA-prohibited substance. Even sports products have gradually eliminated HM from their formulas. Unintentional ingestions may result from the use of medicinal herbs or even the meals ingested by sportspersons. Simple detection methods for HM detection were developed to make the test simple to be conducted outside the lab to avoid any potential controversy. Thus, they can examine questionable items before ingestion. In this study, a fast antibody-based test, referred to as LFA, was developed for the detection of (*S*)-HM in plant samples. The principals were mentioned in Figure 16.

Various membranes, including nitrocellulose, nylon, and polyvinylidene fluoride (PVDF), are used in LFA [45]. In this investigation, however, a nitrocellulose membrane was used as the reaction platform. Nitrocellulose has a high capacity for protein absorption. Additionally, this membrane is wettable in an aqueous solution with a low influence on protein adsorption due to its facile wetting feature. The user is allowed to choose the nitrocellulose pore size depending on the analysis time required for the particular experiment. There is no doubt that this membrane is a popular membrane for LFA development.

In either the test zone or the control zone, SDS was added to the protein solution to prevent its local accumulation in the defined region. For the test zone, several kinds of conjugates, including HM–HSA conjugates, HM–OVA conjugates, and HM-γ-globulin conjugates, were evaluated to identify the conjugates that exhibited the round-shape test zone, greater intensity test zone, and less-intrinsic color in the test zone while retaining the competitive activity against MAb

E8. Preliminary data indicated that HM-γ-globulin conjugates satisfied the criteria for this experiment. In addition to the test zone, the antibody for the control zone was selected from rabbit anti-mouse IgG PAb (ab6709) and goat anti-mouse IgG PAb (ab6780). The early observations indicated that the rabbit-derived PAb produced a round shape with a uniform color over the test zone, but the goat-derived PAb produced a spot with a greater intensity than accumulated exclusively in the center of the control zone. Therefore, rabbit anti-mouse PAb was chosen as the optimal protein for this zone. The quantity of conjugates and antibodies on the membrane was determined based on the smallest number of proteins capable of exhibiting the saturated intensity in their zones.

The strip was treated with a 1% (w/v) BSA solution to reduce the nonspecific binding of MAb E8-colloidal gold nanoparticle conjugates to the uncoated area of the nitrocellulose membrane. PBS-T was used to wash the membranes since excessive BSA altered the results. The PBS-T solution not only made it easier to eliminate dirt via detergent washing, but it also increased the membrane's wettability when the detection mixture was applied.

For typical LFA, the antibody coupled with colloidal gold nanoparticles was kept in the conjugate pad. In certain instances, the system was unable to release the antibody–colloidal gold nanoparticle conjugates or released them too slowly. The conjugate pad was thus excluded from our system. In addition to ensuring the complete release of the antibody–colloidal gold nanoparticle conjugates, omitting the conjugate pad minimized the preparation time of the conjugate pad, which is generally at least 2 h. Because the system required a portion of liquid to moisten and release the antibody–colloidal gold nanoparticles conjugates, the developed LFA required a lesser sample volume (20 μL/sample) than the LFA with conjugate pad (400 μL/sample) [56]. In comparison to the earlier-developed icELISA (50 μL/sample), the sample volume needed is two times less. This increases the adaptability of the assay when the sample amount is limited.

The results of LFA satisfactorily revealed the conjugation of MAb E8 to the colloidal gold nanoparticles (Figure 16). The ionic and hydrophobic interaction between the antibody molecule and the colloidal gold nanoparticles molecule was the expected adsorption mechanism. Thus, it was anticipated that the antibody part of adsorption would be random. Although the random orientation of antibodies on the surface of colloidal gold nanoparticles was less efficient than the exposed-Fv portion layout for (*S*)-HM detection, the outcome was sufficient.

The detection mixture was mixed with the target analyte for 5 min before detection in our detection system to facilitate the interaction between MAb E8–colloidal gold nanoparticle conjugates and the free (*S*)-HM in the sample. Once the sample pad was immersed in the detection mixture, the detection mixture proceeded in an antigravity direction from the sample pad through the nitrocellulose membrane. When the mixture reached the HM-γ-globulin conjugates in the test zone, the remaining variable region on the MAb E8–colloidal gold nanoparticle conjugates attached to the immobilized HM, while the constant region interacted with the anti-mouse antibody in the control zone. The reaction could be directly observed by observing the pinkish spot in the test zone and control zone due to the brilliant hue of colloidal gold nanoparticles. According to these principles, the concentration of (*S*)-HM in the samples was proportional to the pinkish spot of the test zone. Compared to the negative control (5% MeOH), the higher the (*S*)-HM concentration in the sample, the lower the intensity of the pinkish spot on the test zone, but the spot on the control zone remains present constantly regardless of (*S*)-HM concentration.

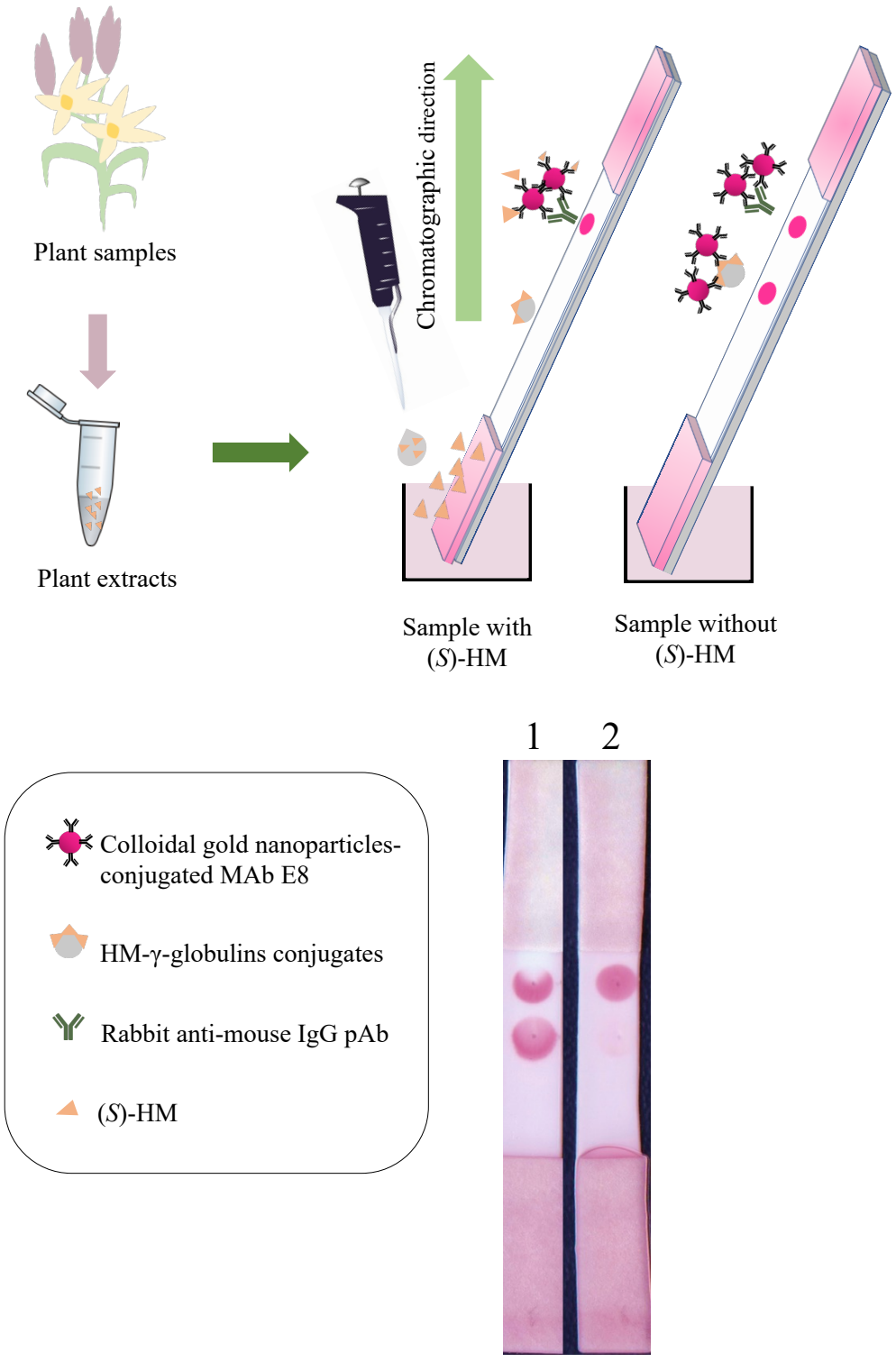

Figure 16 LFA schematic demonstration. The detection mixture flowed in an antigravity direction from the sample pad to the adsorbent pad. Lanes 1 and 2 indicate the result of LFA when using negative control (5% MeOH) and the result of LFA when the sample was 5.00 µg/mL (*S*)-HM, respectively

3.2 Evaluation of sensitivity in lateral flow immunoassay

The sensitivity of LFA might suggest the applicability and usefulness of the test. Ideally, the test should give a positive result when the (*S*)-HM concentration in the sample exceeds 10 ng/mL, which is the WADA's AAF for HM in urine. Nonetheless, the purpose of this study was to identify (*S*)-HM in plant samples to confirm the presence or absence of HM in the suspect plant or food before consumption. There was no clear determination of the minimal quantity of HM in eaten plant material required to produce a negative urine test result. This figure relies on the excretion rate of a particular athlete, which should be investigated in greater depth. Therefore, the sensitivity of the assay needs to be as high as feasible to demonstrate the absence of HM exposure. In this study, the intensity of the pinkish spot in the test zone obtained from various doses of (*S*)-HM (9.77 ng/mL to 2.50 μg/mL) was compared to that obtained from negative control (5% MeOH). The control zones of each strip displayed pinkish spots, whereas the test zones displayed a gradation of intensities (Fig. 17A; test zones). In Lanes 1–9, the concentration of (*S*)-HM decreased as the intensity of the pinkish spots rose. The LOD for LFA was determined to be 156 ng/mL, as the appearance of the spot began at this concentration. ImageJ, a picture analysis program, was used in addition to visual observation to examine the photos. The intensity of the test zone obtained from each (*S*)-HM concentration (*I*) was normalized by using that obtained from 5%MeOH (I_0). The intensity ratio (I/I_0) was plotted against the logarithmic concentration (ng/mL) of (*S*)-HM (Fig. 17B). The intensities obtained from the (*S*)-HM concentration between 19.0 ng/mL and 156 ng/mL showed a positive correlation to the (*S*)-HM concentration. Although this assay was primarily designed for qualitative analysis, this concentration range might be used to estimate the (*S*)-HM concentration in plant samples using this LFA when necessary.

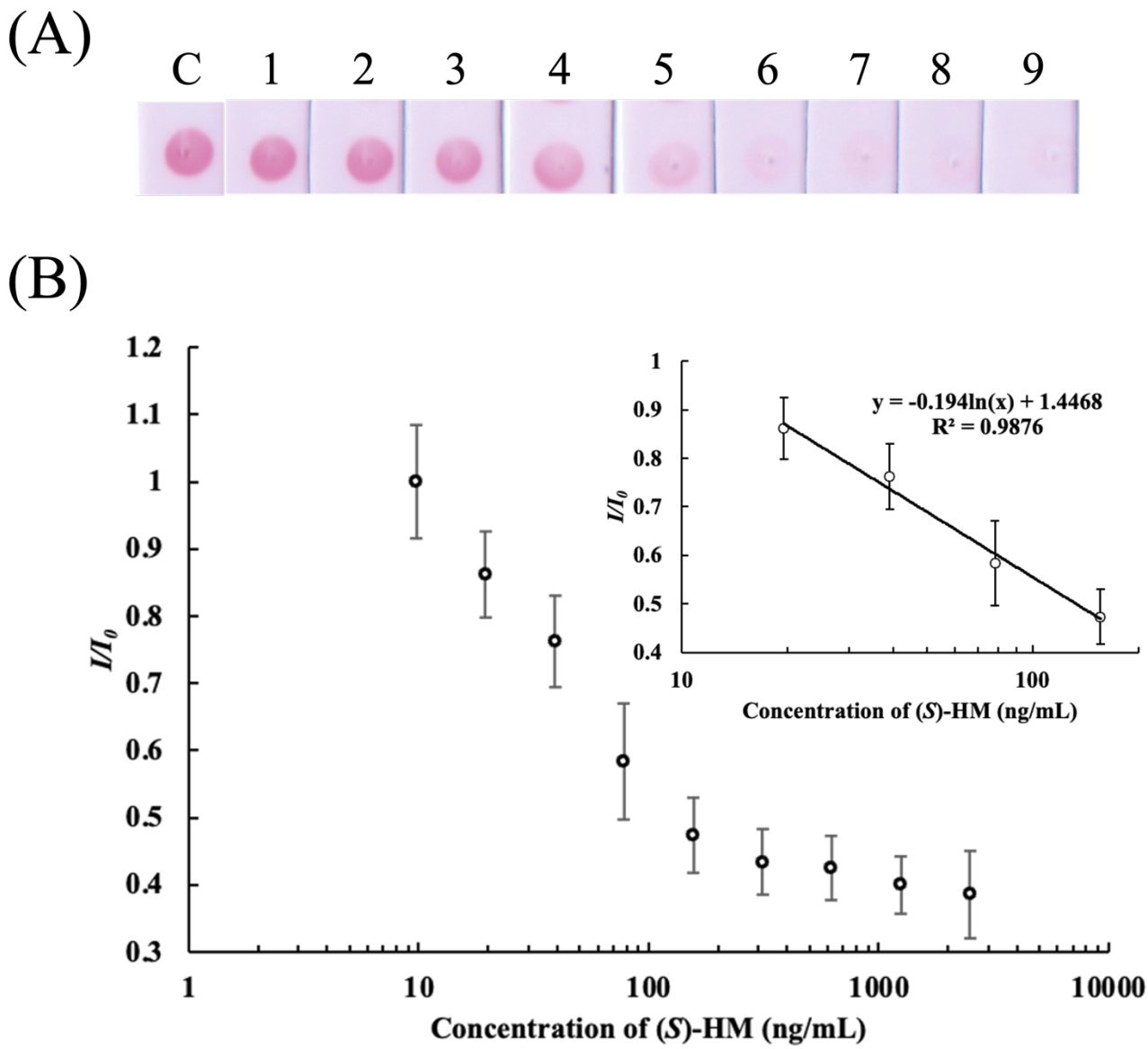

Figure 17 Challenging various concentrations of (*S*)-HM to the LFA. (A) The test zones obtained from LFA using a set of (*S*)-HM concentration that was 2-fold serially diluted from 9.77 ng/mL (Lane 1) to 2.50 μg/mL (Lane 9) and the negative control (5% MeOH; lane C). (B) The standard curve was obtained from the analysis of the strip photos. The error bars were the SD of the (I/I_0) in each concentration obtained from the interday assay. The inset picture was the semiquantitative concentration curve

3.3 Lateral flow immunoassay repeatability test

Two methods were utilized to validate the repeatability of LFA. First, the LOD of the assay was compared (n = 3). The outcome indicated that the LOD remained unchanged at 156 ng/mL. In addition to the LOD findings, the fluctuation of the intensity ratio (I/I_0) obtained from linear concentrations (19.0–156 ng/mL) was studied. The findings acquired on the same day (n = 3) and on a different day (n = 3) were considered and reported using the CV%. The largest variations achieved from intraday and interday testing were 9.96% and 14.9% (Table 5). This demonstrated that the repeatability of LFA was enough for the detection of (*S*)-HM.

Table 5. Repeatability testing of the LFA developed

(*S*)-HM concentration (ng/mL)	**CV (%) [a]**	
	Intra-assay	**Interday**
	(n = 3)	**(n = 3)**
156	9.96	12.0
78.0	9.92	14.9
39.0	3.87	8.84
19.0	2.34	7.41

[a] The calculated values were obtained from ImageJ; the I/I_0 of the test zone of the individual concentration was taken into an account.

CV (%) was calculated using the following equation:

CV (%) = standard deviation (SD) /mean × 100.

3.4 Characterization of MAb E8-colloidal gold nanoparticles conjugates

The MAb E8 was used as the primary detection element in this investigation. Although MAb E8 was well described in the preceding section, the CR of the MAb E8-colloidal gold nanoparticle conjugates may differ from that of the free MAb E8. Additionally, the colloidal gold nanoparticles may adsorb certain compounds on their surface, producing unexpected results for the entire experiment. To investigate the effect of the conjugates on the result of LFA, 27 different natural chemicals were used. Using a screening concentration of 20.0 µg/mL, negative findings were verified for all LFA strips except (*S*)-HM (lane 1) and norlaudanosoline (lane 9), as shown in Figure 18. Notably, spots originating from berberine and tetrahydrobenzylisoquinoline were

visible although icELISA exhibited a low level of CR. This might be related to the fact that the LFA is less sensitive than the icELISA. When the developed LFA is employed with samples containing extraordinarily high levels of berberine and/or tetrahydrobenzylisoquinoline, the test samples have to be analyzed with additional analytical techniques to ensure the actual content. Using a LOD comparison with (*S*)-HM, the CR of MAb E8-colloidal gold nanoparticle conjugates against norlaudanosoline was explored further. The LOD for norlaudanosoline was determined to be 78.0 ng/mL. The estimated CR was 200%, which was close to the icELISA result (223%). Even though a significant CR was reported with norlaudanosoline, this compound was not found in plants. Therefore, this would not interfere with the detection of (*S*)-HM in plant samples.

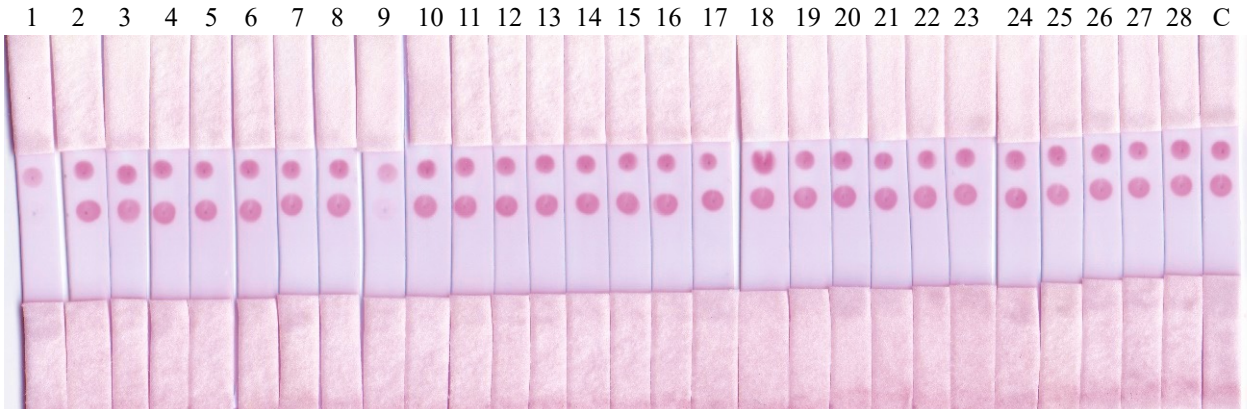

Figure 18 CR of developed LFA. (*S*)-HM (Lane 1), 27 different natural compounds (Lanes 2−28; 20.0 µg/mL), and negative control (5% MeOH; Lane C) were challenged with developed LFA. The cross-reacted compound was norlaudanosoline (Lane 9).

3.5 Actual application of lateral flow immunoassay

The developed LFA was intended to detect (*S*)-HM in plant samples. Thus, the LFA system was tested with seven plants that were used for the icELISA developed in the preceding section. As the LFA results were semiquantitative, two further comparison tests, icELISA and HPLC–UV, were conducted to analyze the real concentration of (*S*)-HM in plant extracts. The concentration listed in Table 6 was the 20-fold diluted concentration (working concentration) of the plant methanolic extracts used to generate the suitable MeOH final concentration (5% MeOH) for icELISA and LFA analyses. Due to the high sugar content and high viscosity of the *Nandina*

domestica candy matrix, the results obtained from icELISA and LFA systems were invalid. Consequently, the candy samples were diluted 20-fold. The results demonstrated that the results of LFA concurred with those of icELISA and HPLC–UV (Table 6). When the concentration of (*S*)-HM in the plant matrix exceeded the LOD of the LFA, substantial positive results were seen (Fig. 19). The intensity was altered when the (*S*)-HM concentration in a matrix fell within or close to the estimation range (19.0–156 ng/mL) of LFA, as demonstrated by three samples: *Aconitum carmichaelii* Debeaux (Bushi, Uchida; Fig. 19, Lane 6), Nanten nodo ame (Brown sugar-flavored; Fig. 19, Lane 8), and Nanten nodo ame (honey-plum-flavored; Fig. 19, Lane 9). This demonstrated that the proposed LFA can be used to determine the concentration of (*S*)-HM in various plant matrices.

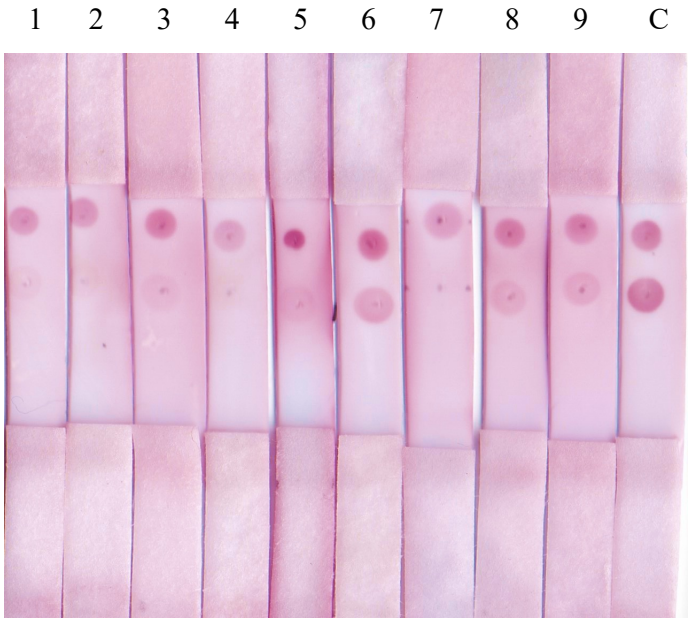

Figure 19 Application of LFA to (*S*)-HM detection in various plants. Positive results were observed on the extracts of *Nandina domestica* Thunb. (fruit; Lane 1), *Nandina domestica* Thunb. (leaf; Lane 2), *Evodia reutaecarpa* (Juss.) Benth. (fruit; Lane 3), *Asarum siebodii* Miq. (root; Lane 4), *Aconitum carmichaelii* Debeaux (houbushi, Uchida; Lane 5), and *Aconitum carmichaelii* Debeaux (Shuchi-Bushi, Uchida; Lane 7). The weak positive results were shown in the leftover strips

Table 6. Analysis of (*S*)-HM content in the sample using LFA, MAb E8-based icELISA, and HPLC–UV

Sample	LFA[a]	(*S*)-HM concentration (μg/mL) [b]	
		icELISA	HPLC–UV
Plant samples			
Nandina domestica (fruit; Lane 1)	+	$1.94 \pm 5.98 \times 10^{-2}$	$2.22 \pm 1.53 \times 10^{-1}$
Nandina domestica (leaf; Lane 2)	+	$8.57 \pm 3.00 \times 10^{-1}$	$5.44 \pm 8.31 \times 10^{-1}$
Evodia rutaecarpa (fruit; Lane 3)	+	$9.74 \times 10^{-1} \pm 1.10 \times 10^{-1}$	$1.40 \pm 9.06 \times 10^{-2}$
Asarum siebodii (root; Lane 4)	+	$4.80 \pm 3.76 \times 10^{-1}$	$3.56 \pm 2.71 \times 10^{-1}$
Aconitum carmichaelii (houbushi, Uchida; Lane 5)	+	$4.05 \times 10^{-1} \pm 1.51 \times 10^{-2}$	$3.57 \times 10^{-1} \pm 2.00 \times 10^{-2}$
Aconitum carmichaelii (Bushi, Uchida; Lane 6)	±	$8.55 \times 10^{-2} \pm 2.60 \times 10^{-3}$	ND
Aconitum carmichaelii (Shuchi-Bushi, Uchida; Lane 7)	+	$1.07 \pm 4.84 \times 10^{-2}$	$1.55 \pm 1.21 \times 10^{-2}$
***Nandina domestica* containing candy**			
Nanten nodo ame (Brown sugar flavored; Lane 8)	±	$2.20 \times 10^{-1} \pm 1.56 \times 10^{-2}$	$1.74 \times 10^{-1} \pm 1.21 \times 10^{-2}$
Nanten nodo ame (Honey-plum flavored; Lane 9)	±	$1.40 \times 10^{-1} \pm 7.33 \times 10^{-3}$	$1.95 \times 10^{-1} \pm 1.26 \times 10^{-2}$

[a] Positive result (+) was noted as the absence of the spot on the test zone and developed the pinkish spot on the control zone. Weak positive result (±) was noted as a weak pinkish spot on the test zone with the presence of a pinkish spot in the control zone, and a negative result (−) was noted as a strong pinkish spot on the test and control zones.

[b] Concentration of (*S*)-HM in each sample was determined using the working concentration (20-fold dilution of the sample extracts).

Note: ND, not detected.

4. Conclusion

This study was undertaken to develop an LFA for the detection of (*S*)-HM in plant samples. The assay was based on the competitive binding of MAb E8–colloidal gold nanoparticle conjugates to immobilized HM on test strips and free (*S*)-HM in the relevant samples. Various validation techniques were used to establish the sensitivity, reproducibility, and selectivity of the LFA, and the assay was applied to actual plant samples to evaluate its performance and precision. Because just a minimal sample volume (20 μL) was needed for analysis, this LFA is excellent for instances with restricted sample volume. Additionally, the use of a preincubation strip format made preparation simpler and avoided the laborious and time-consuming fiber pad preparation phase required in conventional LFAs. The reported LFA is, to the best of our knowledge, the first of its sort.

CHAPTER IV

Selection, Characterization, and Application of the Aptamer for Berberine Detection Method Development

1. Introduction

Japanese medicine (Kampo medicine), with various detailed modifications, is based on similar medicinal theories and therapeutic practices as traditional Chinese medicine. The fundamental concept of medicines is to maintain a balance of mental and physical states [57]. Depending on the underlying reason for an imbalance between mental and bodily states, patients were given a prescription that included a mixture of plants, animals, and minerals. Thus, more than 128 Kampo medicinal formulations are accessible to patients. Due to its extensive history of use, the Kampo medicinal formulation has been refined throughout time to improve its usability and quality. Because Kampo medicine is a mix of plant materials, the Japanese Pharmacopoeia lists the active compounds and/or main compounds test as one of the best techniques to determine quality.

Berberine (BBR) is a distinctive cationic benzylisoquinoline alkaloid initially discovered from goldenseal (*Hydrastis canadensis* L.) [58]. Later, this compound was extracted from several plant species, including barberry root [38] and *Chelidonium majus* Linn. [59]. For Kampo medicine, BBR consists mostly of Coptis rhizome [35], that is, *Coptis japonica* Makino, *Coptis chinensis* Franchet, *Coptis deltoidea*, C. Y. Cheng et Hsiao or *Coptis teeta* Wallich and Phellodendron bark [36], that is, *Phellodendron amurense* Ruprecht or *Phellodendron chinense* Schneider. These herbs served as the foundation for over 10 Kampo medicinal formulations. BBR has a number of pharmacological effects, particularly in relation to metabolic syndromes [37]. Additionally, it was discovered that BBR had antioxidative [38], antitumor [39], and antibacterial [40] properties. A recent study has demonstrated that BBR may be administered in conjunction with probiotics to enhance the hypolipidemic impact on postprandial lipidemia [41]. Although BBR possesses a variety of intriguing pharmacological activities, it is important not to neglect its negative effects. Long-term exposure to BBR may induce gastrointestinal distress [42] and raise the incidence of jaundice [42]. For a balanced BBR intake, reliable and time-efficient BBR detection methods are required.

Aptamers, which are single strands of DNA (ssDNA) or RNA that react to a specific target, have been used to analyze a variety of targets, including peptides, proteins, and even small molecules. The library of random oligonucleotides was screened using SELEX to get the optimal sequence. Even though the selection of highly specific aptamers for several targets has been performed for decades, the selection of aptamers for small molecules remains a challenging endeavor. Small molecules cannot adhere to a solid surface as compared to macromolecules. Thus, it is difficult to separate the aptamer possessing affinity to the target molecule from those that do not.

Regarding the selection of aptamers specific to BBR, a single study was published [60]. Using a biotin-labeled complementary oligonucleotide capture strand, the acquired SELEX was utilized to couple the library to streptavidin-coated agarose beads. However, the cost of synthesizing biotin-labeled complementary strands used for capturing SELEX is rather expensive. Moreover, the complement anchoring sequences impacted the binding ability of their target. The affinity of the aptamer might vary depending on whether it is in its free form or bound form. These constraints affect the overall performance of sensitive aptamer selection.

To overcome the constraints of capture-SELEX, colloidal gold nanoparticles were used as the platform for aptamer selection (GOLD-SELEX) [61]. Colloidal gold nanoparticles possess the ability to adsorb DNA on their surface. The Van der Waals force and strong electrostatic interaction induced by dipolar interaction dominated their interaction. When the target was added to the ssDNA that had been treated with colloidal gold nanoparticles, the high-affinity aptamers interacted with the target and lost their binding to the surface of the colloidal gold nanoparticles.

In this study, unique aptamers against BBR were identified using the GOLD-SELEX approach, and their activity against BBR was measured using a fluorometric assay. Fluorescence emission was observed from the obtained aptamer based on the principles denoted in Figure 20. The light-up phenomenon is observed when the aptamer against BBR is exposed to their target while there is no or low fluorescence emission in the BBR alone or aptamer alone. Additionally, the resulting sequence was adjusted to get the optimal sequence for assay development for BBR detection in Kampo medicine samples. According to our knowledge, this is the first fluorometric microplate-based BBR detection employing aptamer for complex matrices, such as Kampo medication samples. The test used the rapid response of the aptamer to BBR, which can be achieved in ~5 min.

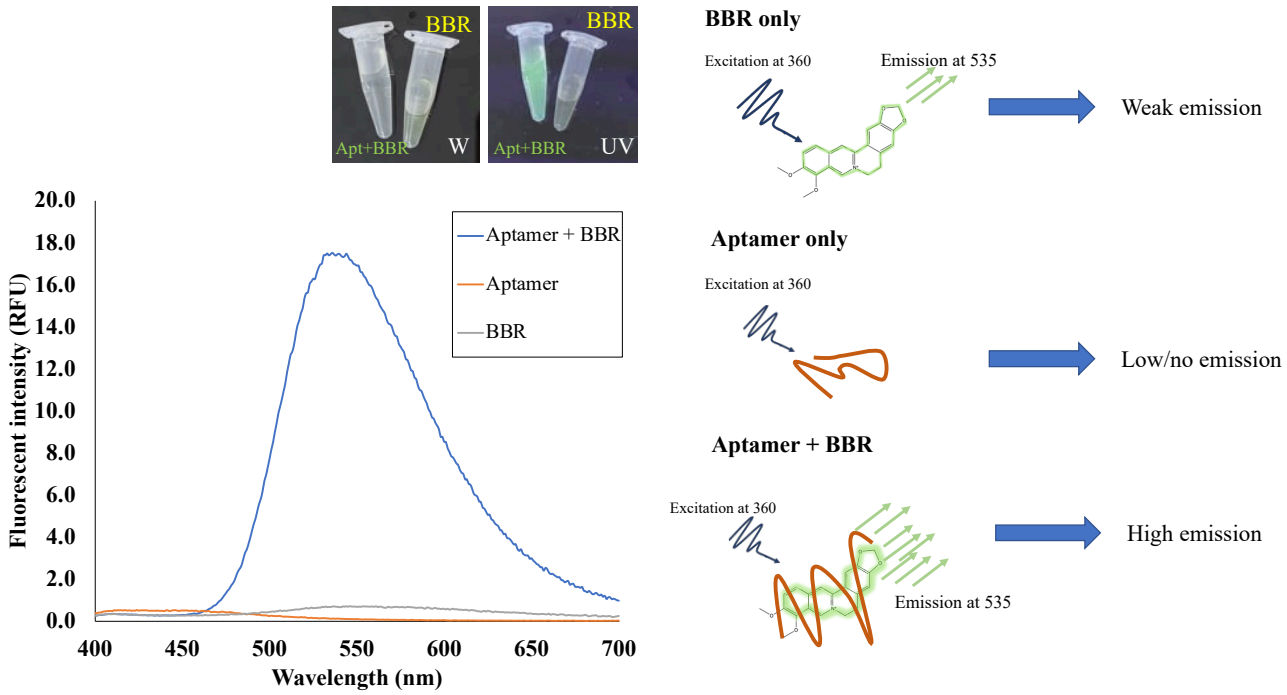

Figure 20 Schematic of the principles of enhancement for BBR detection. Top left of the figure shows the comparison of aptamer mixed with BBR (Apt + BBR) and BBR alone under white light and UV (365 nm). The curve showed the emission fluorescence of BBR, aptamer, and aptamer + BBR. On the right is the expected fluorescence emission in different conditions

2. Material and methods

2.1 Experimental materials and reagents

Berberine hydrochloride (>97% pure) was obtained from Wako Pure Chemical Industries, Ltd. (Osaka, Japan). The colloidal solution of gold nanoparticles (0.0070% wt; 15 nm mean size) was supplied by Tanaka Holding Co. (Kanagawa, Japan). The pMD20-T Vector Cloning Kit, 10× Loading buffer, and the DNA polymerase, PrimeStar HS (premix), were acquired from Takara Bio Inc. (Shiga, Japan). Ethidium bromide solution was acquired from NACALAI TESQUE, INC (Kyoto, Japan). A 100 bp DNA ladder was obtained from Bioneer (Daejeon, Republic of Korea). Prime Taq DNA polymerase with 10× reaction buffer (including $MgCl_2$) and 10 mM dNTP Mixture (2.5 mM of each dNTP) were purchased from Genetbio Co., Ltd. (Daejeon, Republic of Korea). SupreDye v.1.1, a fluorescence sequencing dye, was acquired from Edge BioSystems (CA, USA). All remaining needed reagents were either of an analytical or reagent grade.

2.2 Strain, media, and plasmid

The JM109 *Escherichia coli* was used as the host to obtain the aptamer sequences ligated pMD20-T Vector. The mentioned *E. coli* was grown in LB medium containing 1% Hipolypepton (polypeptone), 0.5% yeast extract, 0.5% NaCl, pH 7.2–7.4) containing ampicillin at a final concentration of 50 μg/mL.

2.3 ssDNA library, primers, and ssDNA

The random ssDNA library was intended to have 80 nucleotides in total. The first and last 20 nucleotides contain primer binding areas, whereas the middle 40 nucleotides are random sequences (5′-AGCAGCACAGAGGTCAGTTC-40N-CCTATGCGTGCTACCGTGAA-3′). The forward primer consisted of the following sequence: 5′-AGCAGCACAGAGGTCAGTTC-3′. The reverse primer had the following sequence: 5′-TTCACGGTAGCACGCATAGG-3′. Moreover, the 5′-phosphorylated reverse primer was used for ssDNA preparation. As the library was supposed to be cloned into the pMD20-T vector, the primers for colony PCR were designed as M13 M4 (5′-GTTTTCCCAGTCACGAC-3′) and M13 RV (5′-CAGGAAACAGCTATGAC-3′) to be forward and reverse primers, respectively. The sequencing primer, which primes the region preceding the cloning site, was designed as 5′-GCAGTGAGCGCAACGCAA-3′ to assist the sequencing process. The ssDNA library, primers, and all additional aptamers that were obtained afterward were synthesized by Fasmac Co., Ltd. (Kanagawa, Japan).

2.4. Preforming GOLD-SELEX

As demonstrated in Figure 21, the ssDNA library (100 μM; 20 μL) was mixed with the 20 mM Tris-HCl (pH 8.0; 180 μL). The mixture was then heated at 95°C for 5 min and put on ice immediately. It was placed for 10 min to ensure that the aptamers fold into their optimal secondary structure. Then, this solution was added to the colloidal gold nanoparticles suspension (1.0 mL) and allowed to incubate at room temperature for 1 h to facilitate the immobilization of the ssDNA to the surface of the colloidal gold nanoparticles. The mixture was then centrifuged at 9,200 × *g* for 30 min. The excess amount of ssDNA that was supposed to be in the supernatant was discarded. Then, the pellet was washed in 1% (w/v) BSA in 20 mM Tris-HCl (pH 8.0; 1.0 mL) and centrifuged at 9,200 × *g* for 30 min. The washing step was repeated three times to ensure that the excess or unbound ssDNA was eliminated. By resuspending the washed pellet with BBR (100

μg/mL) in 20 mM Tris-HCl (pH 8.0; 400 μL), the BBR, the selection reagent, was introduced to the system. The mixture was incubated for 1 h at 37°C before being centrifuged at 20,600 × *g* for 45 min. Absolute isopropanol (600 μL) was added to the supernatant to precipitate it, and it was then incubated for 15 min at room temperature. Subsequently, the pellet was collected by centrifuging at 20,600 × *g* for 30 min. The precipitant was washed with 70% EtOH (400 μL), and the supernatant was eliminated by centrifugation at 20,600 × *g* for 30 min. The residue was let dry at room temperature. The pellet was then redissolved in Tris-EDTA buffer (50 μL) and kept at –20°C until used. The whole process, from library coating, washing, target elution, and ssDNA precipitation was counted as one cycle, and the eluate will be called cycle-1 library ssDNA. The cycle was repeated until the optimum activity of the aptamer pool was obtained. The pressure was given to the system through the reduction of BBR concentration and the reduction of BBR incubation time, as shown in Table 7.

Table 7. Selection condition in each round

Round	Selection compound	Concentration	Time
1	BBR	100 μg/mL	1 h
2	BBR	50 μg/mL	1 h
3	BBR	25 μg/mL	1 h
4	BBR	25 μg/mL	30 min
5	BBR	12.5 μg/mL	1 h
6	BBR	12.5 μg/mL	30 min
7	BBR	6.25 μg/mL	1 h
8	BBR	6.25 μg/mL	30 min

Simple PCR amplification and gel electrophoresis imaging were used to confirm the presence of ssDNA in the eluate. Briefly, the PCR reaction mixture consists of 10 mM dNTP Mixture (1.5 µL), 10× reaction buffer (including $MgCl_2$; 1.5 µL), Prime Taq DNA polymerase (0.3 µL), with either 10 µM of forward primer or reverse primer (0.3 µL), eluate product of each cycle as a template (1.0 µL), and sterile distilled water (SDW; 12.5 µL). The PCR conditions started with initial denaturation (95°C, 5 min) followed by 30 cycles of denaturation (95°C, 30 s), annealing (57°C, 30 s), and extension (72°C, 30 s). The final extension was performed for 7 min at 72°C before being stored at 4°C until usage. A 1% agarose gel stained with ethidium bromide and imaged under UV light was used to verify PCR results (dsDNA).

After a positive result was confirmed by the band, the cycle-1 library ssDNA was amplified by PCR and digested through the lambda exonuclease-mediated method. The ssDNA obtained from each round of GOLD-SELEX was subjected to a check for fluorogenic activity with a concentration of 0.25 µM. The amount of ssDNA library of the cycle-1 was adjusted to 200 pmol and used as the ssDNA material for the next round of GOLD-SELEX.

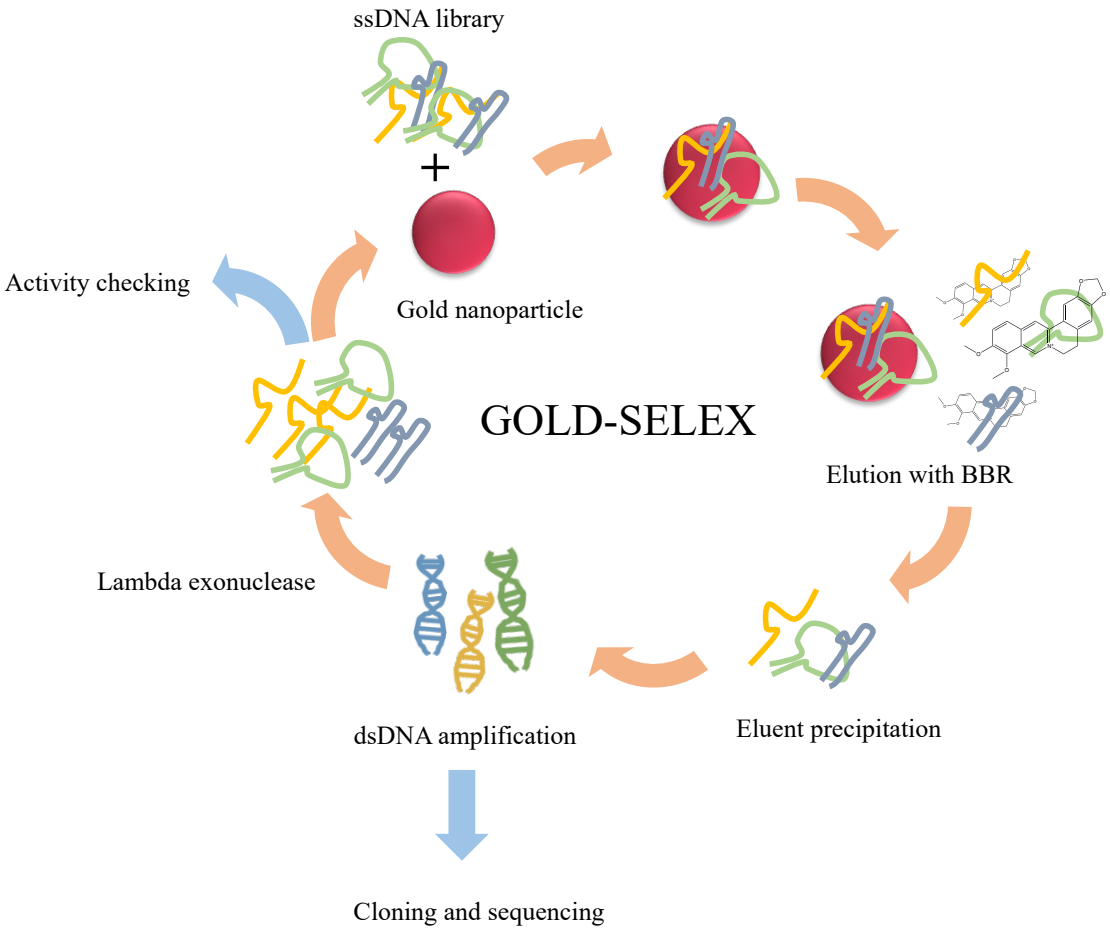

Figure 21 Schematic of GOLD-SELEX process

2.5. ssDNA preparation using lambda exonuclease-mediated method

The phosphorylated dsDNA served as a substrate for ssDNA production. The phosphorylated dsDNA was produced by PCR amplification of the ssDNA library. Briefly, the mixture of PrimeStar HS (50 µL), with either 10 µM of forward primer or phosphorylated reverse primer (6.0 µL), ssDNA cycle library (2 µL), and SDW (45 µL) were added into the thermocycler. The PCR conditions started with initial denaturation (98°C, 1 min) followed by 30 cycles of denaturation (98°C, 10 s), annealing (57°C, 10 s), and extension (72°C, 30 s) before being stored at 4°C until usage. The obtained PCR products (10 µL) were analyzed using gel electrophoresis coupled with ethidium bromide staining. The positive-confirmed PCR products (90 µL) were mixed with enzyme reaction buffer (10 µL) and lambda exonuclease (2 µL) before being incubated at 37°C for 30 min. The digested product was cleaned by phenol–chloroform separation by adding the phenol:chloroform:isoamyl alcohol (25:24:1; 200 µL) followed by mixing for 15 s. The

mixture was centrifuged at 20,600 × *g* for 10 min. The upper layer was precipitated with the DNA precipitation protocol mentioned earlier. The pellet was reconstituted with an appropriate volume of Tris-EDTA buffer and stored at 4°C until usage.

2.6. Microplate-based fluorescence measurement

For activity check of each cycle-ssDNA pool, 0.25 μM of ssDNA library was dissolved in 50 mM Tris-HCl (pH 8.0; 50 μL) and was mixed with BBR standard solution (6.25 μg/mL; 50 μL) in the black 96 well plate. The solution was then incubated at 25°C for 5 min. The fluorescence was recorded using Varioscan Lux (Thermoscientific, Japan) at an excitation wavelength of 360 nm and an emission wavelength of 535 nm. The fluorescence was recorded as the difference between the fluorescence of each cycle-ssDNA pool-BBR complex (F) and the intrinsic fluorescence of BBR (F_0).

When necessary, the activity of the other aptamer was monitored using an identical method. However, aptamer and BBR standard solution were utilized at various and appropriate concentrations.

2.7 Cloning, colony selection, and sequencing of ssDNA

Using a mixture of PrimeStar HS (50 μL), with either 10 μM of nonmodified forward primer or reverse primer (6.0 μL), ssDNA cycle library (2 μL), and SDW (45 μL) in the thermocycler, the appropriate GOLD-SELEX cycle-ssDNA pool was amplified by PCR into the form of dsDNA. The PCR was performed under the following conditions: initial denaturation (98°C, 1 min), 30 cycles of denaturation (98°C, 10 s), annealing (57°C, 10 s), and extension (72°C, 30 s), followed by storage at 4°C until ligation. The PCR product was ligated into the pMD20-T vector using the standard protocol of the pMD20-T Vector Cloning Kit. The white colonies from the blue–white selection technique were selected from multiple plates of the cloned *E. coli*. The total picks were about 80 clones, randomly.

The colonies that exhibited the correct band size were cultured, and their plasmids were extracted using the AccuPrep Plasmid Mini Extraction Kit (Bioneer Corp., Daejeon, Republic of Korea). The plasmids were used as the templates for ssDNA production through the mentioned phosphorylated dsDNA production followed by lambda exonuclease digestion. The ssDNA from each positive colony was primarily checked for fluorescence activity. The highest fluorescence

ssDNA was subjected to analysis of the sequence using SupreDye v.1.1. The secondary structure of the obtained ssDNA was predicted using the internet tool M-fold (http://mfold.rna.albany.edu/).

2.8 Sequence evolution of the obtained aptamer

The sequences of the obtained nucleotides were systematically modified before being used for assay development. The modified sequences were simply synthesized by Fasmac Co., Ltd. (Kanagawa, Japan). The 80-nucleotide sequence was truncated, mutated, and dimerized to obtain the aptamer that increased the fluorescence from the original BBR38. The synthesized aptamers are listed in Table 8.

Table 8. The aptamer sequences used for modification of BBR38

Aptamer name	Sequence
BBR38	5′-AGCAGCACAGAGGTCAGTTCAATAAGGATGAGATATATATTAAATTATGTCATCATAATACCTATGCGTGCTACCGTGAA-3′
BBR38NP	5′-AATAAGGATGAGATATATATTAAATTATGTCATCATAATA-3′
BBR38H1	5′-AATAAGGATGAGATATATAT-3′
BBR38H2	5′-TAAATTATGTCATCATAATA-3′
BBR38S	5′-GATGAGATATATATTAAATTATGTCATC-3′
BBR38S-GC bulge	5′-GATGACATATATATTAAATTATGTCATC-3′
BBR38S-AT bulge	5′-GATGATATATATATTAAATTATATCATC-3′
BBR38S-midGC to AT	5′-GATAAGATATATATTAAATTATGTTATC-3′
BBR38S-midGC to GG	5′-GATGAGATATATATTAAATTATGTGATC-3′
BBR38S cut 2	5′-ATGACATATATATTAAATTATGTCAT-3′
BBR38S cut 4	5′-TGACATATATATTAAATTATGTCA-3′
BBR38S cut 6	5′-GACATATATATTAAATTATGTC-3′

BBR38S cut 8	5′-ACATATATATTAAATTATGT-3′
BBR38S cut 10	5′-ATATATATTAAATTAT-3′
BBR38S cut 12	5′-TATATATTAAATTA-3′
BBR38S cut 14	5′-ATATATTAAATT-3′
BBR38S loop random 1	5′-GACATAVATATTAAATTATGTC-3′
BBR38S loop random 2	5′-GACATATBTATTAAATTATGTC-3′
BBR38S loop random 3	5′-GACATATAVATTAAATTATGTC-3′
BBR38S loop random 4	5′-GACATATATBTTAAATTATGTC-3′
BBR38S loop random 5	5′-GACATATATAVTAAATTATGTC-3′
BBR38S loop random 6	5′-GACATATATATVAAATTATGTC-3′
BBR38S loop random 7	5′-GACATATATATTBAATTATGTC-3′
BBR38S loop random 8	5′-GACATATATATTABATTATGTC-3′
BBR38S loop random 9	5′-GACATATATATTAABTTATGTC-3′
BBR38S loop random 10	5′-GACATATATATTAAAVTATGTC-3′
BBR38S cut 6 A10T	5′-GACATATATTTTAAATTATGTC-3′

BBR38S cut 6 A10C	5′-GACATATATCTTAAATTATGTC-3′
BBR38S cut 6 A10G	5′-GACATATATGTTAAATTATGTC-3′
DBBR38s	5′-GACATATATCTTAAATTATGTCTTTTTTTGACATATATCTTAAATTATGTC-3′
TBBR38s	5′-GACATATATCTTAAATTATGTCTTTTTTTGACATATATCTTAAATTATGTCTTTTTTTGACATATATCTTAAATTATGTC-3′
Reported aptamer	5′-AACATAAATATTAAATTATGT-3′

2.9. Validation of microplate-based BBR fluorescence assay

The developed microplate-based BBR fluorescence assay was validated based on sensitivity, repeatability, and reliability approaches.

The assay sensitivity was evaluated using the 3.3σ/m method by reporting the LOD of the assay where σ was the standard deviation of blank solutions and m was the slope of the calibration curve. The slope of the assay was obtained from the linear range of the curve plotted between F and F_0 and the logarithm of BBR concentration (μg/mL). The various concentrations of BBR (0.78 μg/mL to 25 μg/mL; 50 μL) were challenged with the 0.5 μM TBBR38s in 50 mM Tris-HCl (50 μL).

The repeatability of the assay was determined by reporting the variation in each concentration within the determination range. The variation was reported in the form of CV%, where the CV% was calculated from the variation of $F–F_0$. The assay performed within the same plate (n = 3) is called intra-assay whereas the assay performed between the plates (n = 3) is called interassay.

The reliability of the assay and the performance of the assay through matrices were confirmed by the spike-recovery assay. The assay was challenged by two main types of samples, that is, BBR-containing samples and non-BBR-containing samples. The BBR-containing standard was Kampo medicine preparation no. 58, which contained the BBR source, Coptis rhizome,

whereas non-BBR-containing samples were tap water and Kampo medicine preparation no. 84. Known concentrations of BBR (12.5, 25.0, 50.0, 100, and 200 μg/mL) were spiked into these mentioned matrices and were evaporated at 50°C overnight. The samples were reconstituted with MeOH (1.0 mL) before being used. The amount of BBR was determined by the developed assay either in spiked or nonspiked samples. The recovery was reported as a recovery rate (%) with the following calculation:

$$\text{Recovery rate (\%)} = \frac{\text{Measured amount of BBR} - \text{BBR amount in nonspiked sample}}{\text{Spiked amount of BBR}} \times 100$$

2.10. Sample preparation of Kampo medicine and application of developed assay for BBR detection in Kampo medicine sample

Commercially available 128 Kampo medicine preparations were used in this study for the application of the developed assay. All Kampo medicine preparations were obtained from Tsumura Co. (Japan) in the granule form in the divided sachet. Each Kampo medicine preparation was powdered by a mortar and pestle. After the powder (0.8 g) was dispersed in water, it was sonicated at room temperature for 30 min. The suspension was then centrifuged at 13,200 × *g* for 30 min at 25°C. The supernatant was collected and was then loaded into Diaion HP-20 resin equilibrated with distilled water with a column volume of 5 mL. The water-soluble part was washed 10 times with distilled water (5.0 mL). The leftover residue was finally eluted using MeOH (5.0 mL) four times. The MeOH eluate (20 mL) was evaporated and reconstituted with the same volume of 5% MeOH before being used. The sample was filtered using 0.22 μm filter and used for HPLC–UV analysis and the developed fluorometric-based assay.

All the prepared Kampo medicine samples (50 μL) were mixed with 0.5 μM of TBBR38s in 50 mM Tris-HCl (50 μL). The samples that exhibited a high $F–F_0$ value were picked for further investigation. Therefore, the high BBR content samples were diluted to the appropriate concentration that could fit into the standard curve.

2.11 HPLC–UV for determination of BBR in Kampo medicine preparation

The Kampo medicinal preparation samples were tested as the comparison method for BBR determination. The flow rate of the LC-10AD VP HPLC pump (Shimadzu) was set at 1.0 mL/min. An SPD-10A UV/VIS detector (Shimadzu) whose detection wavelength was set at 345 nm was used. The Cosmosil-Packed Column 5C18-AR-II 4.6 ID × 150 mm, 5 μm particle size (Nacalai Tesque, Kyoto, Japan) was used as the reverse-phase stationary phase. The mobile phase was 30% (v/v) CH_3CN in distilled water with 0.2% (v/v) trifluoroacetic acid. The filtered Kampo medicinal preparation was injected (20 μL) and run with the abovementioned conditions for 30 min. The peak of BBR appeared at the retention time of about 9 min. The determination range of the HPLC–UV was 0.78–50.0 μg/mL. The analytical results were derived from the average of triplicate samples injected.

3. Results and discussion

3.1. Selection of aptamer enhancing fluorescence of BBR through GOLD-SELEX

Small molecules were the group of substances that was difficult to build an aptamer against them. It was extremely challenging to immobilize them on the surface of the selection platform (plate, resin, nanoparticle, and membrane) because of their small size. The small molecule was immobilized on a selection platform using chemical synthesis to produce the aptamer against small molecules. However, the bonded molecule was not the initial form of the molecule. Thus, the aptamer library, rather than the small molecule, was immobilized on the selection platform. There were a variety of strategies for immobilizing ssDNA. In contrast, colloidal gold nanoparticles were used as the immobilized platform in this investigation. The advantage of employing colloidal gold nanoparticles as a platform was that the aptamer could be attached to the surface of the nanoparticles. The immobilization of the aptamer was independent of the anchor sequences of the complement. Thus, the selection was conducted with the stipulation that the aptamers be folded into their original folding configuration. Additionally, colloidal gold nanoparticles are inexpensive and commercially accessible. The selection by colloidal gold nanoparticles may easily distinguish the bound sequence from the eluted sequence. The colloidal gold nanoparticles can be centrifuged and cleaned.

Figure 21 depicts the overall GOLD-SELEX procedure. The initial cycle began with the immobilization of the ssDNA pool, followed by the cleaning of an excessive particle. Once BBR

was introduced into the system, the sequences with a great affinity for BBR were liberated from the surface of the colloidal gold nanoparticles. The released sequences were used as the template for PCR to produce a new library for the subsequent cycle. As the cycle number grew, the system pressure was increased by decreasing the BBR concentration and exposure time. When the template was amplified by general PCR and run on gel electrophoresis, the 80 bps band size confirmed the eluate (Fig. 22). The method was repeated until the ssDNA pool no longer displayed a greater fluorescence level.

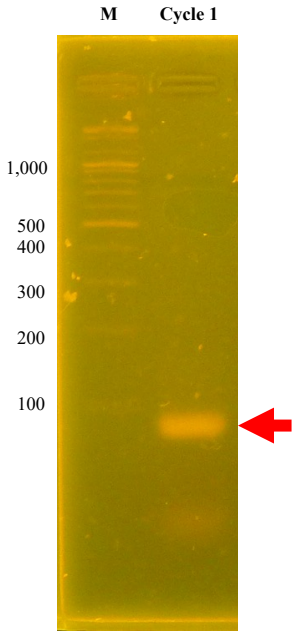

Figure 22 PCR products amplified using cycle 1 ssDNA library eluate as a template. Lane M indicates the 100 bps marker. Lane 1 represents the PCR products when using cycle 1 ssDNA library as a template. The band was expected to be observed under 100 bps marked with a red arrow. The gel electrophoresis was performed using 1% (w/v) agarose

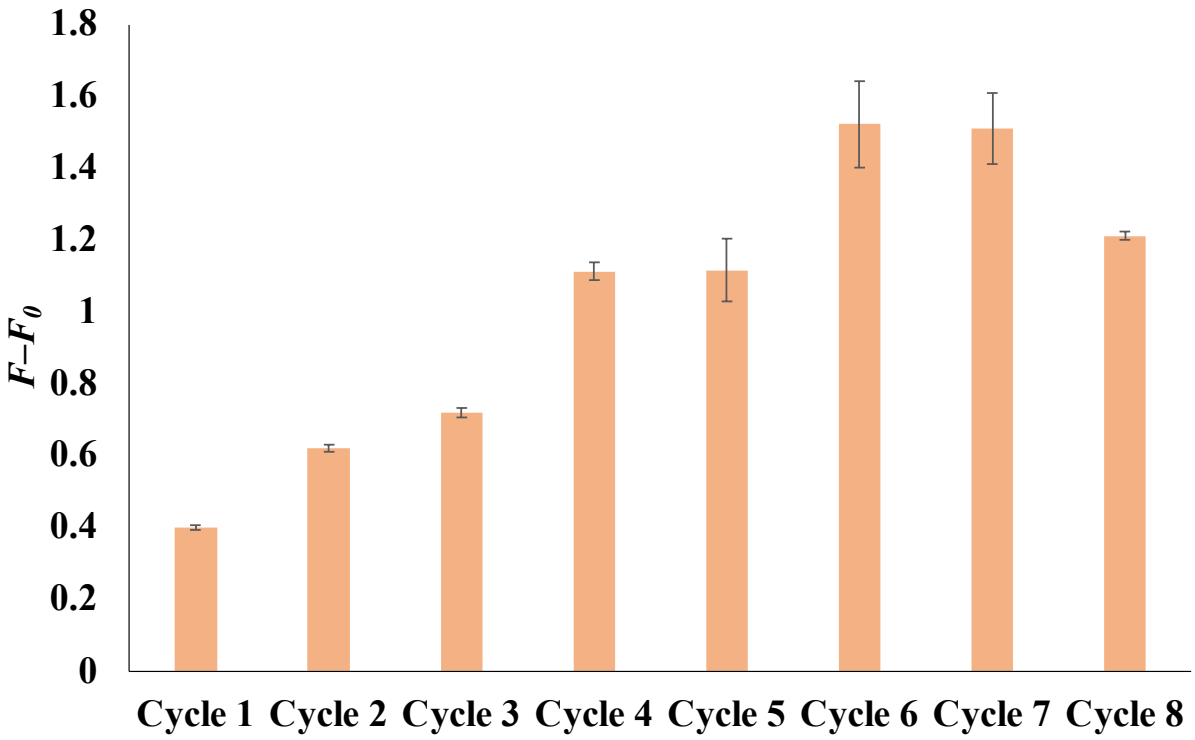

Figure 23 Fluorescence activities of various cycles of ssDNA (0.25 µM) obtained from GOLD-SELEX against BBR (6.25 µg/mL)

According to the results, the fluorescence activity against BBR increased from cycle to cycle until it reached saturation at Cycles 6 and 7 (Fig. 23), which indicated that the sequences that exhibit high fluorescence against BBR were enriched. However, the fluorescence slightly decreased at Cycle 8. This might be because the major sequences in the pool exhibit lower fluorescence when compared to the minor sequences, which might be lost on selection. Thus, the ssDNA library from Cycle 7 was used for cloning further.

The ssDNA library from Cycle 7 was successfully cloned into JM109 *E. coli*. 45 colonies out of a total of 80 sampling colonies exhibited the expected band size at about 250 bps (Fig. 24). The plasmids obtained from these 45 colonies were used as templates for ssDNA syntheses. The fluorogenic activity when these ssDNAs (0.25 µM) were exposed to the BBR (6.25 µg/mL) was investigated. The results indicated that the colony BBR38 exhibited the highest fluorogenic activity (Fig. 25). Thus, the BBR38 sequence was used for further characterization and modification.

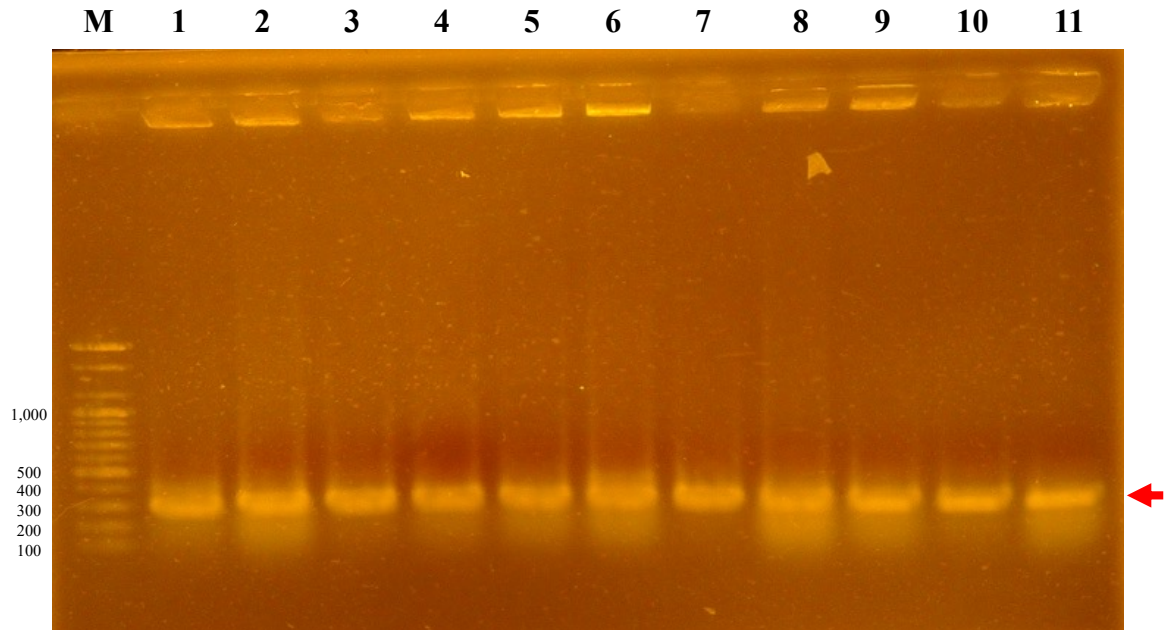

Figure 24 Colony PCR of the colonies selected from Cycle 7 of GOLD-SELEX. Lane M was the 100 bps marker. Lanes 1–10 represented the PCR products from that colony number. The band was expected to be observed at ~250 bps marked with a red arrow. The gel electrophoresis was performed using 1% agarose

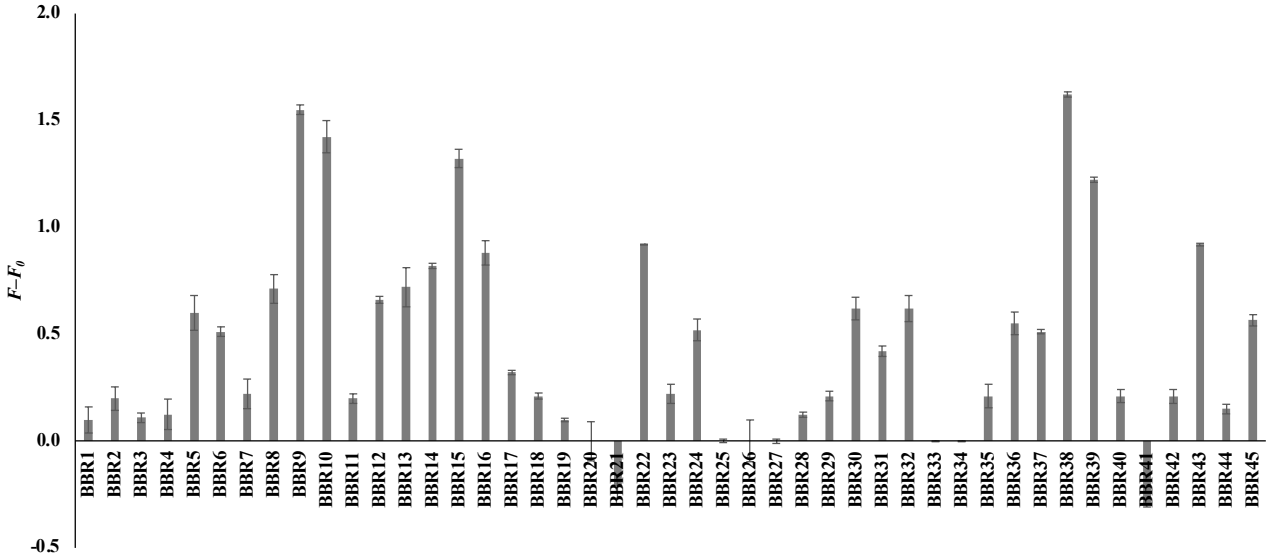

Figure 25 Fluorogenic activity of ssDNA (0.25 µM) against BBR (6.25 µg/mL) from each colony

3.2. Sequence modification of BBR38 for fluorescence enhancement

The complete length of the aptamer could be applied directly to the development of the BBR detection assay. Nevertheless, there was a portion of the sequence that did not contribute to the fluorescence of the BBR–aptamer complex. To get insight into the binding moiety of BBR38 to BBR and to reduce the cost of synthesis, the smallest unit that is capable of fluorescence against BBR needs to be elucidated. Additionally, certain portions of the sequence could be altered to increase the fluorescence intensity.

Initially, the BBR38 was truncated by removing the primer binding site yielding BBR38NP. The constant concentration of BBR (12.5 μg/mL) was utilized to examine the fluorogenicity of aptamers at various concentrations. The results demonstrated that the fluorescence of the original BBR38 was saturated at 5 μM of aptamer, whereas the fluorescence of BBR38NP was not saturated at that concentration (Fig. 26). Furthermore, the overall fluorescence of BBR38NP was greater than that of the original BBR38. Consequently, the primer binding site was found not to be involved in the fluorogenicity of the BBR aptamer.

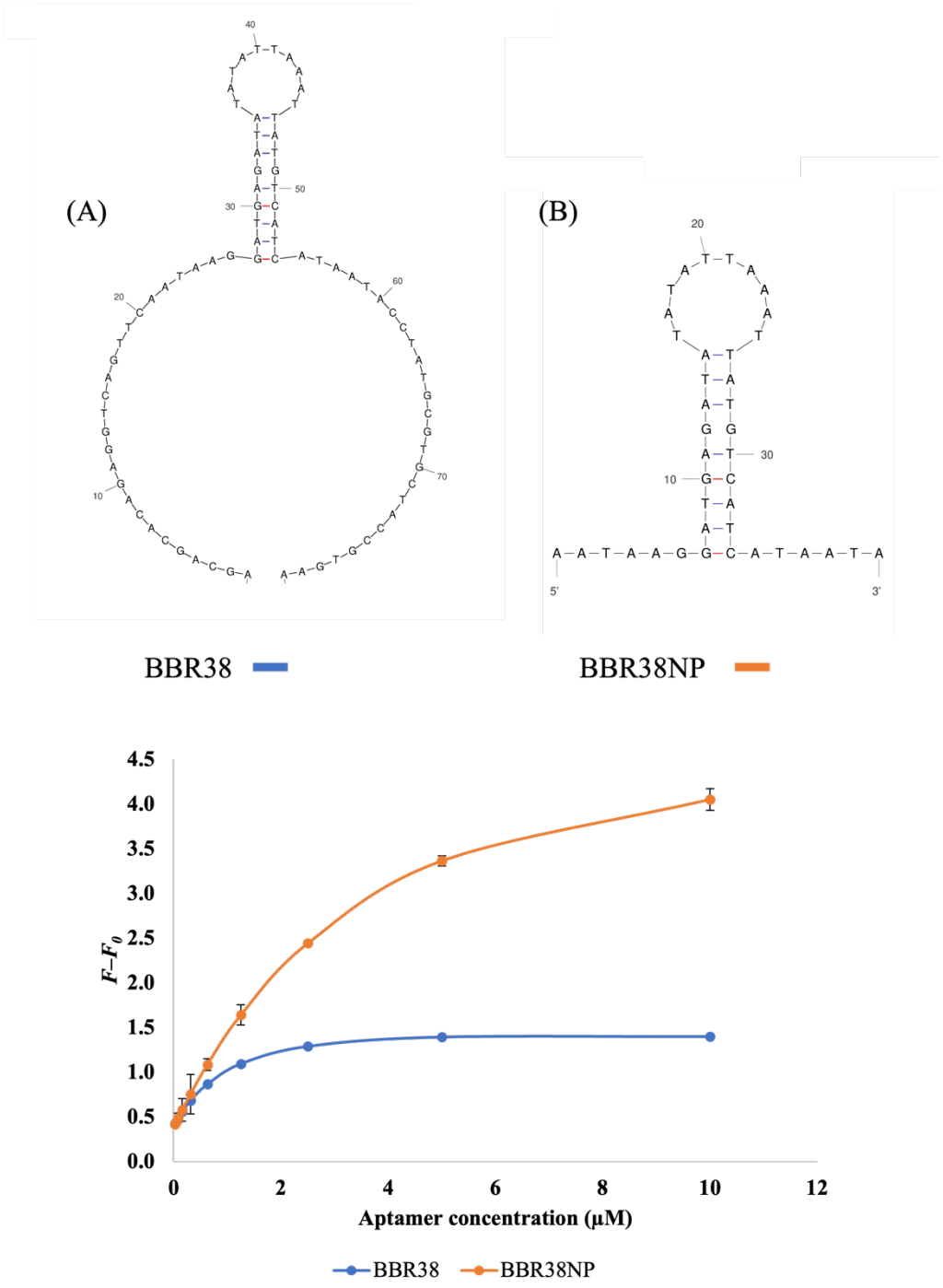

Figure 26 Fluorogenicity of BBR38 and BBR38NP at various concentrations. The blue line indicates the fluorescence obtained from (A) BBR38, while the orange line indicates the fluorescence obtained from (B) BBR38NP. The concentration of BBR in the assay was constant at 12.5 μg/mL. The secondary structures of (A) BBR38 and (B) BBR38NP were predicted using M-fold web server

The BBR38NP sequence was truncated into two halves, BBR38H1 and BBR38H2, to demonstrate the need for the BBR38NP sequence for fluorescence generation against BBR. The results demonstrated that the stem and loop structures of BBR38NP were required for fluorescence (Fig. 27). Neither BBR38H1 nor BBR38H2 exhibited as high level of fluorescence as their parents, BBR38NP, when the sequence was cut in half.

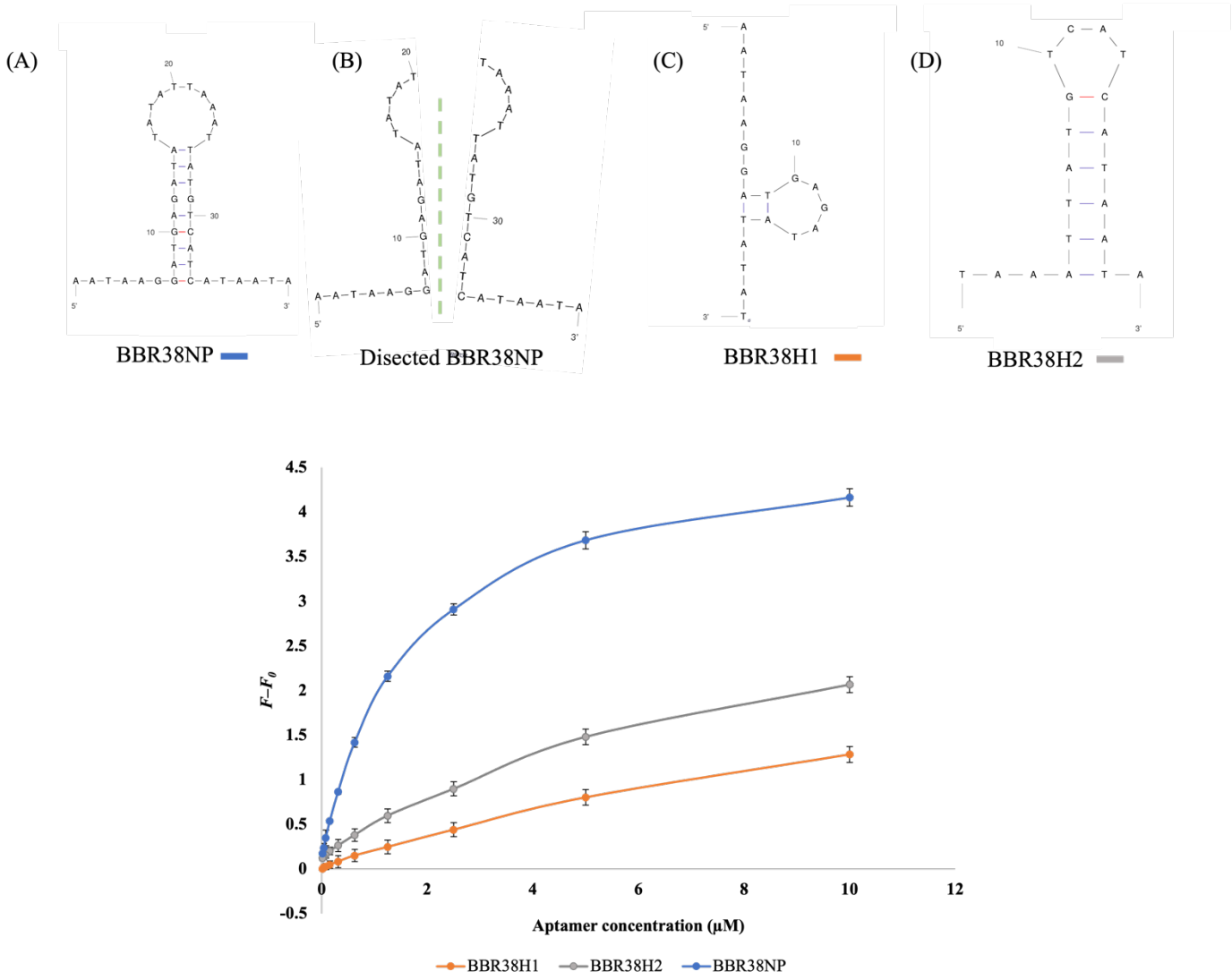

Figure 27 Fluorogenicity of BBR38NP and its half sequences in various concentrations. The blue line indicates the fluorescence obtained from (A) BBR38NP, while the orange and gray lines indicate the fluorescence obtained from (C) BBR38H1 and (D) BBR38H2, respectively. The concentration of BBR in the assay was constant at 12.5 µg/mL. (B) The structure of BBR38NP was cut in half in the middle of the sequence. The secondary structures of (A) BBR38NP, (C) BBR38H1, and (D) BBR38H2 were predicted using M-fold web server

Some BBR38NP parts were not included in the stem-loop design. It was hypothesized that these parts were unnecessary for fluorescence generation. To clarify the hypothesis, the BBR38NP tail was removed, resulting in BBR38S. The results revealed that nonstem-loop tails were not necessary for fluorescence generation, as the fluorescence increased when these tails were removed (Fig. 28). Although the phenomenon was only observed when the aptamer concentration exceeded 1.25 μM, removing these tails would still be advantageous because it would reduce the cost of aptamer synthesis. At this point, it was discovered that the fluorescence of truncated aptamer was comparable to that of previously reported aptamer screening by other aspects [60].

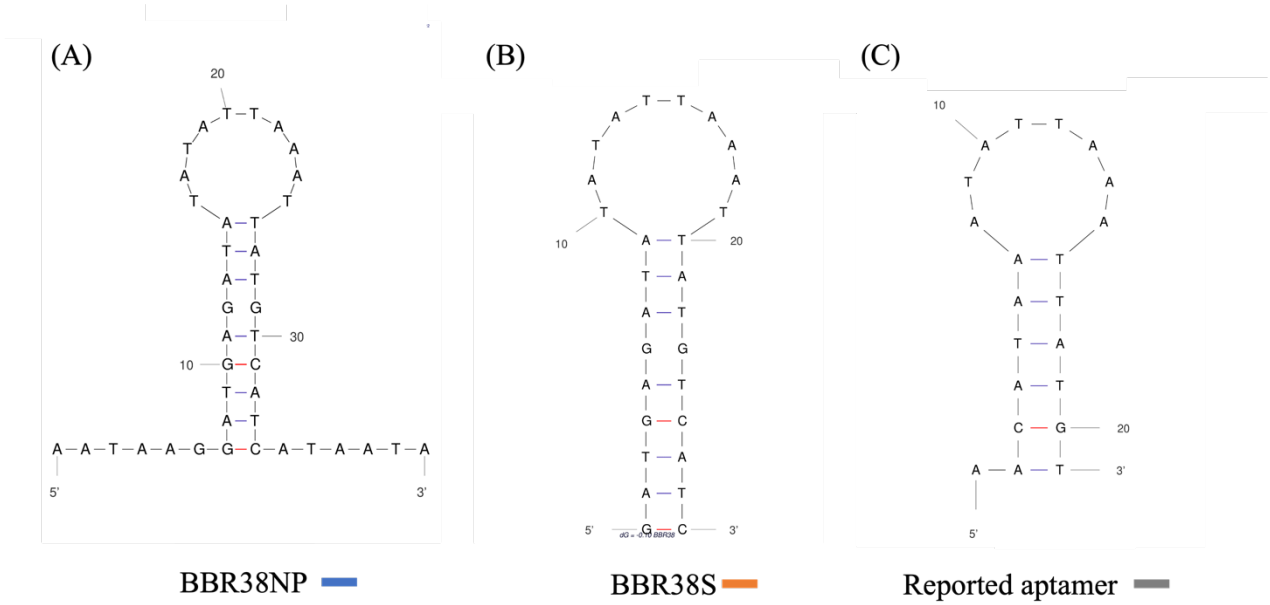

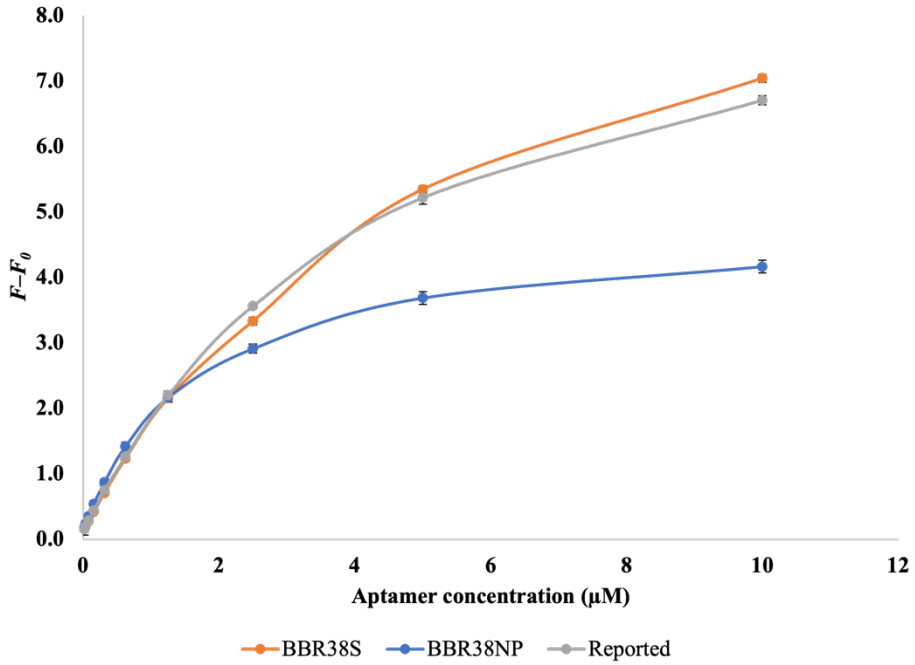

Figure 28 Fluorogenicity of BBR38NP and BBR38S in various concentrations. The blue line indicates the fluorescence obtained from (A) BBR38NP, while the orange and gray lines indicate the fluorescence obtained from (B) BBR38S and (C) reported aptamer, respectively. The concentration of BBR in the assay was constant at 12.5 μg/mL. The secondary structures of (A) BBR38, (B) BBR38NP, and (C) reported aptamer were predicted using M-fold web server

The predicted secondary structure of BBR38S' stem featured one G–G bulge (Fig. 29; circled in red). Mutation was used to investigate the bulge. To close the bulge of G–G, the G6C BBR38S mutation (BBR38S-GC bulge) was created to form the G–C linkage as an example of the bulge's strong bonding. Additionally, the A–T linkage variant with weaker bonding (BBR38S-AT bulge) was used as a comparison. The results demonstrated that the overall fluorogenicity of BBR38S was enhanced when the bulge was closed with either a G–C or an A–T linkage (Fig. 29). Almost identical fluorescence was obtained from these closed bulge forms. This suggested that the bulge in their stem may inhibit fluorescence production. Although the characteristics of the G–C and A–T linkages were comparable, the A–T linkage variant was chosen for further structure modification because its fluorescent was slightly higher than that of the G–C linkage counterparts.

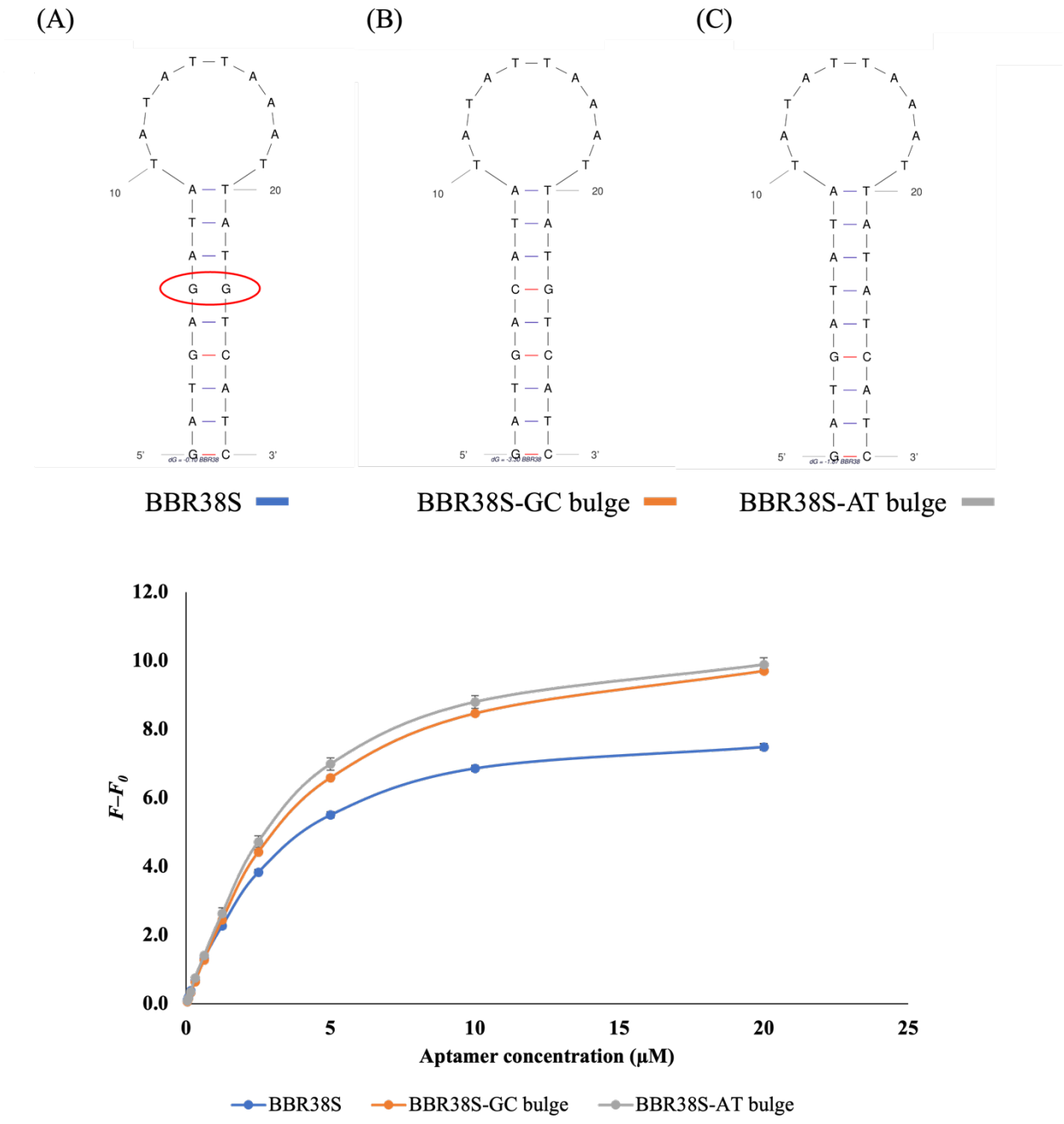

Figure 29 Fluorogenicity of BBR38S and their close bulge variants in various concentrations. The blue line indicates the fluorescence obtained from (A) BBR38S. The orange and gray lines indicate the fluorescence obtained from (B) BBR38S-GC bulge and (C) BBR38S-AT bulge, respectively. The concentration of BBR in the assay was constant at 12.5 µg/mL. The secondary structures of (A) BBR38S, (B) BBR38S-GC bulge, and (C) BBR38S-AT bulge were predicted using M-fold web server. The red circle in structure (A) indicates the bulge in the structure

The middle G–C linkage between G4 and C24 (Fig. 30; circled in red) was examined before further modification. The G–C linkage was changed to an A–T linkage (BBR38S-midGC to AT) because the A–T linkage forms a weaker bond. At this point, the G–G mutation was also altered to represent the open bulge form. The result revealed that the mutation in this linkage decreases the fluorescence of the original BBR38S (Fig. 30). This corresponded to the changes in predicted secondary structures from its parent. Thus, the G–C bond between G4 and C24 was required for fluorescence production.

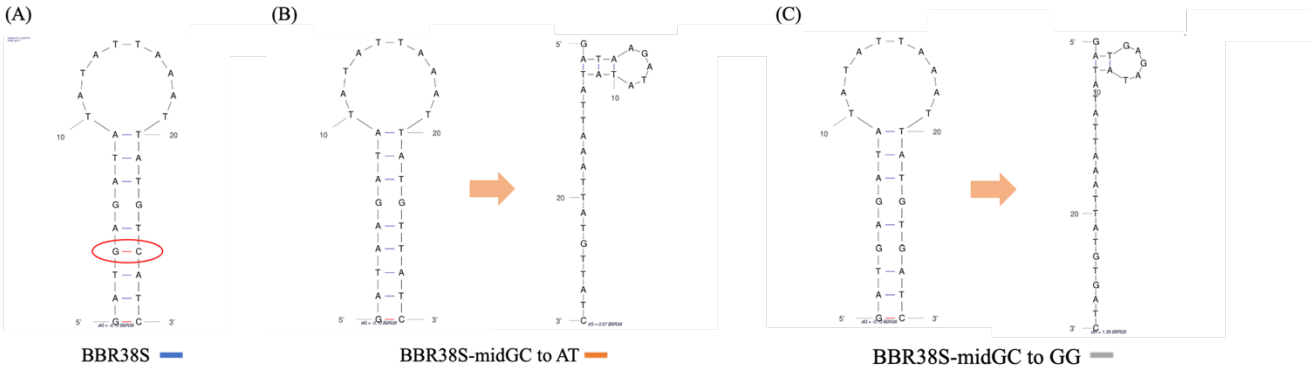

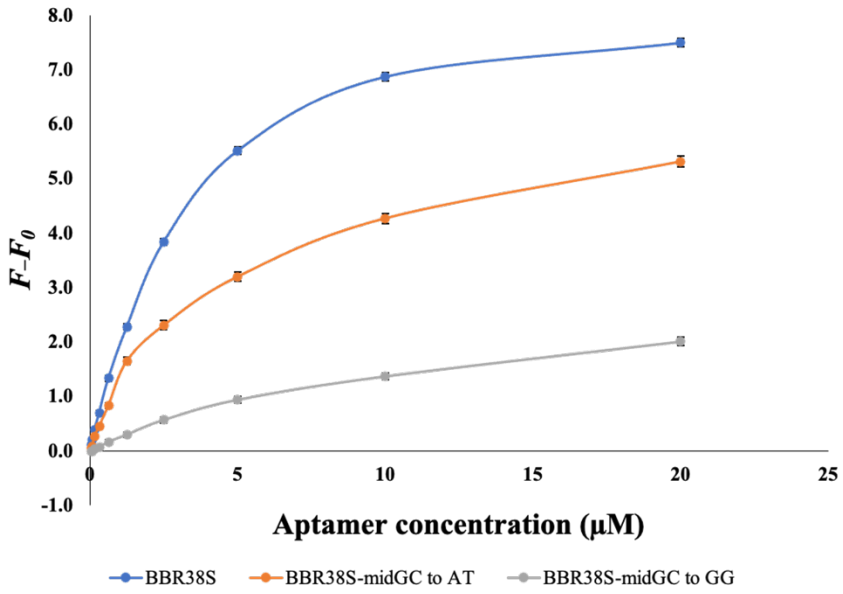

Figure 30 Fluorogenicity of BBR38S and their middle bulge modification variants in various concentrations. The blue line indicates the fluorescence obtained from (A) BBR38S. The orange and gray lines indicate the fluorescence obtained from (B) BBR38S-midGC to AT and (C) BBR38S-midGC to GG, respectively. The concentration of BBR in the assay was constant at 12.5 μg/mL. The secondary structures of (A) BBR38S, (B) BBR38S-midGC to AT, and (C) BBR38S-midGC to GG bulge were predicted using M-fold web server. The structures prior the arrow of (B) and (C) were the expected structures. The red circle in structure (A) indicates the bulge in the structure

The BBR38S-AT bulge was further reduced to yield minimal fluorogenic structure results. Each time, two nucleotides were removed from the stem of BBR38S-AT, as the stem is composed of complementary bases. To compare fluorescence, a total of eight forms of truncated BBR38S-AT (ranging from 2 to 14 nucleotides) were utilized. As shown in Figure 31, the fluorescence increased to the same degree when 2–6 nucleotides were removed. When eight nucleotides were removed from the initial structure, lower fluorescence was observed as compared with the BBR38S-AT bulge. When more than eight nucleotides were removed from the initial structure, the fluorescence decreased dramatically. This corresponds to the predicted secondary structures of the aptamers. The BBR38S-AT bulge stem-loop was maintained until cutting the six nucleotides (Fig. 31D). The removal variants of 2–6 nucleotides displayed nearly identical fluorescence. Therefore, BBR38S cut 6 (Fig. 31D) was selected for further truncation as the minimal structure capable of exhibiting high fluorescence.

(A) (B) (C) (D)

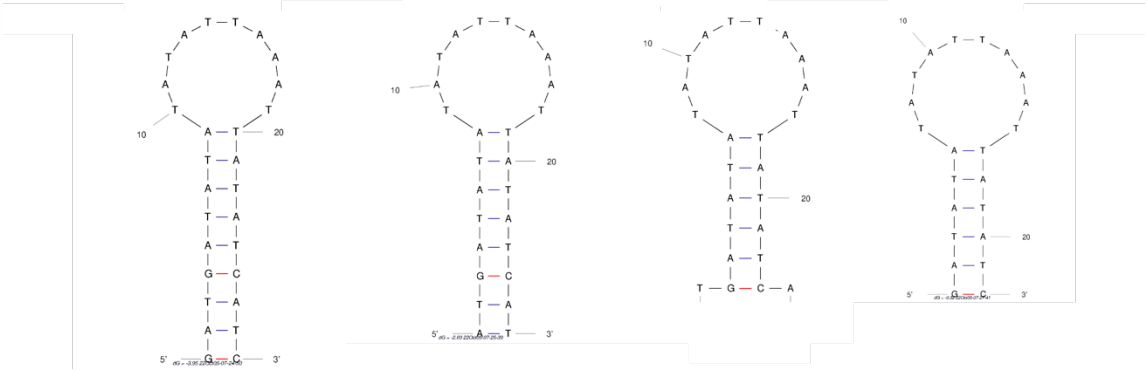

BBR38S-AT bulge. BBR38S cut 2 BBR38S cut 4 BBR38S cut 6

(E) (F) (G) (H)

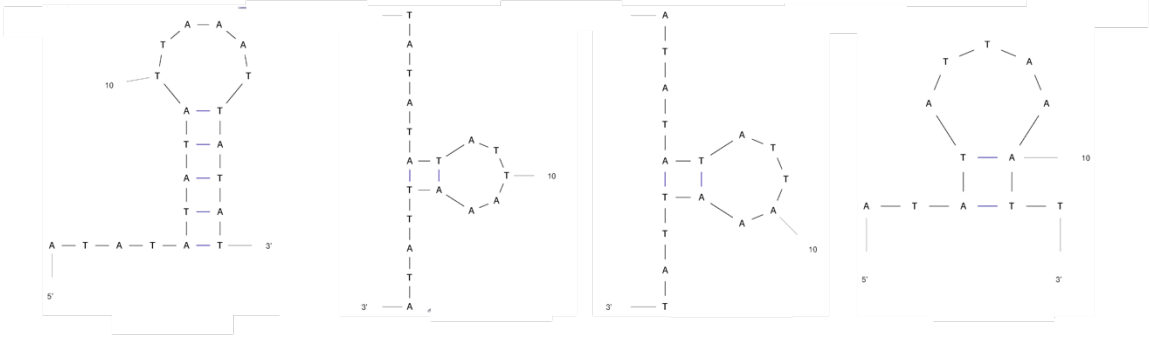

BBR38S cut 8 BBR38S cut 10 BBR38S cut 12 BBR38S cut 14

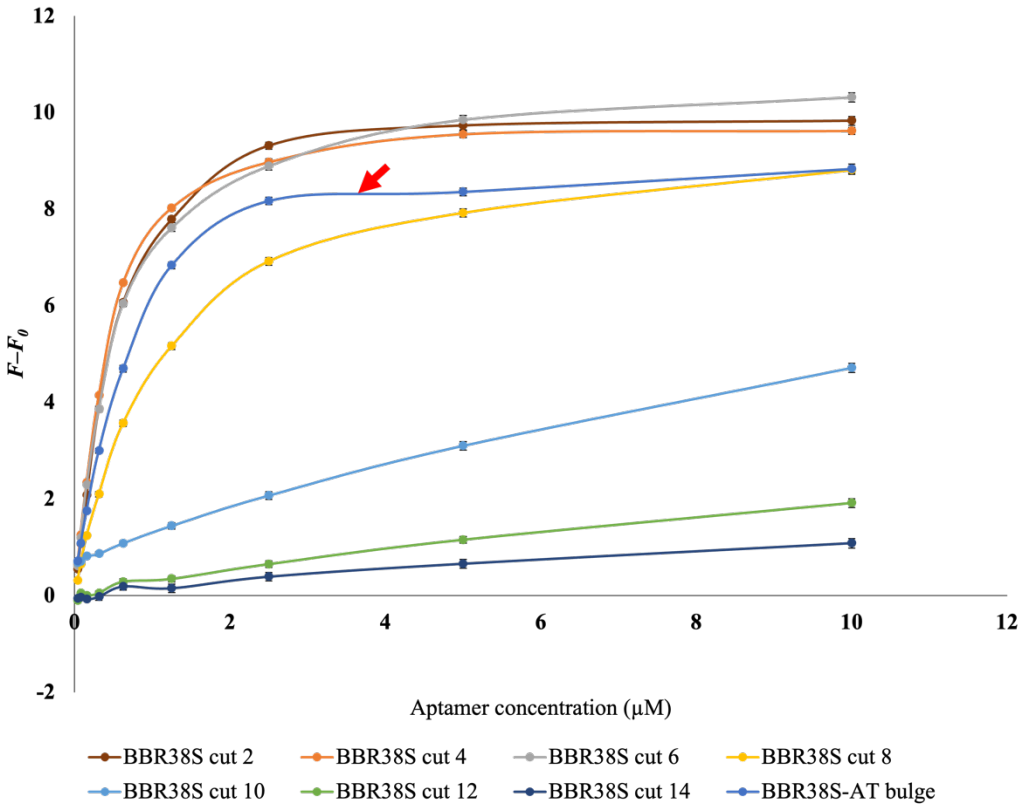

Figure 31 Fluorogenicity of BBR38S-AT bulge and their truncated variants in various concentrations. The concentration of BBR in the assay was constant at 12.5 μg/mL. The blue line indicates the fluorescence obtained from (A) BBR38S-AT bulge. The other lines indicate the fluorescence obtained from (B) BBR38S cut 2, (C) BBR38S cut 4, (D) BBR38S cut 6, (E) BBR38S cut 8, (F) BBR38S cut 10, (G) BBR38S cut 12, and (H) BBR38S cut 14, by their indicated colors in the curve. The secondary structure of (A) BBR38S-AT bulge and (B–H) truncated BBR38S (removal of 2–14 nucleotides) were predicted using M-fold web server. The red arrow in the curve indicates the fluorescence obtained from the BBR38S-AT bulge curve

After focusing on the stem, the loop of the structure is also of interest. The loop nucleotides (nucleotide positions 6–18) were mutated using nonself-mutation. The ssDNA pool, which contained nucleotides other than the original nucleotides, was used to screen the important position. The ssDNA pool of any position which could exhibit higher fluorescence than the BBR38S cut 6 was further investigated in depth. However, the nucleotides at positions 6 and 18 were omitted from the mutation because this position was the origin of the stem. The results found that the only position that enhanced the fluorescence was nucleotide at position 10. Thus, the nucleotide at position 10 was further mutated.

The detailed mutation results revealed that the BBR38S cut 6 A10T (Fig. 32B) and BBR38S cut 6 A10C (Fig. 32C) showed almost identical fluorescence, which was the highest fluorescence among their variants, whereas the BBR38S cut 6 A10G (Fig. 32D) showed enhanced fluorescence at a lower concentration. However, the fluorescence was decreased at a higher concentration. Thus, the BBR38S cut 6 A10C variant was selected as the candidate for modification further.

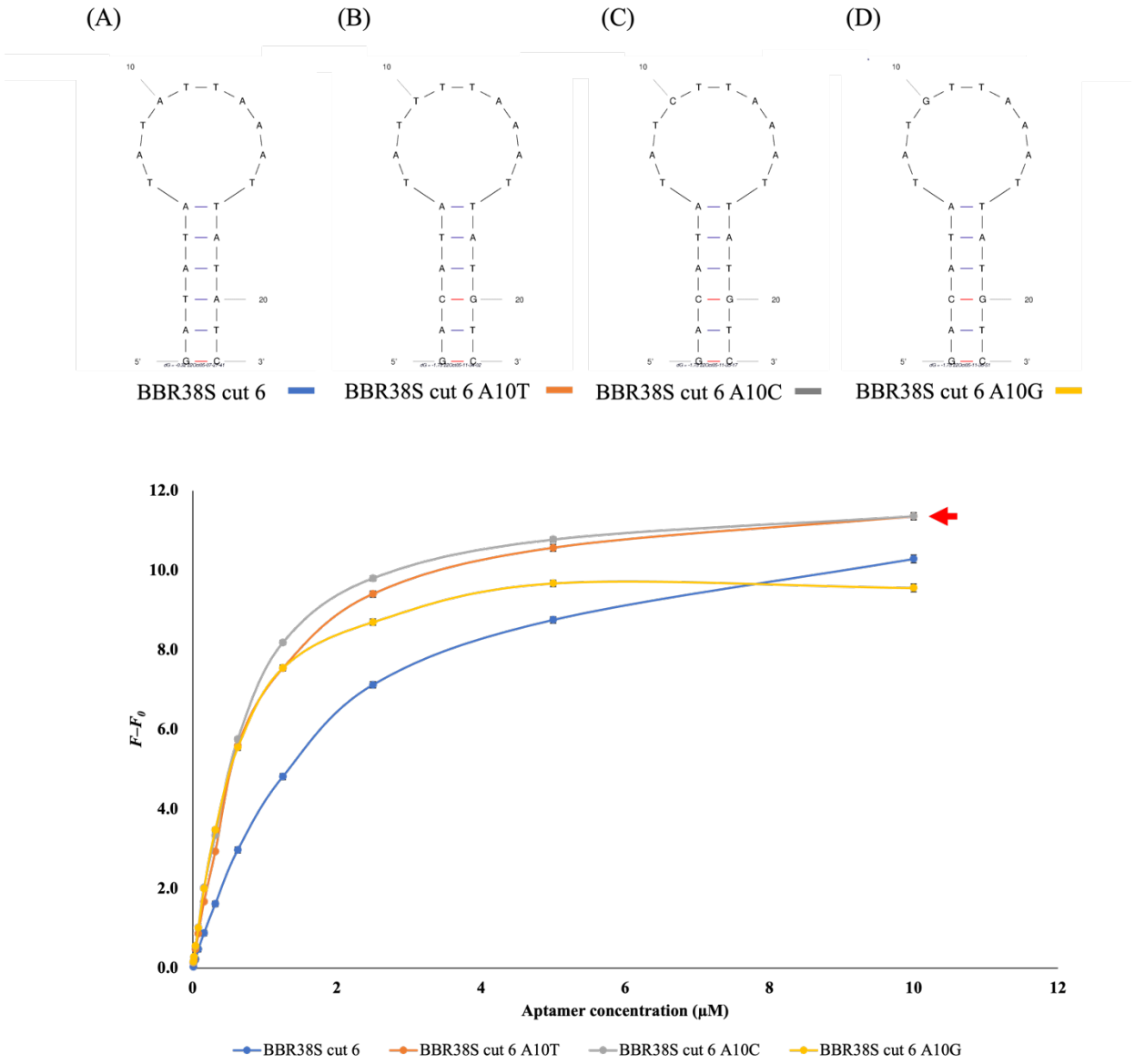

Figure 32 Fluorogenicity of BBR38S cut 6 and their loop mutation variants in various concentrations. The blue line indicates the fluorescence obtained from (A) BBR38S cut 6. The orange, gray, and yellow lines indicate the fluorescence obtained from (B) BBR38S cut 6 A10T, (C) BBR38S cut 6 A10C, and (D) BBR38S cut 6 A10G, respectively. The concentration of BBR in the assay was constant at 12.5 μg/mL. The secondary structure of (A) BBR38S cut 6, (B) BBR38S cut 6 A10T, (C) BBR38S cut 6 A10C, and (D) BBR38S cut 6 A10G were predicted using M-fold web server. The red arrow indicated the superior fluorescence obtained from (B) BBR38S cut 6 A10T and (C) BBR38S cut 6 A10C

One technique for improving the performance of the aptamer was to polymerize the active aptamer [62]. The flexible T-7 linker, which consisted of the repeat of seven thymine nucleotides, was used in this study to polymerize the BBR38S cut 6 A10C into dimers and trimers. The aptamers (1 μM) were challenged with various concentrations of BBR to demonstrate the clear performance of polymerization. The results found that the aptamers exhibited higher fluorescence when the number of polymers was increased (Fig. 33). Although the linear range of these three variants was almost identical, the higher fluorescence intensities facilitate the ability to identify the BBR-containing sample from the impurity noise that might be contained in some samples. The calculated LODs of monomer, dimer, and trimer aptamers were 0.627 μg/mL, 0.566 μg/mL, and 0.431 μg/mL, respectively. These results indicated that the detection limit of these aptamers has slightly improved. Thus, the TBBR38s were used as the detection element for further study.

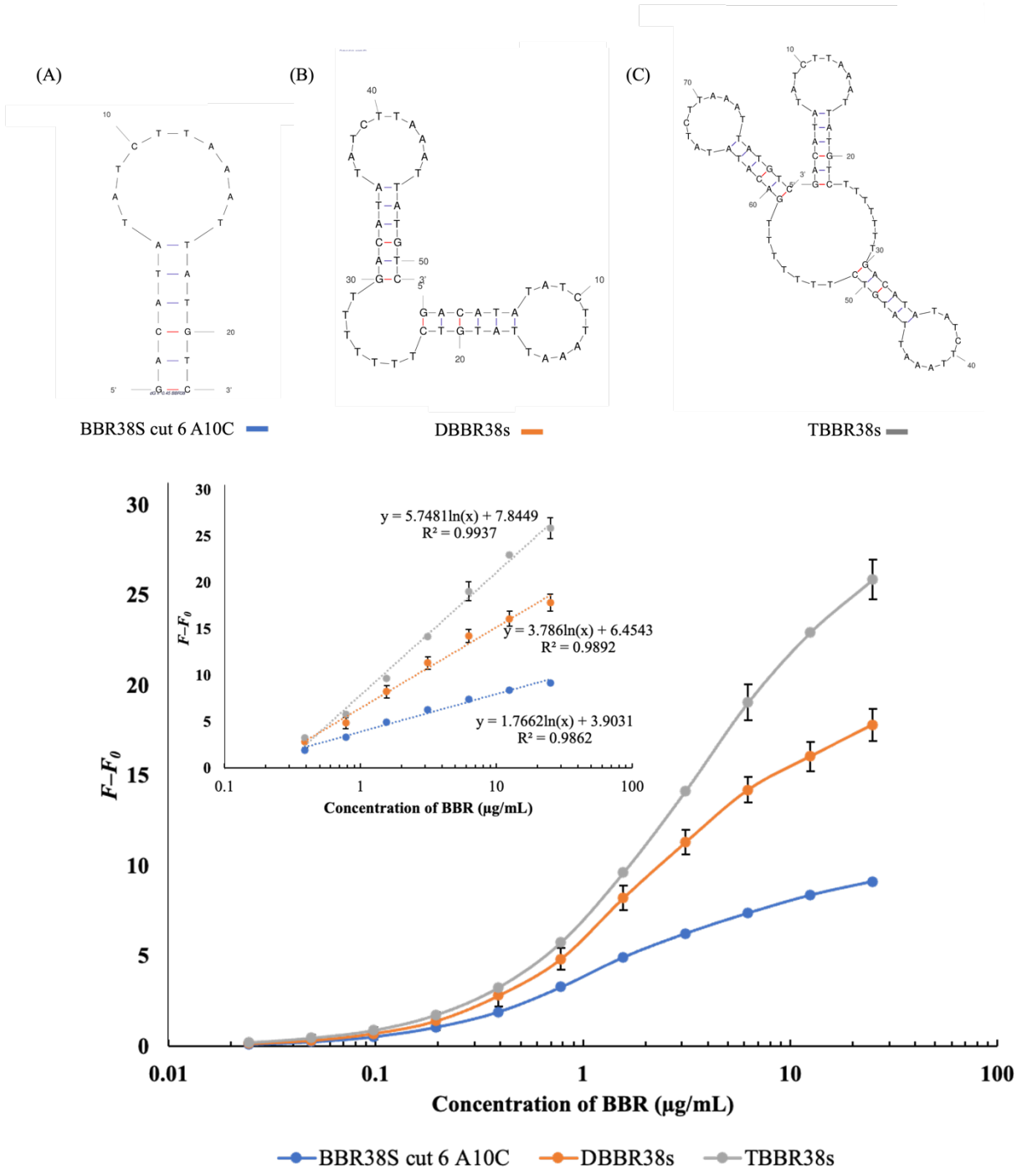

Figure 33 Activity of BBR38S cut 6 A10C and their polymer variants against various concentrations of BBR. The inset figure shows the linearity range of the curve. The blue, orange, and gray lines indicate the fluorescence obtained from (A) BBR38S cut 6 A10C, (B) DBBR38s, and (C) TBBR38s, respectively. The secondary structure of (A) BBR38S cut 6 A10C, (B) DBBR38s, and (C) TBBR38s were predicted using M-fold web server.

3.3. Microplate-based BBR detection using aptamer

In this study, the aptamer was used as a label-free fluorescent-based BBR detection. As demonstrated in Figure 20, the intrinsic fluorescence of BBR was weak, as was the intrinsic fluorescence of aptamers, which showed low or no emission of the fluorescence when excited at 360 nm. When the BBR was mixed with the appropriate aptamer, the fluorescence was enhanced by the interaction between the aptamer and the BBR. The error from the matrix or intrinsic fluorescence of the sample, which could interfere with the result, was eliminated by using the fluorescence differences between generated fluorescence (F) and intrinsic fluorescence (F_0). Under the provided circumstances, the fluorescence sensing system of BBR for detection in the matrix can be achieved.

3.4 Assessment of TBBR38s reactivity

A fluorometry-based BBR detection assay was used to investigate TBBR38s' reactivity. The constant concentration of TBBR38s (1 μM) was mixed with various concentrations of BBR (Fig. 34). The linear determination range was found to be 0.780–25.0 μg/mL, with a calculated LOD of 0.431 μg/mL. The developed method was not as highly sensitive as the other established methods such as HPLC–UV (LOD; 0.7 ng/mL) [63] and electrochemical method (LOD; 0.14 μM) [64]. However, the advantage of the developed method is a 5 min analysis time. Moreover, the assay could be conducted with multiple samples at the same time. This decreases the labor-intensiveness of the analytical method. In modern times, the antibody was the detection element that generally compared with aptamer. It was found that the sensitivity of this developed assay was almost identical to the icELISA developed using MAb against BBR (LOD; 740 ng/mL) [65] and was superior to the assay developed by single-chain variable fragment against BBR (LOD was not reported; mg level) [66]. Thus, this method could be used as an alternative method for antibody-based assays, which require an animal for production and take a long time to produce.

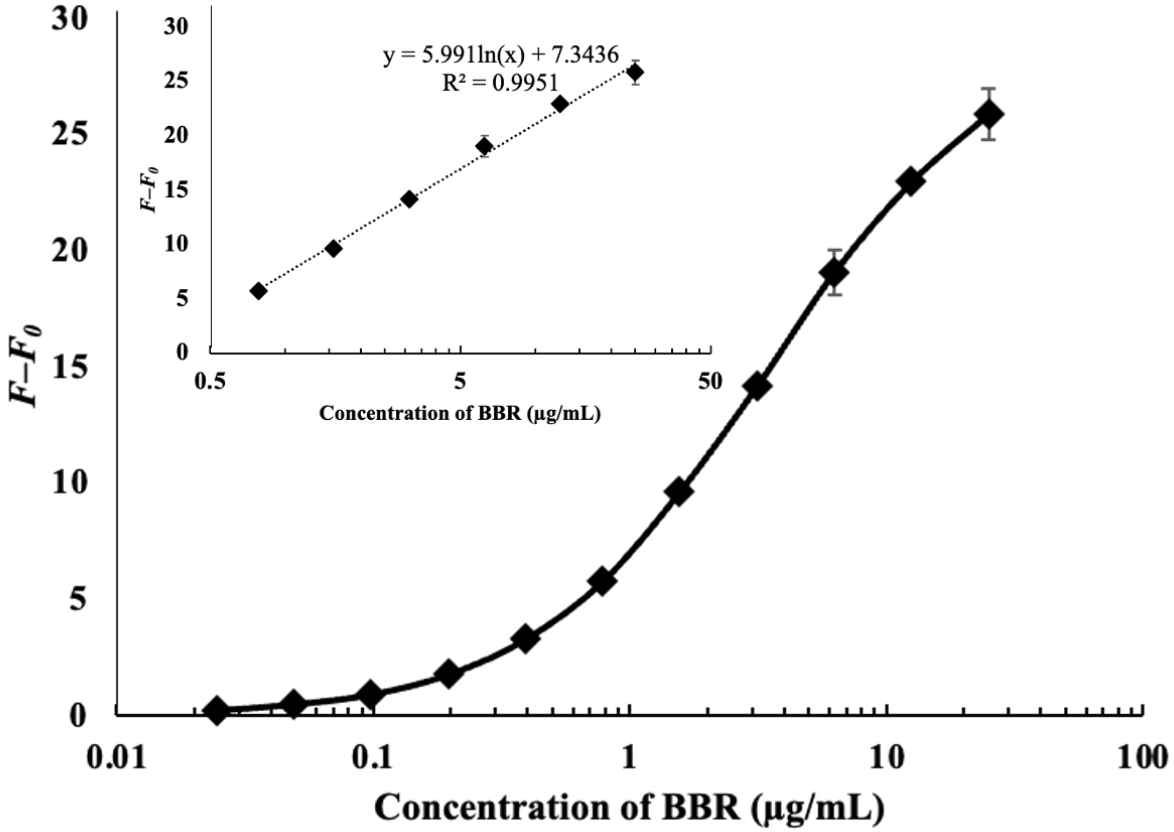

Figure 34 Standard curve for determination of BBR using fluorometric-based assay. The constant concentration of TBBR38s was applied as 1 µM. The inset shows the linear determination range for BBR (0.780–25.0 µg/mL).

3.5. Selectivity of TBBR38s

The aptamer is comprised of a set of limited nucleotides (A, T, C, and G). The arrangement of these nucleotides could interact with the target compound as the pocket or other patterns. There are some possibilities that the aptamer selected from one compound could bind to the nontarget compound because of the small molecular size of the small molecules. Thus, the CR test was performed in this study. Twenty compounds (25 µg/mL) were evaluated with the developed assay. The results found that the fluorescence was obtained from some structurally related compounds such as dihydroberberine and coptisine (Fig. 35). The fluorescence intensities of these compounds were less than half of those of BBR. Dihydroberberine seemed to be the compound that has to be considered when the sample containing a high amount of this compound was analyzed. The CR might be due to the minimal structure differences between BBR and dihydroberberine

(hydrogenation). The Coptis rhizome and Phellodendron bark were highlighted as the target plants because the assay was developed to analyze the BBR content in Kampo medicine preparation. According to JP18th, the BBR content in Coptis rhizome and Phellodendron bark should be higher than 4.2% (42 mg/g) and 1.2% (12 mg/g), respectively [35, 36]. The dihydroberberine content was reported in *Coptis chinensis* Makino (Rhizome) and *Phellodendron chinense* Schneider (Bark) as 37.6 µg/g [67] and 22.4 µg/g [68], respectively. The dihydroberberine content was more than 500 times lower than the BBR in each sample. The variance that could be found in BBR detection, specifically in Kampo medicine preparation, was expected to be minimal. Thus, the TBBR38s could be a good candidate for the development of a BBR detection system in Kampo medicine preparation samples.

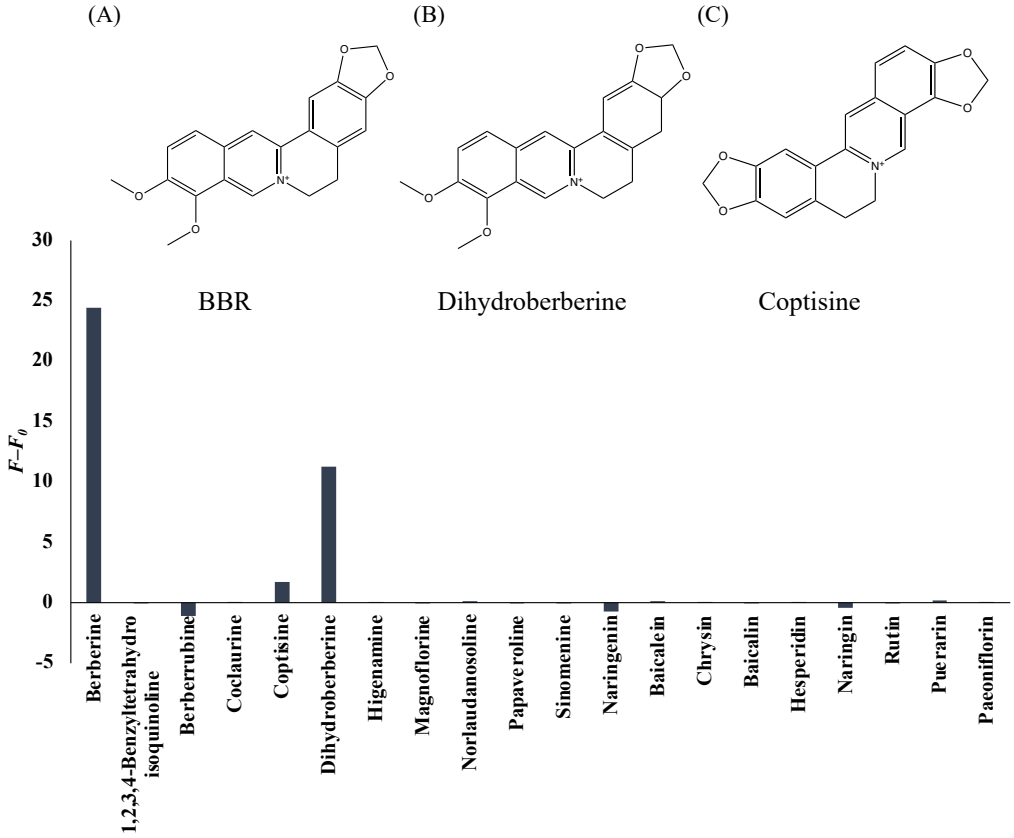

Figure 35 CR of TBBR38s against various natural compounds (25.0 µg/mL). The compounds were evaluated with a constant concentration of TBBR38s (1 µM). The structures on top were the cross-reacted compounds, i.e., (B) dihydroberberine and (C) coptisine compared with (A) BBR

3.6. Validation of TBBR38s-based assay

The coefficient of variation (CV, %) was used to report the assay's repeatability. The variations of each detectable concentrations of BBR (25.0, 12.5, 6.25, 3.13, 1.56, and 0.780 μg/mL) were assessed by means of intra (n = 3) and interassay (n = 3). As demonstrated in Table 9, the variation within the plate was in a range of 0.168% to 2.66%, whereas the variation between the plates was in a range of 4.09% to 4.95%. This indicates that the developed assay has sufficient repeatability.

Table 9. Variation of the developed TBBR38s-based assay indicated by intra and interassay CV (%)

BBR concentration (μg/mL)	CV (%)	
	Intra-assay	Interassay
	(n = 3)	(n = 3)
25.0	0.168	4.73
12.5	2.08	4.09
6.25	1.58	4.28
3.13	0.400	4.33
1.56	1.24	4.35
0.780	2.66	4.95

Above values indicate the CV calculated from the below formula:
CV = standard deviation (SD) /mean × 100.

Moreover, the accuracy of the assay was represented through a spike-recovery test. The test sample was comprised of Kampo medicine preparation no. 58, which contained the BBR source, the Coptis rhizome, while the non-BBR-containing samples comprised tap water and Kampo medicine preparation no. 84 with spiking BBR (12.5, 25.0, 50.0, 100, and 200 μg). The results showed that the recovery was between 91.2% and 108% (Table 10). This indicated that the developed assay was sufficiently accurate for Kampo medicine preparation analysis.

Table 10. The percentages of recovery obtained from spiked BBR in various samples

Sample	Spiked amount of BBR (μg)	Measured amount of BBR (μg)	CV (%)	Recovery amount (μg)	Recovery (%)
Tap water	0.00	0.00	ND	0.00	ND
	12.5	11.4	0.439	11.4	91.2
	25.0	24.2	0.867	24.2	96.8
	50.0	49.5	4.46	49.5	99.0
	100	105.2	4.32	105	105
	200	194	2.00	194	97.1
Kampo no. 58	0.00	298	0.751		
	12.5	311	0.712	13.1	105
	25.0	326	1.02	28.1	112
	50.0	352	1.75	54.0	108
	100	395	1.41	97.4	97.4
	200	510	1.89	212	106
Kampo no. 84	0.00	0.501	2.00		
	12.5	12.2	0.823	11.7	93.6
	25.0	26.0	4.27	25.5	102
	50.0	52.2	10.7	51.7	103
	100	103	5.09	102	102
	200	200	3.38	199	99.7

Note: ND, not detected.

3.7. Actual application of the developed fluorometric-based assay

To check the performance of the fluorometric-based assay, 128 Kampo medicine preparations were used as the sample for BBR determination. There was a total of 15 Kampo medicine preparations that were positive with screening tests, that is, Kampo nos. 14, 15, 37, 46, 50, 57, 58, 67, 73, 80, 91, 93, 113, 120, and 136. The positive Kampo medicine preparations corresponded to the preparations containing Coptis rhizome and Phellodendron bark reported by the company. Thus, these preparations were analyzed further to obtain the exact amount of BBR in the samples. The results showed that the BBR content obtained from the fluorometric-based assay corresponded to that obtained from HPLC–UV (Table 11; Fig. 36). This indicated that the fluorometric-based assay could be used for Kampo medicine preparation analysis along with the conventional method. Even so, the contents of BBR were revealed in these Kampo medicine preparations in this study. The discussion in the dimension of the recommended dosage for efficacy

and safety needs to be further investigated with more complete information. Because the BBR was not the only active ingredient in the Kampo medicine preparation, there are usually synergistic pharmacologically active compounds in the combination of herbal medicine. However, this evaluation might be beneficial as a representative of the standardization of the Kampo medicine preparations using BBR as the biological markers.

Table 11. BBR content in the various Kampo medicine preparations determined using developed fluorometric-based assay and HPLC–UV.

Sample	**Fluorometric-based assay**		HPLC–UV	
	BBR amount (μg/g dry wt)	**SD**	**BBR amount (μg/g dry wt)**	**SD**
Kampo no. 14	398	14.8	384	31.4
Kampo no. 15	708	6.86	614	22.2
Kampo no. 37	380	26.1	578	21.0
Kampo no. 46	261	13.9	220	16.9
Kampo no. 50	604	13.2	652	4.96
Kampo no. 57	573	16	529	9.35
Kampo no. 58	388	9.58	458	7.43
Kampo no. 67	301	12.3	269	7.02
Kampo no. 73	308	12.4	307	17.5
Kampo no. 80	459	12.7	446	6.14
Kampo no. 91	912	21.9	914	94.9
Kampo no. 93	287	11.5	290	9.54
Kampo no. 113	206	14.7	312	16.7
Kampo no. 120	1610	102	1751	122
Kampo no. 136	447	10.5	535	16.5

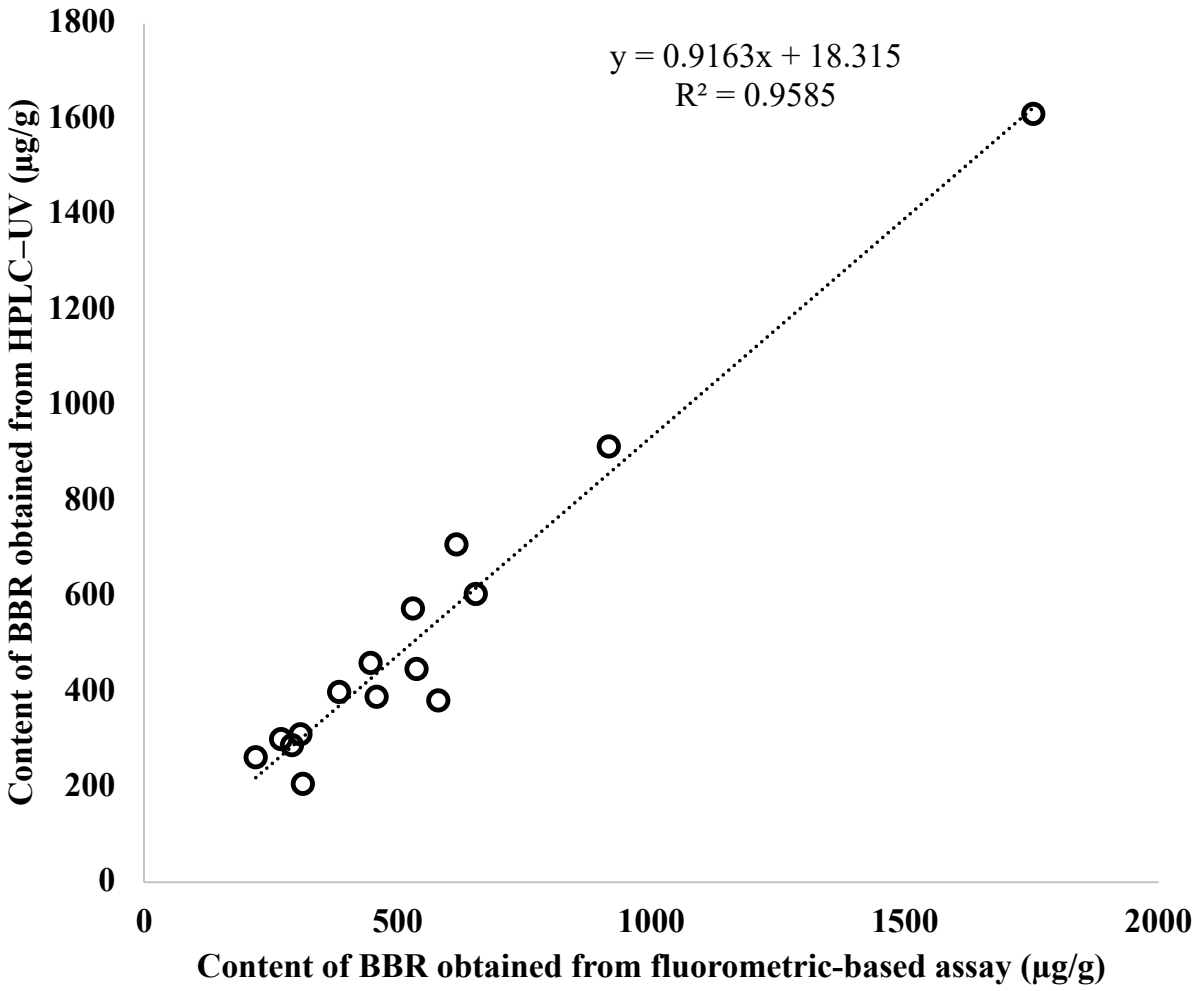

Figure 36 Correlation plot between the BBR content obtained from HPLC–UV and fluorometric-based assay

4. Conclusion

In this study, the aptamer against BBR was successfully selected from GOLD-SELEX process. To make the structure more fluorescent, the obtained structure was truncated, modified, and polymerized. The final sequence (TBBR38s) was successfully applied for the development of BBR detecting assay. The microplate-based BBR detection using TBBR38s has a linearity range of 0.780–25.0 μg/mL, with an LOD of 0.431 μg/mL. Various validation methods, that is, repeatability, precision test, and accuracy test, were used to confirm the reliability of the assay. Even the developed assay sensitivity was not superior to that of established methods. However, the assay has the benefit of short detection time (5 min) with the ability to analyze multiple samples at one time. Moreover, the assay linearity range and LOD were comparable to that of icELISA developed using MAb, which generally takes at least 4 h to obtain the result. The developed assay was used for detecting the BBR in Kampo medicine preparation samples where the correlation between the content obtained from HPLC–UV and that of the developed assay was revealed. Thus, this assay could be used as the alternative or used for BBR-containing sample screening along with the other analytical methods.

Chapter V

Conclusion

Benzylisoquinoline alkaloids are important pharmacologically active substances derived from plants. They were obtained from a variety of medicinal plants used in several traditional medicine formulations. The quality of benzylisoquinoline alkaloids from natural sources is often managed by controlling their concentration. Several techniques, such as HPLC–UV, electrochemical approach, and GC–MS, were developed to detect these alkaloids. However, these procedures required numerous rounds of time- and labor-intensive sample processing and required a relatively large amount of organic solvent. To circumvent these constraints, biological detection techniques have been developed to replace or complement traditional approaches. Biochemical tests for the detection of the valuable alkaloids HM and BBR were established in this thesis.

HM was the first alkaloid of interest, which was detected using specially developed immunoassays because it is on the WADA list of banned substances. Thus, the detection methods that could detect HM in samples of medicinal plants were crucial for sports communities. Immunizing mice with HM–BSA conjugates made using a CDI-mediated approach led to the successful production of the Anti (*S*)-HM MAb (MAb E8). It was possible to clone a sustainable source of MAb E8, a colony E8 hybridoma, by hybridizing myeloma cells with immunized splenocytes. The purified MAb E8 was highly sensitive with a high degree of specificity for (*S*)-HM. The MAb E8 was subsequently employed in the development of icELISA. The repeatability, precision, and dependability of the assay were ensured by the application of various validation techniques. Consequently, a cost-effective, high-throughput, and straightforward assay for detecting (*S*)-HM was developed. The developed assay can detect (*S*)-HM in plant samples. Therefore, this method could be used as an alternative to established methods or in conjunction with them for simple screening of (*S*)-HM-containing plants. It is noteworthy that this is the first immunoassay for detecting (*S*)-HM.

To extend the benefits of MAb E8, this research was conducted to develop an LFA for detecting (*S*)-HM in plant samples. The developed LFA made detection possible in versatile scenarios. The assay is predicated on the competitive binding of MAb E8–colloidal gold nanoparticle conjugates to immobilized HM on test strips and free (*S*)-HM in the corresponding samples. Several validation techniques were used to establish the sensitivity, reproducibility, and

selectivity of the LFA. The real samples were used to evaluate the performance of the assay. Because only a small sample volume (20 μL) was required for the analysis, this LFA is ideal for situations involving small sample volumes. Additionally, the application of a preincubation strip format simplified preparation and eliminated the laborious and time-consuming fiber pad preparation phase required for conventional LFAs. To our best knowledge, the reported LFA is the first of its kind.

The second focus of this study was BBR, the yellow pharmacologically active alkaloid. BBR was contained in various Kampo medicine preparations. Effective BBR screening and detection techniques were required to standardize these Kampo medicine preparations. Here, the aptamer-based BBR detection assay was developed. The GOLD-SELEX approach was successful in finding the aptamer against BBR that allows fluorescence amplification of BBR. The structures were modified to obtain the final trimer sequence (TBBR38s). The detection is based on the ability to generate the fluorescence of the BBR–aptamer complex. A comparable sensitive assay to the icELISA was developed. Multiple validation techniques, including repeatability, precision, and accuracy tests, were utilized to confirm the dependability of the assay. The assay was superior to the established immunoassays in terms of shorter detection time and nonanimal usage. Moreover, the aptamer sequence did not require an expensive refrigerator or liquid nitrogen for sustainable production as it was stored as digital data. The developed assay was used to detect BBR in samples of Kampo medicine preparations, and a high positive correlation between the content determined using HPLC–UV and that of the developed assay was observed. Consequently, this assay could be used as an alternative or in conjunction with other analytical techniques for the screening of BBR-containing samples.

There are no excellent analytical techniques in the world. The user must select the detection method that best corresponds to the specific scenario at hand. The biochemical assays developed in this study may not be the most effective assays because their sensitivity was lower than that of some conventional methods. However, biological assays can be used in situations where such specific detection equipment is unavailable. Additionally, the developed biochemical assays can be utilized for the early screening of samples to reduce the amount of labor required for the actual analytical work.

References

[1] Hagel JM, Facchini PJ. Benzylisoquinoline alkaloid metabolism: a century of discovery and a brave new world. *Plant Cell Physiol*. 2013;54(5):647-72. doi: 10.1093/pcp/pct020.

[2] Bessi I, Bazzicalupi C, Richter C, Jonker HR, Saxena K, Sissi C, Chioccioli M, Bianco S, Bilia AR, Schwalbe H, Gratteri P. Spectroscopic, molecular modeling, and NMR-spectroscopic investigation of the binding mode of the natural alkaloids berberine and sanguinarine to human telomeric G-quadruplex DNA. *ACS Chem Biol*. 2012;7(6):1109-19. doi: 10.1021/cb300096g.

[3] Dinsmore WW. Available and future treatments for erectile dysfunction. *Clin Cornerstone*. 2005;7(1):37-45. doi: 10.1016/s1098-3597(05)80047-x.

[4] Qian JQ. Cardiovascular pharmacological effects of bisbenzylisoquinoline alkaloid derivatives. *Acta Pharmacol Sin*. 2002;23(12):1086-92.

[5] Bowman WC. Neuromuscular block. *Br J Pharmacol*. 2006 Jan;147 Suppl 1(Suppl 1):S277-86. doi: 10.1038/sj.bjp.0706404.

[6] Liscombe DK, MacLeod BP, Loukanina N, Nandi OI, Facchini PJ. Evidence for the monophyletic evolution of benzylisoquinoline alkaloid biosynthesis in angiosperms. *Phytochemistry*. 2005;66(20):2501-20. doi: 10.1016/j.phytochem.2005.04.044.

[7] Shields VD, Smith KP, Arnold NS, Gordon IM, Shaw TE, Waranch D. The effect of varying alkaloid concentrations on the feeding behavior of gypsy moth larvae, *Lymantria dispar* (L.) (Lepidoptera: Lymantriidae). *Arthropod Plant Interact*. 2008;2(2):101-7. doi: 10.1007/s11829-008-9035-6.

[8] Park IK, Lee HS, Lee SG, Park JD, Ahn YJ. Antifeeding activity of isoquinoline alkaloids identified in *Coptis japonica* roots against *Hyphantria cunea* (Lepidoptera: Arctiidae) and *Agelastica coerulea* (Coleoptera: Galerucinae). *J Econ Entomol*. 2000;93(2):331-5. doi: 10.1603/0022-0493-93.2.331.

[9] Sellier MJ, Reeb P, Marion-Poll F. Consumption of bitter alkaloids in *Drosophila melanogaster* in multiple-choice test conditions. *Chem Senses*. 2011;36(4):323-34. doi: 10.1093/chemse/bjq133.

[10] Krug E, Proksch P. Influence of dietary alkaloids on survival and growth of *Spodoptera littoralis*. *Biochem Syst Ecol.* 1993;21(8):749-56. doi: 10.1016/0305-1978(93)90087-8.

[11] Rangelov Kozhuharov V, Ivanov K, Ivanova S. Higenamine in plants as a source of unintentional doping. *Plants* (Basel). 2022;11(3):354. doi: 10.3390/plants11030354.

[12] Sheng X, Himo F. Enzymatic *Pictet-Spengler* reaction: computational study of the mechanism and enantioselectivity of norcoclaurine synthase. *J Am Chem Soc*. 2019;141(28):11230-238. doi: 10.1021/jacs.9b04591.

[13] Nishihachijo M, Hirai Y, Kawano S, Nishiyama A, Minami H, Katayama T, Yasohara Y, Sato F, Kumagai H. Asymmetric synthesis of tetrahydroisoquinolines by enzymatic *Pictet-Spengler* reaction. *Biosci Biotechnol Biochem*. 2014;78(4):701-7. doi: 10.1080/09168451.2014.890039.

[14] Kosuge T, Yokota M. Letter: Studies on cardiac principle of aconite root. *Chem Pharm Bull*. 1976;24(1):176-8. doi: 10.1248/cpb.24.176.

[15] Hong H, Lee YI, Jin D. Determination of *R*-(+)-higenamine enantiomer in *Nelumbo nucifera* by high-performance liquid chromatography with a fluorescent chiral tagging reagent. *Microchem J*. 2010;96(2):374-9. doi: 10.1016/j.microc.2010.06.011.

[16] Pyo MK, Lee DH, Kim DH, Lee JH, Moon JC, Chang KC, Yun-Choi HS. Enantioselective synthesis of (*R*)-(+)- and (*S*)-(-)-higenamine and their analogues with effects on platelet aggregation and experimental animal model of disseminated intravascular coagulation. *Bioorg Med Chem Lett*. 2008;18(14):4110-4. doi: 10.1016/j.bmcl.2008.05.094.

[17] Park JE, Kang YJ, Park MK, Lee YS, Kim HJ, Seo HG, Lee JH, Hye Sook YC, Shin JS, Lee HW, Ahn SK, Chang KC. Enantiomers of higenamine inhibit LPS-induced iNOS in a macrophage cell line and improve the survival of mice with experimental endotoxemia. *Int Immunopharmacol*. 2006;6(2):226-33. doi: 10.1016/j.intimp.2005.08.007.

[18] Stajić A, Anđelković M, Dikić N, Rašić J, Vukašinović-Vesić M, Ivanović D, Jančić-Stojanović B. Determination of higenamine in dietary supplements by UHPLC/MS/MS method. *J Pharm Biomed Anal*. 2017;146:48-52. doi: 10.1016/j.jpba.2017.08.017.

[19] Ahmad W, Jantan I, Bukhari SN. *Tinospora crispa* (L.) Hook. f. & Thomson: a review of its ethnobotanical, phytochemical, and pharmacological aspects. *Front Pharmacol*. 2016;7:59. doi: 10.3389/fphar.2016.00059.

[20] Hibino T, Yuzurihara M, Kase Y, Takeda A. synephrine, a component of evodiae fructus, constricts isolated rat aorta via adrenergic and serotonergic receptors. *J Pharmacol Sci*. 2009;111(1):73-81. doi: 10.1254/jphs.09077fp.

[21] Huang YF, He F, Wang CJ, Xie Y, Zhang YY, Sang Z, Qiu P, Luo P, Xiao SY, Li J, Wu FC, Liu L, Zhou H. Discovery of chemical markers for improving the quality and safety control of *Sinomenium acutum* stem by the simultaneous determination of multiple alkaloids using UHPLC-QQQ-MS/MS. *Sci Rep*. 2020;10(1):14182. doi: 10.1038/s41598-020-71133-4.

[22] Zhang N, Lian Z, Peng X, Li Z, Zhu H. Applications of higenamine in pharmacology and medicine. *J Ethnopharmacol*. 2017;196:242-52. doi: 10.1016/j.jep.2016.12.033.

[23] Yang B, Ma S, Zhang C, Sun J, Zhang D, Chang S, Lin Y, Zhao G. Higenamine attenuates neuropathic pain by inhibition of NOX2/ROS/TRP/P38 mitogen-activated protein kinase/NF-κB signaling pathway. *Front Pharmacol*. 2021;12:716684. doi: 10.3389/fphar.2021.716684.

[24] Romeo I, Parise A, Galano A, Russo N, Alvarez-Idaboy JR, Marino T. The antioxidant capability of higenamine: insights from theory. *Antioxidants* (Basel). 2020;9(5):358. doi: 10.3390/antiox9050358.

[25] Bai X, Ding W, Yang S, Guo X. Higenamine inhibits IL-1β-induced inflammation in human nucleus pulposus cells. *Biosci Rep*. 2019;39(6):BSR20190857. doi: 10.1042/BSR20190857.

[26] Chen Y, Guo B, Zhang H, Hu L, Wang J. Higenamine, a dual agonist for β1- and β2-adrenergic receptors identified by screening a traditional Chinese medicine library. *Planta Med*. 2019;85(9-10):738-44. doi: 10.1055/a-0942-4502.

[27] Park SO, Hong CY, Paik SW, Yun-Choi HS. Determination of blood concentration of higenamine by high pressure liquid chromatography. *Arch Pharm Res*. 1987;10(1):60-6. doi: 10.1007/bf02855622.

[28] World Anti-Doping Agency. The 2022 WADA prohibited list. Available online: https://www.wada-ama.org/sites/default/files/resources/files/2022list_final_en.pdf.

[29] Malhotra B, Kulkarni GT, Dhiman N, Joshi DD, Chander S, Kharkwal A, Sharma AK, Kharkwal H. Recent advances on *Berberis aristata* emphasizing berberine alkaloid including phytochemistry, pharmacology and drug delivery system. *J Herb Med*. 2021;27:100433. doi:/10.1016/j.hermed.2021.100433.

[30] Zhang Q, Piao XL, Piao XS, Lu T, Wang D, Kim SW. Preventive effect of *Coptis chinensis* and berberine on intestinal injury in rats challenged with lipopolysaccharides. *Food Chem*

Toxicol. 2011;49(1):61-9. doi: 10.1016/j.fct.2010.09.032.

[31] Yashiki(Tohi) K, Kiso A, Zhou YY, Iwasaki D, Kambara T, Mizutani K. The effects of *Coptis japonica* root extract and its key component, berberine, on human subcutaneous adipocytes. *J Soc Cosmet Chem*. 2009;43(4):274-80. doi: 10.5107/sccj.43.274.

[32] da Silva AR, de Andrade Neto JB, da Silva CR, Campos Rde S, Costa Silva RA, Freitas DD, do Nascimento FB, de Andrade LN, Sampaio LS, Grangeiro TB, Magalhães HI, Cavalcanti BC, de Moraes MO, Nobre Júnior HV. Berberine antifungal activity in fluconazole-resistant pathogenic yeasts: action mechanism evaluated by flow cytometry and biofilm growth inhibition in *Candida* spp. *Antimicrob Agents Chemother*. 2016;60(6):3551-7. doi: 10.1128/AAC.01846-15.

[33] Okunade AL, Hufford CD, Richardson MD, Peterson JR, Clark AM. Antimicrobial properties of alkaloids from *Xanthorhiza simplicissima*. *J Pharm Sci*. 1994;83(3):404-6. doi: 10.1002/jps.2600830327.

[34] Zhang Y, Xu L, Qiu J, Sun M, Xia C, Zhou Z, Liu T. Provenance variations in berberine content of *Phellodendron amurense*, a rare and endangered medicinal plant grown in Northeast China. *Scand J For Res*. 2014;29(8):725-33. doi: 10.1080/02827581.2014.978885.

[35] Japanese Pharmacopoeia 18th Edition (JP18th) Coptis rhizome. 2022:1988-9.

[36] Japanese Pharmacopoeia 18th Edition (JP18th) Phellodendron bark. 2022:2096-7.

[37] Pérez-Rubio KG, González-Ortiz M, Martínez-Abundis E, Robles-Cervantes JA, Espinel-Bermúdez MC. Effect of berberine administration on metabolic syndrome, insulin sensitivity, and insulin secretion. *Metab Syndr Relat Disord*. 2013;11(5):366-9. doi: 10.1089/met.2012.0183.

[38] Abd El-Wahab AE, Ghareeb DA, Sarhan EE, Abu-Serie MM, El Demellawy MA. *In vitro* biological assessment of *Berberis vulgaris* and its active constituent, berberine: antioxidants, anti-acetylcholinesterase, anti-diabetic and anticancer effects. *BMC Complement Altern Med*. 2013;13:218. doi: 10.1186/1472-6882-13-218.

[39] Liu D, Meng X, Wu D, Qiu Z, Luo H. A natural isoquinoline alkaloid with antitumor activity: studies of the biological activities of berberine. *Front Pharmacol*. 2019;10:9. doi: 10.3389/fphar.2019.00009.

[40] Peng L, Kang S, Yin Z, Jia R, Song X, Li L, Li Z, Zou Y, Liang X, Li L, He C, Ye G, Yin

L, Shi F, Lv C, Jing B. Antibacterial activity and mechanism of berberine against *Streptococcus agalactiae*. *Int J Clin Exp Pathol*. 2015;8(5):5217-23.

[41] Wang S, Ren H, Zhong H, Zhao X, Li C, Ma J, Gu X, Xue Y, Huang S, Yang J, Chen L, Chen G, Qu S, Liang J, Qin L, Huang Q, Peng Y, Li Q, Wang X, Zou Y, Shi Z, Li X, Li T, Yang H, Lai S, Xu G, Li J, Zhang Y, Gu Y, Wang W. Combined berberine and probiotic treatment as an effective regimen for improving postprandial hyperlipidemia in type 2 diabetes patients: a double blinded placebo controlled randomized study. *Gut Microbes*. 2022;14(1):2003176. doi: 10.1080/19490976.2021.2003176.

[42] Rad SZK, Rameshrad M, Hosseinzadeh H. Toxicology effects of *Berberis vulgaris* (barberry) and its active constituent, berberine: a review. *Iran J Basic Med Sci*. 2017;20(5):516-29. doi: 10.22038/IJBMS.2017.8676.

[43] Yalow RS, Berson SA. Immunoassay of endogenous plasma insulin in man. *J Clin Invest*. 1960;39(7):1157-75. doi: 10.1172/JCI104130.

[44] Sakamoto S, Putalun W, Vimolmangkang S, Phoolcharoen W, Shoyama Y, Tanaka H, Morimoto S. Enzyme-linked immunosorbent assay for the quantitative/qualitative analysis of plant secondary metabolites. *J Nat Med*. 2018;72(1):32-42. doi: 10.1007/s11418-017-1144-z.

[45] Nuntawong P, Putalun W, Tanaka H, Morimoto S, Sakamoto S. Lateral flow immunoassay for small-molecules detection in phytoproducts: a review. *J Nat Med*. 2022;76(3):521-45. doi: 10.1007/s11418-022-01605-6.

[46] McKeague M, Derosa MC. Challenges and opportunities for small molecule aptamer development. *J Nucleic Acids*. 2012; 2012:748913. doi: 10.1155/2012/748913.

[47] Xiufen W, Hiramatsu N, Matsubara M. The antioxidative activity of traditional Japanese herbs. *Biofactors*. 2004;21(1-4):281-4. doi: 10.1002/biof.552210155.

[48] Tsai FY, Lui LF, Chang B. Analysis of diuretic doping agents by HPLC screening and GC-MSD confirmation. *J Pharm Biomed Anal*. 1991;9(10-12):1069-76. doi: 10.1016/0731-7085(91)80046-c.

[49] Feng YR, Wang B, Li GJ, Kang WJ, Lian KQ, Lu XL. Determination of higenamine in multi-matrix by gas chromatography-mass spectrometry combined with derivatization technology. *J Food Drug Anal*. 2020;28(1):124-31. doi: 10.1016/j.jfda.2019.09.002.

[50] Erlanger BF. The preparation of antigenic hapten-carrier conjugates: a survey. *Methods*

Enzymol. 1980;70(A):85-104. doi: 10.1016/s0076-6879(80)70043-5.

[51] Sakamoto S, Yusakul G, Tsuneura Y, Putalun W, Usui K, Miyamoto T, Tanaka H, Morimoto S. Sodium periodate-mediated conjugation of harringtonine enabling the production of a highly specific monoclonal antibody, and the development of a sensitive quantitative analysis method. *Analyst*. 2017;142(7):1140-48. doi: 10.1039/c6an02751b.

[52] Sakamoto S, Nagamitsu R, Yusakul G, Miyamoto T, Tanaka H, Morimoto S. Ultrasensitive immunoassay for monocrotaline using monoclonal antibody produced by *N,N′*-carbonyldiimidazole mediated hapten-carrier protein conjugates. *Talanta*. 2017;168:67-72. doi: 10.1016/j.talanta.2017.03.028.

[53] Sakamoto S, Kohno T, Shimizu K, Tanaka H, Morimoto S. Detection of ganoderic acid A in *Ganoderma lingzhi* by an indirect competitive enzyme-linked immunosorbent assay. *Planta Med*. 2016;82(8):747-51. doi: 10.1055/s-0042-104202.

[54] Guo ZY, Zhang ZY, Xiao JQ, Qin JH, Zhao W. Antibacterial effects of leaf extract of *Nandina domestica* and the underlined mechanism. *Evid Based Complement Alternat Med*. 2018;2018:8298151. doi: 10.1155/2018/8298151.

[55] Sakamoto S, Yusakul G, Nuntawong P, Kitisripanya T, Putalun W, Miyamoto T, Tanaka H, Morimoto S. Development of an indirect competitive immunochromatographic strip test for rapid detection and determination of anticancer drug, harringtonine. *J Chromatogr B Analyt Technol Biomed Life Sci*. 2017;1048:150-54. doi: 10.1016/j.jchromb.2017.01.032.

[56] Sakamoto S, Kikkawa N, Kohno T, Shimizu K, Tanaka H, Morimoto S. Immunochromatographic strip assay for detection of bioactive *Ganoderma* triterpenoid, ganoderic acid A in *Ganoderma lingzhi*. *Fitoterapia*. 2016;114:51-5. doi: 10.1016/j.fitote.2016.08.016.

[57] Wang PL, Kaneko A. Introduction to Kampo medicine for dental treatment-Oral pharmacotherapy that utilizes the advantages of Western and Kampo medicines. *Jpn Dent Sci Rev*. 2018;54(4):197-204. doi: 10.1016/j.jdsr.2018.03.004.

[58] Habtemariam S. Berberine pharmacology and the gut microbiota: A hidden therapeutic link. *Pharmacol Res*. 2020;155:104722. doi: 10.1016/j.phrs.2020.104722.

[59] Och A, Zalewski D, Komsta Ł, Kołodziej P, Kocki J, Bogucka-Kocka A. Cytotoxic and proapoptotic activity of sanguinarine, berberine, and extracts of *Chelidonium majus* L. and *Berberis thunbergii* DC. toward hematopoietic cancer cell lines. *Toxins* (Basel).

2019;11(9):485. doi: 10.3390/toxins11090485.

[60] Wang J, Zhang Y, Wang H, Chen Y, Xu L, Gao T, Pei R. Selection and analysis of DNA aptamers to berberine to develop a label-free light-up fluorescent probe. *New J Chem*. 2016;40(11):9768-73. doi: 10.1039/c6nj02290a.

[61] Chatterjee B, Kalyani N, Anand A, Khan E, Das S, Bansal V, Kumar A, Sharma TK. GOLD SELEX: a novel SELEX approach for the development of high-affinity aptamers against small molecules without residual activity. *Mikrochim Acta*. 2020;187(11):618. doi: 10.1007/s00604-020-04577-0.

[62] Vorobyeva M, Vorobjev P, Venyaminova A. Multivalent aptamers: versatile tools for diagnostic and therapeutic applications. *Molecules*. 2016;21(12):1613. doi: 10.3390/molecules21121613.

[63] Chang YX, Qiu YQ, Du LM, Li CF, Wu H. Simultaneous determination of palmatine and berberine using cucurbit[7]uril as mobile phase additive by HPLC. *J Liq Chromatogr Relat*. 2011;34(20):2629-39. doi: 10.1080/10826076.2011.593073.

[64] Geto A, Pita M, De Lacey AL, Tessema M, Admassie S. Electrochemical determination of berberine at a multi-walled carbon nanotubes-modified glassy carbon electrode. *Sens Actuators B Chem*. 2013;183:96-101. doi: 10.1016/j.snb.2013.03.121.

[65] Kim JS, Tanaka H, Shoyama Y. Immunoquantitative analysis for berberine and its related compounds using monoclonal antibodies in herbal medicines. *Analyst*. 2004;129(1):87-91. doi: 10.1039/b311304c.

[66] Kim JS, Masaki T, Sirikantaramas S, Shoyama Y, Tanaka H. Activation of a refolded, berberine-specific, single-chain Fv fragment by addition of free berberine. *Biotechnol Lett*. 2006;28(13):999-1006. doi: 10.1007/s10529-006-9033-7.

[67] Li CL, Tan LH, Wang YF, Luo CD, Chen HB, Lu Q, Li YC, Yang XB, Chen JN, Liu YH, Xie JH, Su ZR. Comparison of anti-inflammatory effects of berberine, and its natural oxidative and reduced derivatives from *Rhizoma Coptidis in vitro* and *in vivo*. *Phytomedicine*. 2019;52:272-83. doi: 10.1016/j.phymed.2018.09.228.

[68] Tan L, Wang Y, Ai G, Luo C, Chen H, Li C, Zeng H, Xie J, Chen J, Su Z. Dihydroberberine, a hydrogenated derivative of berberine firstly identified in Phellodendri Chinese cortex, exerts anti-inflammatory effect via dual modulation of NF-κB and MAPK signaling pathways. *Int Immunopharmacol*. 2019;75:105802. doi: 10.1016/j.intimp.2019.105802.

ACKNOWLEDGEMENTS

On behalf of my advisors, Professor Satoshi Morimoto, Professor Hiroyuki Tanaka, and Associate Professor Seiichi Sakamoto, I would like to express my profound and sincere gratitude. They have always inspired, advised, encouraged, and trusted me throughout the course of my research and preparation of this thesis. With their assistance and opportunities, the purpose of my life is to grow.

I am grateful to Professor Tomofumi Miyamoto of the Graduate School of Pharmaceutical Science at Kyushu University for his insightful comments and ideas on my dissertation.

Additionally, I would like to express my profound thanks and gratitude to Associate Professor Boonchoo Sritularak of the Faculty of Pharmaceutical Sciences, Chulalongkorn University, Thailand and Assistant Professor Gorawit Yusakul of the School of Pharmacy, Walailak University, Thailand who inspired me and instilled in me a passion for study.

In addition, I would like to convey my thanks and admiration to Kanta Noguchi, Kei Minami, and Hiroki Uchiyama for their everyday assistance, emotional support, and encouragement.

I'd also want to thank the members of our department and the Thai exchange students for their friendship and support.

Lastly, I would want to thank my family for their love and support, which have allowed me to reach my objective.

Poomraphie Nuntawong